Genetic dissection of circuits underlying the modular structure of the Superior Colliculus

Laura Masullo

MRC Laboratory of Molecular Biology

University of Cambridge

This dissertation is submitted for the degree of

Doctor of Philosophy

Peterhouse

March 2019

Declaration

This dissertation is the result of my own work and includes nothing which is the outcome of work done in collaboration except as declared in the *Statement of Contribution*. All the work described in this dissertation was carried out in the Neurobiology Division of the Medical Research Council Laboratory of Molecular Biology, under the supervision of Dr. Marco Tripodi.

It is not substantially the same as any that I have submitted, or, is being concurrently submitted for a degree or diploma or other qualification at the University of Cambridge or any other University or similar institution. I further state that no substantial part of my dissertation has already been submitted, or, is being concurrently submitted for any such degree, diploma or other qualification at the University of Cambridge or any other University or similar institution.

It does not exceed 60,000 words, excluding figures, tables, appendices and bibliography, as specified by the Degree Committee.

Statement of contributions

Due to the interdisciplinary nature of this project, some of the data presented was acquired and analysed with the help of the following collaborators:

Dr. Letizia Mariotti (Tripodi Lab): acquired and analysed part of the electrophysiological recordings *in vitro* (Chapter 3), contributed to the implementation of the double-sensor system for head movement tracking (Chapter 5), assisted with the analysis of optogenetics data (Chapter 6) and conducted the *in vivo* electrophysiology experiments (Chapter 7).

Nicolas Alexandre (Tripodi Lab): contributed to the implementation of the double-sensor system for head movement tracking (Chapter 5).

Dr. Paula Freire-Pritchett (LMB Bioinformatics Unit): developed the software for the analysis of RNAseq datasets (Chapter 3).

Jerome Boulanger (LMB Light Microscopy Unit): developed the software for the analysis of 3D images acquired with light sheet microscopy (Chapter 3).

All experiments in this thesis were conceived and designed by my PhD supervisor, Dr. Marco Tripodi, and myself, with additional input from other investigators for the experiments they contributed to.

Summary

In order to successfully interact with the environment, animals need to produce accurate movements towards specific positions in space. A crucial region of the brain that guides such goal-oriented movements is the superior colliculus (SC), an evolutionary conserved structure of the midbrain. While several lines of research in different model organisms have confirmed that the SC contributes to the initiation of orienting movements, how functionally distinct neuronal groups within the SC are organized to support the production of such motor outputs is poorly understood.

One of the reasons why the intrinsic circuit organization of the SC remains elusive is the lack of genetic characterization of the neuronal populations of the motor SC. Here, we performed RNAseq to screen for genetic markers for neuronal subpopulations in the motor SC. We identified a transcription factor, *Pitx2*, which is exclusively expressed in a subpopulation of glutamatergic neurons in the motor domain of the SC. Strikingly, this population of neurons displays a non-homogenous distribution within the motor layer of the SC, being organised in clusters along the mediolateral and anteroposterior axis. We mapped the pre-synaptic network and the post-synaptic targets of Pitx2^{ON} neurons, unveiling that this modular population receives direct inputs from motor and sensory cortical regions, as well as several midbrain nuclei involved in movement control, and sends projection along the cephalomotor pathway. We then asked whether these modules may act as functional units, each integrating multimodal sensory information and encoding a specific feature of head movement, the main ethologically relevant orienting behaviour in rodents. Optogenetic activation of this modular population in freely moving animals produced a stereotyped, robust head motion characterised by a pronounced quantal nature; furthermore, the amplitude of the elicited head movement varied based on the modular unit activated. Our results suggest that distinct clusters of genetically defined neurons produce head displacement along a characteristic vector.

In conclusion, we found that a population of premotor neurons in the SC is organised in a modular conformation and we suggest that such modularity may represent a physical implementation of a discontinuous motor map for orienting movements encoded in the mouse SC. Our work complements previous observations of periodicity in SC circuitry, as well as its afferent and efferent systems. Exploiting the genetic toolkit available in the mouse, our work begins to address the functional relevance of this modularity and paves the way for future experiments to investigate principles of sensorimotor integration in SC circuits.

Acknowledgements

I would like to thank my supervisor *Marco Tripodi* for giving me the opportunity to join the lab, entrusting me with this exciting project and supervising me through its realisation.

I would also like to thank the following people:

Letizia Mariotti, a great collaborator, brilliant scientist and exceptional friend; I will forever be grateful for her unconditional help and constant support during my PhD. I could not have asked for a better companion to embark on this demanding project.

Members of the Tripodi Lab, for scientific discussions, coffee breaks and moral support.

Michael Hastings, for his advice throughout my graduate studies.

Claire Knox and the Biological Services group, for their invalueable technical assistance.

Steve Scotcher and the LMB Mechanical Workshop, for finding a way to accommodate all my last minute requests.

Peterhouse, and in particular my MCR committee, for providing a home away from home.

My parents and *Giulio*, for always offering the source of greatest comfort and unrivalled encouragement.

Table of contents

List of abbreviations

AAV	Adeno-associated virus
AC	Anterior cingulate cortex
AChE	Acetylcholinesterase
APN	Anterior pretectal nucleus
AUD1	Primary auditory cortex
C1-C3	Spinal cord, cervical segments 1-3
ChR1/2	Channelrhodopsin 1/2
CL	Central lateral nucleus of the thalamus
CM	Central medial nucleus of the thalamus
Cun	Cuneiform nucleus
DN	Dentate nucleus
EMG	Electromyogram
FEF	Frontal eye fields
FF	Fields of Forel
FISH	Fluorescent *in situ* hybridisation
FN	Fastigial nucleus
IC	Inferior colliculus
III	Oculomotor nucleus
IP	Interposed nucleus
LGv	Ventral part of the lateral geniculate complex
LH	Lateral habenula
LHA	Lateral hypothalamic area
LTA	Light-triggered average

M1	Primary motor cortex
M2	Secondary motor cortex
MDRN	Medullary reticular nucleus
MM	Mammillary nucleus
Mobp	Myelin-associated oligodendrocyte basic protein
MRN	Midbrain reticular nucleus
NOT	Nucleus of the optic tract
NPC	Nucleus of the posterior commissure
Onecut 2/3	One Cut Homeobox 2/3
$\mathbf{p_{adj}}$	Adjusted p-value
PAG	Periacqueductal gray
PB	Parabrachial nucleus
PBG	Parabigeminal nucleus
PF	Parafascicular nucleus
PFA	Paraformaldehyde
PH	Posterior hypothalamic nucleus
Pitx2	Paired-like homeodomain transcription factor 2
PMv	Ventral premammillary nucleus
PN	Paranigral nucleus
PPN	Peduncolopontine nucleus
PRN	Pontine reticular nucleus
RGC	Retinal ganglion cell
RPF	Retroparafascicular nucleus
RSPL	Retrosplenial cortex
S1	Primary somatosensory cortex

S1 BF	Primary somatosensory cortex, barrel fields
S1 LL	Primary somatosensory cortex, lower limb
S1 M	Primary somatosensory cortex, mouth
S1 N	Primary somatosensory cortex, nose
S1 T	Primary somatosensory cortex, trunk
S1 UL	Primary somatosensory cortex, upper limb
S2	Secondary somatosensory cortex
SAI	Stratum album intermediale
SAP	Stratum album profundum
SC	Superior colliculus
SC_{dg}	Superior colliculus, deep gray
Sc_{iga}	Superior colliculus, intermediate gray a
Sc_{igb}	Superior colliculus, intermediate gray b
SCm	Superior colliculus, motor related
Sc_{op}	Superior colliculus, optic layer
scRNAseq	Single-cell RNA sequecing
SCs	Superior colliculus, sensory related
SC_{sg}	Superior colliculus, superficial gray
Sc_{zo}	Superior colliculus, zonal layer
SGI	Stratum griseum intermediale
SGN	Suprageniculate nucleus
SGP	Stratum griseum profundum
SGS	Stratum griseum superficiale
SNc	Substantia nigra, pars compacta
SNr	Substantia nigra, pars reticulata

SO	Stratum opticum
SOM	Somatostatin
Sp5O	Spinal trigeminal nucleus oralis
STA	Spike-triggered average
STN	Subthalamic nucleus
SUM	Supramammillary nucleus
SZ	Stratum zonale
Tfap2d	Transcription factor AP-2 delta
TRN	Tegmental reticular nucleus
TSD	Torsional standard deviation
TVA	Tumour virus receptor A
V1	Primary visual cortex
vGAT	Vescicular GABA transporter
vGluT2	Vescicular glutamate transporter 2
Visc	Visceral area
VM	Ventral medial nucleus of the thalamus
VTA	Ventral tegmental area
WT	Wild-type
ZI	Zona incerta
2P	Two-photon

1. Introduction

1.1 The neuroscience of space

Together with time, space is one of the most intuitive concepts to grasp and yet one of the most controversial to define. Physicists and philosophers have entertained discussions about the very nature of space for centuries. At one point in history, the debate became a royal matter; in the early 18th century, Queen of Great Britain and keen philosopher Caroline of Ansbach asked two thinkers from opposing philosophical currents to exchange letters on the subject. Representing continental rationalists, German philosopher Gottfried Liebniz believed space coincided with the spatial relations between objects, implying it would not exist without the things it connects; on the other side of the Channel, English absolutist Samuel Clarke expressed his Newtonian views of an absolute space, conceived as a property of the physical world[1]. This exchange ignited a new fire in the European intellect of the time, and many others joined in the discussion. Among all, the work of Immanuel Kant attempted to engage with both views and at the same challenge their assumption that all knowledge about the world is ultimately derived from sensory impressions.

> *"Space is not something objective and real, nor a substance, nor an accident, nor a relation; instead, it is subjective and ideal, and originates from the mind's nature in accord with a stable law as a scheme, as it were, for coordinating everything sensed externally".*

In his *Inaugural Dissertation* of 1770[2], Kant expresses the idea that space is just a concept humans use to make sense of the world, rather than a real entity. It is therefore a representation of the mind, not a physical dimension. Kant's view is in clear disagreement with the work of physicist Albert Einstein and mathematician Hermann Minkowski, who established the generally accepted and experimentally confirmed view of space as a physical entity that, together with time, defines a boundless four-dimensional continuum known as spacetime. Nonetheless, Kant's philosophical speculation resonates well with our own intuitive explanation of how we perceive the world. In defining separate areas of competence for physical and psychological takes on the matter, it provides an excellent starting point for understating how space is represented in the brain. Indeed, successful interaction with the environment around us relies on our ability to process spatial information according to multiple coding systems. The most important defining feature of such coding system is the spatial frameworks through which they operate; these can be tied to a particular body part, hence defining *egocentric* reference frames, or fixed with respect to the outside world, therefore termed *allocentric* reference frames. Modern neuroscience has proven that the brain makes use of both types of neural representation according to the requirements of the behavioural task involved.

1.1.1 Navigating in space

Navigation is a fundamental spatial task that a vast majority of animal species employ as a way to survive and thrive in their environment. Ethological observations of animals in their habitat provide fascinating examples of how species have evolved to successfully exploit their territories through extensive exploration. For example, elephants in north-western Namibia have some of the largest home ranges ever recorded in the animal kingdom; their seasonal movements, linked to rainfall, forage preference and availability[3-5], can extend up to 625 km and often involve reaching isolated waterholes without the possibility to use stable landmarks along the way[6]. While one could presume that such seasonal migrations might be however linked to mnemonic processes, several studies have reported successful navigation in animals exploring unknown territories in the wild. For example, resident Burmese pythons in southern Florida, which were displaced by up to 36 km from their home territory, showed remarkable ability to orient homeward relative to the capture location and return to within 5 km of their original position[7].

Significant progress has been made in our understanding of how behaviours such as navigating long distances in familiar or novel environments are supported by allocentric spatial frameworks, both in terms of where spatial maps are stored in the brain and how the

metric of such motion is encoded. While conducting behavioural studies in lab rats, Edward Tolman first inferred that neural circuits might encode a cognitive map providing an internal representation of space[8]. In the past 40 years, experimentalists have provided explanation of the biological substrates of such representation. Through a combination of behavioural and electrophysiological recordings, O'Keefe and colleagues first described the existence of neurons in the rodent hippocampus that show tuning to specific spatial locations in the animal's environment, which they named "place cells"[9], and postulated that these findings corroborated Tolman's theory of cognitive maps for spatial representation in the brain. In the 1990s, experimental results regarding a second type of spatial response in hippocampal circuits were published; this functional class of newly defined "head direction cells" was shown to signal the direction an animal is facing[10,11]. Most recently, May-Britt and Edvard Moser, demonstrated the existence of an additional class of spatially tuned cells in the enthorinal cortex, referred to as "grid cells", that fire when the animal is positioned in a repeating hexagonal grid of fields in its environment[12,13]. Many other spatial responses have since been observed and the path integration mechanisms operating through interaction among distinct functional cell types remain only partially understood[14]. Nevertheless, these findings point at the existence of a specialized system centred around the hippocampus, which encodes a cognitive map of space in allocentric coordinates to support orientation and navigation tasks.

1.1.2 Interacting with space

Our ability to interact with the environment around us extends much beyond the comparatively simple act of navigating it. We are surrounded by objects that we are able to grasp and manipulate; whether it is to grab a cup of coffee or hit a tennis ball, we are able to judge the spatial position of an object and execute accurate target-oriented movements. In order to interact coherently with objects in our surroundings, we also need an egocentric representation of space; that is, we need to be able to judge the spatial position of a target with respect to ourselves.

In *The Foundation of Science*[15], the French mathematician Henry Poincaré states:

> "*When it is said then that we 'localize' such and such an object at such and such a point of space, what* does it *mean? It simply means that we represent to ourselves the movements it would be necessary to make to reach that object".*

Thus, Poincaré suggests that motion is at the heart of the perceptual construction of space and in fact the very nature of the perceptual representation of space lies in the planning of actions. If such a strong connection exists between space and motion, then one can assume that the spatial framework that sustains such interactions with the surroundings should concern an area of space directly addressable by the motor task involved. The notion of a separate representation in the brain for the space immediately around the body was first introduced by neurophysiological studies in the 1970s[16,17] and subsequently elaborated and expanded by Graziano and Rizzolatti[18,19], who introduced the term *peripersonal space*. Their pioneering work in cats and primates provided initial observations that visually responsive neurons in premotor cortical areas, such as area 6 and the ventral premotor cortex, code stimulus position in spatial, rather than retinal coordinates[20-22]. This suggests that these neuronal populations are involved in the generation of a stable, body-centred reference frame necessary for programming visually guided movements. We now appreciate that the primate brain stores multiple egocentric representations of space centered on different body parts (i.e., hand-centered, head-centered, and trunk-centered)[23]; a justification for this apparently redundant strategy for spatial representation comes from neurophysiological studies in monkeys, which revealed that neurons in the putamen, area VIP, and inferior area 6 have motor functions as well as multisensory functions[24]. For this reason, peripersonal representations can be considered interfaces between the multisensory and motor domains, capable of encoding the location of objects of interest by integrating information from multiple sensory modalities to generate suitable motor acts.

1.2 Orienting actions: translating the world into motor space

The neurophysiological studies on the representation of peripersonal space corroborate Poincaré's intuition regarding the existence of a univocal relationship between the representation of space in egocentric coordinates and the encoding of a motor map of actions that allow us to interact with it. Studying networks that underlie orienting movements of the eye and head towards nearby stimuli can therefore represent a valid experimental approach to the more general investigation of the representation of space as a function of the self. Before moving on to describe the anatomical and functional properties of circuits underlying such behaviours, it is important to consider how goal-oriented actions are routinely employed by animals to interact with their environment, the context in which they are recruited and the type of sensory information that can elicit them.

1.2.1 Goal-oriented actions

Eye movements. Many higher mammals, including humans, non-human primates and cats, have an oculomotor range wide enough (± 55° in humans[25]) to allow for visual targets to be reached solely with a rapid movement of the eye between fixation points, a saccade. In fact, while reading a book or looking out of the window of a moving vehicle, we can find examples of a type of gaze control revolving entirely around the generation of saccades.

The fundamental anatomical feature of the eye that explains the execution of saccades is the fovea, a small pit containing a high density of photoreceptors located near the centre of the retina. It provides high acuity vision for a visual angle of roughly 5°, or 0.03% of the visual field[26], so animals need to constantly and synchronously move their eyes to sequentially extract high-resolution visual information from a larger portion of the world. Additionally to scanning the visual field, saccades contribute to a wide range of oculomotor behaviours; for example, they can represent reflexive movements towards a novel sensory cue manifesting unexpectedly in the environment, or they can be memory-guided movements generated towards a point in space in which the target had been previously presented. Saccades can also be performed as remembered sequences of gaze shifts as part of a learned task, such as while playing a musical instrument[27]. The study of saccades has been a very prolific area of research in the context of goal-oriented movements, as they are easily accessible to laboratory measurement and clinical evaluation. Furthermore, their dynamic properties can be easily delineated; saccades are ballistic movements that display consistent relationship among their amplitude, speed and duration[28], thus providing an ideal motor readout to investigate neural processes underlying their planning and execution. As their accuracy and latency during a task have been consistently reported in laboratory experiments and clinical assessment, defects in saccade performance have also been widely employed as a diagnostic tool for neurological conditions, such as Parkinsonian disorders[29].

Head recruitment. As mentioned above, higher mammals can employ saccades to reach targets in a broad range of positions in their visual fields. However, even in primates, the area of the visual space explored engaging saccades only is much smaller than its full potential. The stereotypical strategy adopted by animals to reach targets in peripheral regions of the visual space is executing concomitants, coordinated head rotations. Pioneering work by Bizzi and collegues revealed the fundamental principles dictating eye-head coordination[30-32]. By monitoring head and eye movements while recording electromyograms (EMG) from neck muscles, these studies in monkeys elucidated the eye and head kinematics involved in a typical spontaneous gaze shift generated to follow a target appearing at unexpected time and location from stationary coordinates. Under these particular

experimental conditions, the eyes appear to perform a saccade with a short delay from stimulus presentation to reach the target; the gaze shift thus produced brings the visual target in line of sight with little contribution from the head (< 2°). The head instead begins its rotation later and continues until after the gaze shift is completed, resulting in a compensatory movement of the eye in the opposite direction at matching speed [31] (Fig. 1.1a).

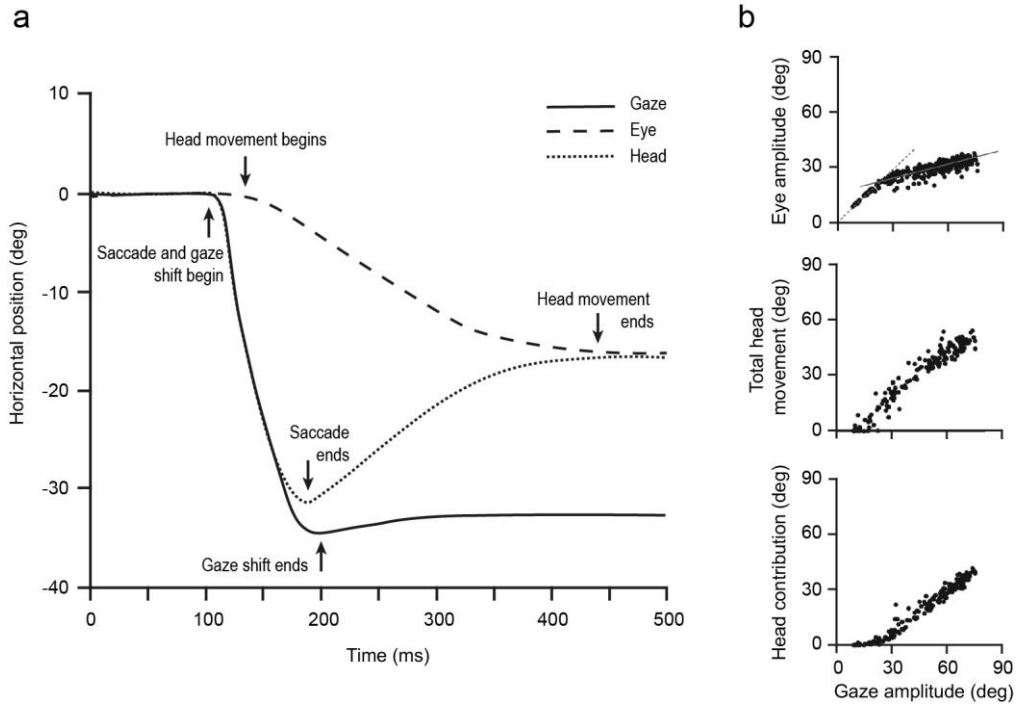

Figure 1.1 | Eye-head coordination in monkeys during visually guided gaze shifts.
a, Example of a gaze shift (solid line) generated through a combination of eye (dashed line) and head (dotted line) movements, aimed to follow a target appearing at unexpected time and location from stationary coordinates. **b**, Relative contribution of the eyes and head to gaze shifts of different amplitudes along the horizontal axis of movement. The amplitude of eye movements (top) shows a 1-1 relationship with the amplitude of overall gaze shift within a range of 5-20° (dotted line), but this declines with larger gaze shifts (solid line). The total head movement amplitude (middle) increases linearly across the full range of amplitudes of gaze shift; however, the head contribution to gaze shift (defined as movement that contributes to the overall change in the direction of the line of sight, bottom) relates linearly to gaze shift only for larger gaze amplitudes (30°+). Adapted from Freedman, 2008[26].

While recordings of eye and head motion seem to suggest that eye movement commands are generated before those for head displacement, increase in EMG signals from agonist neck muscles is recorded before that observed in ocular muscles[31,33], suggesting that the neuronal discharges leading to muscle contraction may be delivered in inverted order to what one might conclude from the motion data. In fact, the timing of head and eye movement initiation, as well as their contribution to overall gaze shift, are not fixed parameters in

orienting behaviour. The amplitude of the overall intended gaze shift plays a major role in the orchestration of eye-head coordination, with ampler gaze shift manifesting from a larger head-to-eye contribution than smaller gaze shifts[34] (Fig. 1.1b). The onset time of head displacement relative to saccade initiation is also modulated by the nature of the gaze shift, decreasing monotonically as the gaze shift amplitude increases until it appears synchronously to, or even anticipating, the eye rotation[35]. Further evidence of how flexibly these motor plans can be implemented in orienting comes from species such as bats and barn owls, characterized by a much more limited oculomotor range; during orienting, these animals perform head rotations that account for almost the entire gaze shifts[36,37]. This effect is also apparent in animals that lack a fovea, such as rodents; during visual orienting, head rotations produce the desired gaze shift and the concomitant rapid eye movements produced lack much of the precise metric described for primates. In fact, it has been stipulated that such eye movements might correspond to quick phases of vestibular and optokinetic nystagmus, regarded as the evolutionary forerunners of saccades[38].

Altogether, while head and eye movements have been traditionally considered tightly coupled motor plans for the performance of desired gaze shifts, the two can be executed somewhat independently during orienting based on the requirements of the task and the ethological relevance they carry.

1.2.2 Sensing a non-visual space

Most of the studies of goal-oriented behaviours summarised so far employed visual cues to elicit movement, or were conducted in animals that rely on vision as a fundamental source of sensory information. However, successful interaction with the environment can be obtained integrating very different types of sensory information according to their ethological relevance. For nocturnal animals with low acuity vision for example, sensing the environment through touch and hearing represents a meaningful strategy. Considering how animals perceive their surroundings as a whole is key to understanding fundamental processes of sensorimotor integration. Rather than tackling the anatomical and neural mechanisms underlying touch and hearing, this section provides a brief summary of their behavioural capabilities and their engagement in active sensing. Indeed, while the perception of tactile and auditory cues might appear a passive process, animals that rely on this alternative sensory systems engage in active auditory and somatosensory tasks comparable to the scanning of the visual field by foveated eyes.

Auditory orientation. Species that are able to navigate space efficiently in darkness often show a heightened ability to use auditory signals to locate objects of interest in space. The passive acoustic properties of the pinna, the only visible part of the ear, make it capable of amplifying or attenuating sounds based on the direction from which they reach the ear. In humans and other primates with virtually immobile ears, the spectral profile of the auditory signal reaching the ear is tightly linked to head position; ear mobility confers the ability to orient the pinnae independently of the head, breaking the univocal correspondence between acoustic signal properties and head position. Together with head movements, pinnae rotations are often observed in rodents, cats and bats upon presentation of an auditory cue[39-41]. While a wide variety of animals display such mobility, it is still unclear how ear rotations act to improve sound localization; it has been suggested that they could play a role in improving signal-to-noise ratio and obtaining multiple samples of an acoustic object in a short time span[40]. In addition to visual targets, auditory signals are effective triggers of orienting movements. Primate studies have reported that auditory saccades and head movements can be precisely executed towards the sound source following an equivalent strategy to visually guided movements[42].

Tactile orientation. Similarly to vision in primates, rodents and other small mammals reconstruct their tactile sensory space by actively moving their somatosensory organs. The sensory system engaged in such exploration relies on the tactile stimulation of prominent arrays of sensitive whiskers, also knows as vibrissae, which are swept back and forth to interact with objects during exploration. This behaviour, referred to as exploratory whisking, consists of a periodic protraction and retraction of the whiskers, typically occurring at 7-12 Hz, lasting several seconds at a time. Interestingly, animals are able to modify a number of spatial and temporal parameters of their whisking behaviour, including amplitude, velocity and midpoint, according to environmental conditions, as well as their motivational state[43]. In fact, in addition to providing sensory information to guide targeted movement of the head towards point of interest in space, whisking can also assume the role of a goal-oriented task in itself. In a much less frequent pattern of whisking, known as foveal whisking, the vibrissae are thrust forward to contact objects with low-amplitude movements at a higher frequency range of 15-25 Hz[44]. Rodents routinely make use of somatosensory information to guide their execution of accurate orienting movements of the head and trunk. A unique example is provided by the tactile orienting behaviour of the naked mole rat. These burrowing animals are functionally blind and possess poor sound localization abilities[45,46]; instead, they rely on the displacement of their somatic vibrissae to provide information on their surroundings[47]. Displacement of even a single hair can produce a turn of head and body to bring the snout around the stimulated area[48].

Sonar localisation. Extracting information about a dark environment using somatosensation may be an excellent strategy for burrowing species, but it certainly does not provide a viable option for those that navigate in flight. Instead, echolocating bats are able to emit temporally coordinated sequences of vocalization and then process the returning signal, extracting meaningful information about the location and physical features of objects in space. Similarly to what is observed for whisking in rodents, the emission of sonar vocalization is a highly dynamic process that involves the adaptation of, among others, the frequency and duration of vocalisations during target approach based an audiovocal feedback[49]. As a potential object of interest is detected in the surroundings, a form of "active listening" is engaged and leads to the production of sonar sound groups (SSGs), clusters of vocalizations characterised by increased echolocation pulse rate and decreased pulse duration that provide high-resolution information about the sensory space[50,51]. The returning echoes shape the motor behaviour of the animal, leading to pinnae and head rotations, as well as changes in flight trajectory.

In summary, animals routinely employ a diverse array of goal-oriented actions that allow them to interact with their peripersonal space. Considering the ethological relevance of such behaviours, as well as the sensory information that drives them, is a key factor in the design of experimental approaches to the study of gaze control in laboratory animals. Regardless of the precise nature of the motor plans employed in the process, all goal-oriented actions are bound to be the result of precise integration of relevant sensory inputs, matched with an appropriate attentional state that provides a cognitive framework for motor execution; identifying a platform for such sensorimotor integration processes in the brain holds the key to study the neural substrates of spatial-motor representations.

1.3 The superior colliculus: a unique spatial hub

Given the diversity of motor plans underlying goal-oriented tasks, as well as the sensory information that directly drives them, it is somewhat surprising to find that all of the sensory and motor functions described so far in the context of orienting are found represented in a single brain region. The superior colliculus (SC) is a central node in the mediation of sensorimotor transformations and the production of appropriate goal-oriented behaviours. Historically regarded as a key centre for the initiation of visually guided saccades in higher mammals, it is now evident that the repertoire of SC-mediated motor programmes is extremely wide and its representation varied across species. This section contains an

overview of the role of the SC in guiding orienting behaviours, as well as some evidence for its involvement in broader cognitive processes of attention.

1.3.1 Eye movements

The earliest indication of SC involvement in the production of goal-oriented motor tasks comes from studies of saccadic eye movements. Observations from experiments in head-restrained monkeys and cats have laid the foundations to our understanding of SC-mediated control of gaze. In the 1970s, it was first suggested that there exist neurons in the SC that fire bursts of action potentials prior to the manifestation of contraversive saccades, and that these neurons display a clear firing preference towards saccades of a given amplitude and direction[52,53]. Furthermore, these eye-movement-related neurons are distributed across the SC according to the properties of their preferred saccade; large contraversive saccades are represented caudally and smaller saccades rostrally, while both upwards and downwards directions are represented in each hemisphere, in the medial and lateral portions of the SC respectively[54] (Fig. 1.2).

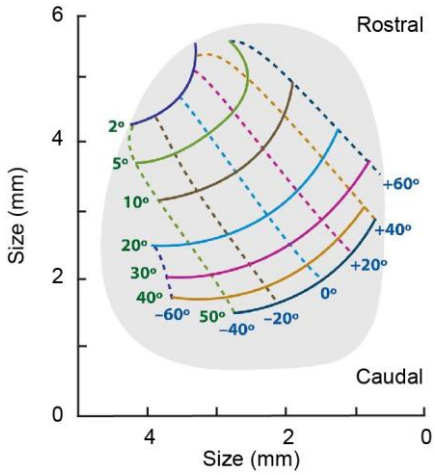

Figure 1.2 | Topographical organization of saccadic eye movements in the primate SC. Schematic representation illustrating topographical distribution of contralateral saccadic eye movements in the primate SC, encoded in retinotopic coordinates. Dashed lines define isodirectional bands, while solid lines show isoradial organisation of movement vectors. Green and blue numbers refer to the radial and directional values of each band respectively. Adapted from Gandhi and Katnani, 2011[55].

A number of studies employed micro-stimulation of the motor SC to infer causality and sufficiency of SC activity in generating orienting movements of the eye in monkeys, cats and

rodents[56-58], and confirm the observations of topography in the organisation of saccade vectors[59]. The importance of stimulation parameters on the motor output produced was also assessed; stimulation frequency does not appear to modify the amplitude or direction of the saccade produced, but it does affect the speed at which these movements are performed. Similar variations in movement velocity are also observed for physiologically produced saccades; indeed, visually guided saccades are faster than memory-guided eye movements of comparable metric[60,61] and the underlying neural discharge is more vigorous when the visual target remains illuminated[62]. On the other hand, stimulus duration appears to be an important determinant of the amplitude of motion produced. While this might not appear to be in accordance with the hypothesis of motor tuning of SC premotor units, prolonged stimulation produces a "staircase" of saccades interrupted by brief inter-saccadic intervals[56,63-65] (Fig. 1.3), suggesting that longer stimulations might instead produce a concatenation of motor events of similar metric.

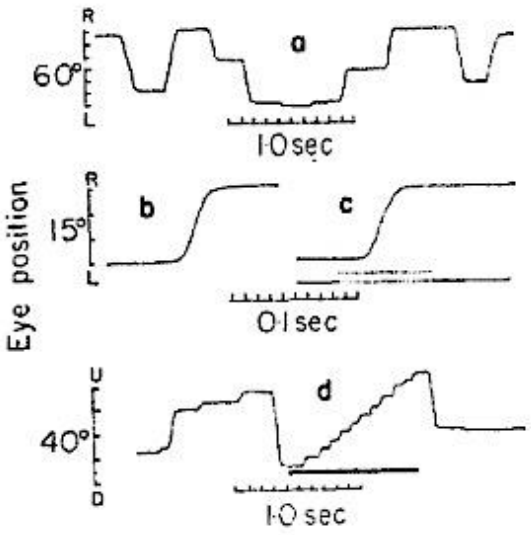

Figure 1.3 | Staircase of saccades evoked by electrical stimulation in the monkey SC.
a, Motion trace of spontaneous saccadic eye movements occurring along the horizontal axis. **b**, **c**, Single saccade occurring spontaneously (**b**) or triggered by brief electrical stimulation (**c**), tracked along the horizontal component of movement. **d**, Staircase of vertical saccades elicited by prolonged SC stimulation. Adapted from Robinson et al., 1972[56].

1.3.2 Head movements

Many of the early studies designed to elucidate the role of the SC in orienting were carried out in head-restrained primates; as a consequence, the involvement of collicular circuits in the generation of head movements was initially overlooked. Instead, later studies confirmed that the same SC premotor units that display high-frequency bursts of activity preceding

head-restrained saccades also fire significantly before the onset of head rotation[66], suggesting that these units are encoding a desired gaze shift regardless of the individual components of head and eye movement that this will entail. In support of these observation, micro-stimulation of the SC in cats and monkeys when the head is unrestrained leads to coordinated eye and head movement of comparable metric to visually guided gaze shifts[67-71].

As previously discussed, the contribution of eye and head to the overall gaze shift produced depends on many factors, including the amplitude of gaze shift, and is markedly different across species. These behavioural observations led to the hypothesis of a distinct control system for head and eye movements in the brain; on the contrary, the results of SC micro-stimulation in head-free conditions suggest a tight coupling of head and eye movement control. Interestingly, a number of studies that looked at EMG data from neck muscles upon SC stimulation provide a possible way to reconcile both views. Indeed, low-frequency stimulation in the SC is insufficient to evoke a gaze shift, but leads to small increase in EMG signal in contralateral deep neck muscles[72]. When the head is unrestrained, similar sub-threshold stimulations can trigger head-only movements that precede the onset of a gaze shift[73,74]. These results support the hypothesis that SC output is processed along two distinct pathways in the brain stem: an oculomotor pathway that produces the eye movement component of the gaze shift and a cephalomotor pathway that exerts control over the neck muscles. A fundamental difference between the two is that the oculomotor pathway is under the potent inhibitory control of pontine omnipause neurons, which prevents saccade generation until the SC output reaches a threshold. A significantly weaker gating mechanism exists on the head pathway, which allows the execution of head-only movements preceding the full onset of gaze shift[74-77].

1.3.3 Tactile orienting

As described previously, many animals, especially nocturnal species, rely to a much smaller extent on vision to interact with their surroundings; instead, tactile orienting is often a preferred strategy. The SC has been shown to assume a central role in the orchestration of movement of tactile structures, in particular whiskers. Notably, electrical stimulation of the SC triggers movement of these structures; this effect is particularly evident in species that commonly employ these sensors to interpret their sensory space, such as rats, hamsters, bats and cats[37,58,78,79]. SC-dependent vibrissae movement has been extensively characterised in rats. While stimulation of the motor cortex can result in rhythmic contractions of whisker pads[80], induced SC activation produces sustained whisker protraction independent of cortical activity and with much shorter latencies and current thresholds[79]. Unlike what is observed

with saccades, whisk amplitude is not topographically mapped onto SC premotor neurons, but is rather modulated by stimulation parameters. Instead, different whisker pads are engaged when the stimulation site is changed, with protractions of the contralateral and ipsilateral whisker pads evoked from dorsal and ventral regions respectively[79].

1.3.4 Auditory and sonar localization

Further evidence of the universality of SC function in orienting comes from studies that have looked at its involvement in organising movement of auditory structures, as well as the production of vocalisations used for object detection.

Pinnae movements. Firstly, the SC has been implicated in the control of ear orientation with respect to surrounding sounds in a vast number of species. Early lesion studies in cats reported significant deficits in the orientation of the pinna to a sound source[81]. Complementary evidence is provided by electrical stimulation experiments in the same species, which reportedly produce contralateral or bilateral pinna movements[82,83]. A remarkable observation comes from micro-stimulation studies in bats, where it was reported that contralateral pinnae movements can be evoked with low stimulation currents (under 25 μA) and are produced with short latency from stimulation (20 ms)[37]; these parameters are comparable to what is reported for saccades upon SC micro-stimulation in primates. Furthermore, a pronounced organisation of pinnae displacement vectors has been observed in bats and cats[37,78], and more loosely in rodents and monkeys[58,84]. This comparative approach suggests that the SC has adapted through evolution to orchestrate with maximum efficiency the motor plans that are most relevant to the species.

Sonar vocalisations. Perhaps one of the most compelling pieces of evidence for the SC as a unique spatial hub is its involvement not only in the orienting of auditory structures, but also in the production of sonar vocalization used by echolocating bats to find and capture preys in their surroundings. Moss and colleagues developed an experimental system to record neural activity from freely moving bats chronically implanted with multi-channel electrodes in the motor SC while monitoring sonar vocalisations produced to track objects of interest in space. SC activity was found to be increased shortly before vocal onset[85], in agreement with earlier micro-stimulation studies that had reported sonar vocalisations, as well as topographically organized pinnae and head movements, upon SC activation in the same species[37]. In a more recent effort to elucidate how the SC of bats uses spatial information deriving from auditory feedback from sonar vocalisations, Moss and colleagues developed an echo model "to construct the instantaneous acoustic sensory space of the bat each time it vocalized and

received echoes from physical objects in its flight path"[51]. By expressing this information in 3D egocentric coordinates, the authors were able to isolate units in the SC that display a fixed tuning profile for particular object distances, which appeared to be sharper when auditory feedback was provided through SGGs rather than single vocalisations. In fact, the preferred distance encoded by cells in the SC was altered during SGGs production, favouring the representation of closer objects. Therefore, the activity of the SC sensorimotor population and its tuning to specific sensory features can be modulated by the context in which objects are presented in space, pointing to the involvement of this midbrain region in spatial attention.

1.3.5 Spatial attention in the SC

Traditional cognitive theories would propose the existence of two clearly distinct brain regions, dedicated to the selection and the initiation of actions respectively, whose serial activation leads to the performance of an appropriate motor task[86]. However, more recent experimental work and theoretical models have suggested that these processes might be carried out in parallel by overlapping brain regions as animals are continuously engaged in sensing and acting on their environment[87-90]. Consistently with this view, many studies have confirmed a higher cognitive role for the SC than previously recognised. A first line of research suggested a role for the SC in covert attention, that is the act of selectively attending to a spatial target by performing a goal-oriented action. Kustov and collegues observed that the expected end points of saccades generated by micro-stimulation of the SC could be deviated towards the position of spatial cues transiently introduced before the onset of stimulation, supporting the idea that the SC is involved in reflexive attentional shifts[91]. Furthermore, neuronal activity in the SC is directly modulated by peripheral cues: when these are presented before the target of a saccade, the latency of the performed eye movement is decreased and it is associated with a larger neuronal discharge. This effect is particularly apparent when the position of the cue matches that of the saccade target[92]. Delivery of relevant SC micro-stimulation was also shown to be an effective replacement to visual cues in guiding tasks of motion change detection tested using change-blindness[93,94], which refers to the inability to detect changes in the visual scene when these are preceded by the transient modification of the full visual field (such as a blank screen)[95]. Complementary to this body of evidence, chemical inactivation of SC circuits suggest that not only collicular activity is sufficient to evoke attention-like changes in performance, but also that it is necessary to explain the observed improvement in performance recorded in cued tasks. In one study, monkeys were asked to identify the direction of motion adopted by dots in a previously cued patch, while ignoring that occurring in an un-cued patch. When the visual

cue was placed in a region of the visual field affected by SC inactivation, performance was severely impaired and animals showed a tendency to choose the motion occurring in the distractor patch. When no competing stimulus was presented, SC inactivation had little impact on task performance, indicating that the deficit previously described was due to the inability to filter distracting sensory content rather than to the presence of a distractor in its own right[96].

The experimental evidence reported so far clearly highlights the importance of the SC in generating a diverse range of spatially accurate motor plans, as well as promoting attentional frameworks to support the appropriate action. While the nature of the inputs engaged to this end have changed through evolution, the SC has retained its role as a unique spatial hub, effectively providing a representation of peripersonal space based on the most ethologically relevant sensory modalities. From this stems its ability to orchestrate coordinated orienting movements to targets, again regardless of the motor groups recruited downstream. In this sense, the SC can be seen as a universal encoder of goals, rather than actions. Because of this versatility, it can be postulated that studying the anatomy and physiology of collicular networks might help elucidate more general, fundamental principles of sensorimotor integration.

1.4 Anatomical substrates for sensorimotor integration in the SC

Reconstructing the anatomical organisation and connectivity patterns of a brain region might not be the most exhaustive approach to understanding the types of computations performed by its neural networks, but it can certainly help refining our hypothesis regarding their capabilities. In the case of the SC, the unique anatomical features of the region provide an excellent starting point to illustrate some principles of sensorimotor integration implemented locally.

1.4.1 Lamination defines functional domains

One of the most striking anatomical features of the SC is its lamination, clearly highlighted by the variation in fibre density along the dorsoventral aspect of the SC, as well as by the variation in size and density of the cell bodies located in each layer (Fig. 1.4).

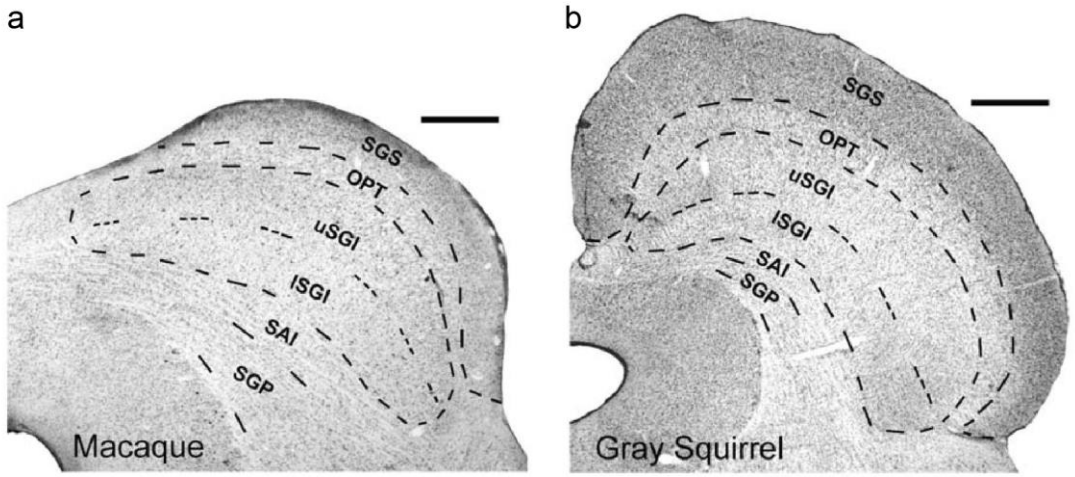

Figure 1.4 | Cytoarchitecture of the SC.
a, **b**, Coronal section through the SC of adult macaque (**a**) and gray squirrel (**b**), showing the conserved pattern of lamination across species; however, the SGS is notably thicker in the squirrel, while the SGI larger in the macaque (scale bars: 1 mm). Adapted from May, 2006[97].

Following a pattern conserved among vertebrate species, lamination defines a superficial and a deep domain within the SC, generally referred to as visual sensory and multimodal motor SC domains respectively. Each of these domains is further divided into sublayers as marked by the evident alternation between white and gray matter. The superficial SC is composed by: the outermost *stratum zonale* (SZ), a narrow and almost cell-free lamina, the intermediate *stratum griseum superficiale* (SGS), containing a high concentration of cell bodies of various shapes and sizes, and the ventral *stratum opticum* (SO), which instead shows an abundance of fibre terminations from retinal afferents. Similarly, the motor SC domain is further divided into (from dorsal to ventral): the *stratum griseum intermediale* (SGI), populated by numerous premotor units, the *stratum album intermediale* (SAI), containing a high density of fibres running from the dorsomedial to the ventrolateral aspects of the SC, the cell-rich *stratum griseum profundum* (SGP) and lastly the *stratum album profundum* (SAP), a thin layer of fibres adjacent to the periaqueductal gray (PAG)[97].

While the overall organisation of the SC into layers is conserved in mammals, variations can be appreciated in the anatomical composition of collicular domains across species. Strikingly, the visual SGS varies substantially in size (Fig. 1.4), suggesting that collicular structures have evolved to represent sensory information differently according to their ethological relevance. The organization of collicular circuits into an orderly laminar structure serves a key role in sensorimotor transformation; the functional relevance of this compartmentalization is better appreciated in light of the connectivity pattern of these sublaminae.

1.4.2 Inputs to the SC

Sensory inputs. An important player in the definition of collicular layers is the segregation and organization of incoming sensory inputs. Superficial layers are specifically targeted by a proportion of retinal ganglion cells (RGCs), the size of which varies significantly among species; in mice, 85%–90% of RGCs project to the SC[98], while only 10% of primate RGCs project to the area[99]. Most retinal terminals target the contralateral SGS in rodent species with little binocular overlap, while a complex pattern of ipsi- and contralateral retinal projections is observed in the SGS of higher mammals[100]. Additionally, visual information is delivered to the SGS via an indirect pathway involving visual and extrastriate cortical regions. Visual information from both direct and indirect pathways is retinotopically organised within the SGS, converging on different dendritic locations of individual cells[101,102]. This visual retinotopic map corresponds to the underlying motor map encoded by premotor neurons in the deeper layers[56,103], thus establishing an ideal anatomical platform for sensorimotor transformation.

From the prospective of network economy, it makes sense to exploit this existing visuo-motor axis and map onto it inputs from other sensory modalities. The existence of auditory maps in the SGI has been described in a number of mammalian species[104-106]; auditory inputs seem to converge with visual information locally, where the representation of auditory space is adapted to the existing visuo-motor map even when there is a mismatch between the direction of the eye and the ear[105,107,108]. The source of auditory input to the SGI is varied among species, although a few nuclei, namely the external nucleus of the inferior colliculus (IC), the nucleus of the brachium of the IC and the dorsal nucleus of the lateral lemniscus, contribute in most mammalian species. Similarly, somatosensory information is relayed to the intermediate layers of the SC and mapped to represent the physical world, as the eye perceives it. Two major sources of somatosensory inputs are the primary somatosensory cortex (S1) and the trigeminal nucleus of the medulla; their inputs are somatotopically organised to create a representation of the body in register with the visual map, in which central visual space is represented in the anterior SC while peripheral locations are mapped posteriorly[109-111]. While all these sensory modalities are represented in the SC across species, the abundance of fibres relaying information about particular senses is known to be different according to the relevance of that sensory modality for guiding behaviour. This suggests that throughout evolution, the SC has developed to store and bring into congruence the sensory information that is most relevant to produce appropriate sensory-guided behaviours. An example that illustrates this principle is provided by studies in snakes, a species that uses infrared radiation as a preferred source of spatial information. The optic tectum, homologous

to the mammalian SC, contains infrared-sensitive neurons that respond to the appearance of warm objects in their receptive fields[112], suggesting that rather than the quality of sensory flow into the SC, it is the logic in its use that is conserved in collicular regions.

The majority of single neurons in the SGI receive visual, auditory and somatosensory information; multisensory convergence in these cells results in integrated responses that are different to those elicited when a single sensory modality is presented. The key parameters employed to compute such integration appear to be related to both the physical properties of the stimuli and their spatial-temporal relationships. These principles of multisensory integration apply not only to the activity of individual SGI neurons, but also to the behavior of the animal during multisensory orientation tasks[78].

Motor-related inputs. In addition to sensory inputs, a number of non-sensory afferents converge in the SGI to control the execution of spatially tuned movements. The basal ganglia, a collection of subcortical nuclei widely implicated in process of action selection and execution, exert an inhibitory influence on a number of motor systems, including the SC. The substantia nigra pars reticulata (SNr) is largely responsible for the high-frequency, tonic inhibitory input to the premotor population of the ipsilateral SGI[113]. Transient suppression of activity in the SNr is deemed necessary for the production of SC-driven orienting behaviours, based on observations of reduction in firing rates in the SNr during oculomotor tasks in monkeys[114] and head movements in cats[115], as well as increase in saccade frequency upon pharmacological inhibition of SNr neurons[116]. A substantial additional source of inhibition is possibly provided by the subthalamic zona incerta (ZI), although the significance of its interaction with the SC remains elusive[117].

Neuromodulatory systems also contribute to the coordination of SC-mediated motor plans. In this context, the cholinergic afferent system has been studied in greatest detail due to abundance of acetylcholinesterase (AChE) signal in the SGI. Bilateral projections from the peduncolopontine nucleus (PPN) and the lateral dorsal tegmental nucleus are the main provider of cholinergic inputs to the region. PPN neurons display saccade-related activity in monkeys and it has been shown that their cholinergic release in the SC can lower firing threshold of SGI neurons and facilitate their direct activation by SGS activity[118].
How the complexity of sensory and motor information is ultimately interpreted and transformed in motor commands is still unknown. A number of anatomical studies have highlighted a striking modular organization of the motor layers of the colliculus. A series of AChE-dense patches, roughly 300 μm wide, were first described to tile the SGI along the mediolateral and anteroposterior axes[119,120]; other molecular markers, such as calbindin,

parvalbumin and nitric oxide synthase, were later identified as having a modular arrangement within the motor layer. Furthermore, many of the inputs to the SGI described so far, including SNr, terminate in patches[119,121-123], suggesting that understanding the network computations occurring within these modules could provide key information about collicular function.

1.4.3 Anatomical outputs of the SC

Control of orienting behaviour. In light of the evident involvement of the SC in the selection and execution of orienting behaviour, the most extensively characterised collicular output pathways are those originating in its motor domain, in particular those linked to the generation of orienting movements. These motor plans are organised by a set of nuclei in the brain stem, many spread across various segments of the reticular formation. The paramedian reticular nucleus of the pons and the midbrain reticular nucleus (MRN) are two prominent examples of such collicular targets[124]; together, they specialize in the control of the horizontal component of saccades. The control of the vertical component has instead been linked to burst activity in the rostral interstitial nucleus of the medial longitudinal fasciculus and the interstitial nucleus of Cajal, both targeted by collicular efferents[125].

As described in the previous section, electrophysiological and EMG studies of SC activity in head-free conditions suggested that the collicular pathways in control of eye and head movements during gaze shifts might be partially segregated. Indeed, the most relevant downstream targets for the generation of head turns appear to be the contralateral medullary reticular formation (MDRF) and the cervical spinal cord. The first contains premotor neurons that organise movements of the head[84] and is targeted by SGI and SGP cells terminating most abundantly in the gigantocellular reticular nucleus[126-129]. The tectospinal pathway is instead composed of a small number of neurons, often concentrated in the lateral SGI, that send sparse afferent fibres to the cervical segments of the spinal cord, where they appear to synapse onto local interneurons[130,131]. While their features vary substantially across species, it is generally thought that these direct tectospinal connections provide a more modest contribution to gaze control than the ones terminating in the MDRF.

Contribution to higher cognitive functions. The SGI is also the site of origin of prominent ascending pathways, which highlights the contribution of collicular networks to higher cognitive functions, such as attention and decision-making. The main targets of these projections are thalamic nuclei such as the pulvinar and the mediodorsal nucleus[132]. The former projects in turn to cortical areas involved in the control of spatial attention, notably

the lateral intraparietal area[133] which contains a salience map that can guide visual attention and saccadic eye movements[134]. The pulvinar has been implicated in attention processes in primates; its activity is modulated by manipulations of spatial attention and lesions of the region lead to neglect syndrome and attentional deficits[135], as well as defects in visuomotor coordination of grasping behaviour if these lesions are provided early in life[136]. These neglect-like deficits are comparable to those reported during SC inactivation[96], suggesting that this pathway might indeed be responsible for mediating SC-related control of visual attention. Areas of the prefrotal cortex, including the frontal eye fields (FEF), are indirectly targeted by the SC via its connection with the mediodorsal thalamic nucleus; this informs the cortex on motor signals about saccades, as well as visual information from the SC[137]. In turn, FEF can cause attention-like changes in the processing of visual signals in the extrastriate cortex[138]; as a consequence, one could imagine the input of the SC as a regulator of cortico-cortical feedback mechanisms for spatial attention.

1.4.4 Intracollicular circuits for sensorimotor processing

The experimental evidence summarized so far points to the existence of a highly organized intracollicular network to support the transformation of sensory information with high spatial content into a coherent motor plan. It is perhaps surprising to find that to date, relatively little is known about the intrinsic SC circuitry that performs this function. *In vitro* whole-cell clamp experiments have been most informative about the anatomical and physiological circuitry underlying intralaminar communication between sensory and motor domain, as well as horizontal interactions within distinct functional layers.

Interlaminar connectivity is a fundamental anatomical substrate for processes of sensorimotor integration; given the correspondence between visual maps in the superficial layers and motor maps in the SGI, it could be deduced that a pronounced vertical organization in this communication axis ought to exist. Indeed, anatomical studies have confirmed that the main local targets of SGS cells lie in the SGI area immediately beneath it[139,140]. Electophysiological studies have corroborated these observations, demonstrating that bursts of activity can be induced in SGI neurons upon extracellular electrical stimulation in the SGS[141]. Studies that employed glutamate uncaging to provide spatially accurate excitation in the SGS at different dorsal-ventral coordinates confirmed that the intra-collicular pathway from visual to premotor layer is robust, columnar and excitatory[141].

Connections within the intermediate layers have also been addressed to understand the circuit principles underlying the competition among different populations of premotor cells during the generation of orienting behaviour appropriate to the incoming sensory flow. Models of collicular function hypothesize two fundamental circuit principles: on one hand, long-range inhibition is necessary to suppress the activity of premotor cells that would trigger the production of unwanted orienting behaviours; secondly, short-range recurring excitation reinforces the execution signal for the correct motor plan. At present, we have only a partial picture of the structure and physiology of local circuits that would sustain these models. Anatomical and physiological studies of tecto-tectal connections have been interpreted in favour of the hypothesis of long-range inhibition[142-144]; however, many of these studies involved extracellular stimulation, which carries the intrinsic confounding effect presented by stimulation of fibres of passage arising from structures outside the SC, such as the SNr. In fact, *in vitro* electrophysiology experiments using glutamate uncaging suggest that inhibitory synaptic circuits within the SGI might be even more spatially restricted than the excitatory ones[141,145]; these observations are compatible with a role of local inhibiton in the "clipping" of the duration of premotor cell activity rather than its contribution to a long-range competitive mechanism.

In summary, decades of research regarding the anatomical organisation of collicular networks have identified some fundamental principles of circuit design that are likely key contributors to their capability of generating spatially accurate orienting actions. Firstly, their lamination provides an anatomical substrate for sensorimotor transformation, forming a vertical axis along which visual information shapes the activity of ventrally located premotor units. Secondly, the multimodal motor layers of the SC provide a platform for input convergence, where incoming information of sensory and motor nature is brought into congruence according to a spatial logic; interestingly a modular design is adopted in the organisation of these afferents, suggesting this anatomical feature might be instrumental for processes of sensorimotor transformation. The emergence of these collicular maps allows efferents to relay the product of such integration to downstream partners in the form of spatially accurate motor commands. While our current hypothesis on the contribution of collicular circuits to the gaze control network is enhanced by these anatomical observations, little is known about how different cell groups within the SGI are organised and work together to produce coherent motor plans.

1.5 Genetic approach to neural circuits

Part of the reason behind the current limitation in our understanding of collicular circuits stems from the fact that most studies have tried to define collicular populations based on their morphology, electrophysiological properties, location within the SC or even tuning to particular aspects of the sensory or motor space. As made evident in the previous sections, none of these strategies has proved sufficient to isolate functionally homogeneous classes of neurons in the SC; yet, dissecting the complex collicular circuit into its functional building blocks seems to be a fundamental step to take in an effort to define the precise principles of sensorimotor integration adopted in this network.

1.5.1 A universal definition of cell types

Understanding the organizational logic of neural circuits requires deciphering the biological basis of neuronal diversity and defining their identity on a level that operates across all previously employed classifiers. In a review published in the Philosophical Transactions of the Royal Society in 2010[146], Sydney Brenner writes:

> *"Since the essence of all biological systems is that they are encoded as molecular descriptions in their genes and since genes are molecules and exert their functions through other molecules, the molecular explanation must constitute the core of understanding biological systems".*

The genetic profile of a neuron is indeed the single most reliable indicator of the identity of the cell, being the intrinsic determinant of its morphological and physiological properties, as well as a key player in its localisation within a network during development. Recent experimental efforts involving single cell RNA sequencing (scRNAseq) from dissociated nervous tissue have indeed corroborated the validity of the genetic approach in defining neuronal cell types. In the retina, a structure containing some of the best characterised cell types in the central nervous system, scRNAseq has identified distinct markers that correlate to previously described types, as well as suggesting novel types[147]. Looking at cell transcriptome in brain regions where the definition of cell types is more controversial, such as the SC, might provide a novel starting point in the interrogation of circuit function and organisation, yielding unique insights in the contribution of distinct functional groups to the production of goal-directed motion.

1.5.2 Genetics of neural circuits

Of course the idea of applying genetic tools to the study of biological systems in general, and the nervous system in particular, is one whose potential was recognized decades ago. In the late 1960s, pioneering work by Seymour Benzer first introduced the idea of genetic analysis of behaviour by describing unique behavioural phenotypes associated with *Drosophila Melanogaster* mutants[148]. Soon after, Benzer and colleagues went on to stipulate that genes and genetic mosaicism could be employed to dissect the development and function of the nervous system, similarly to how "the scalpel cleaves a biological system along anatomical lines"[149]. In an effort to determine the complete structure of the nervous system, Sidney Brenner pioneered the study of genetics in *Caenorhabditis elegans*[150], which resulted in the production of the complete wiring diagram of the nervous tissue in this organism that shapes the experimental approaches of nematode physiologists all over the world[151]. For a couple of decades from its inception, the field of neural circuit genetics remained exclusive to invertebrate research; however, the advent of mouse transgenesis in the early 1980s[152-154] brought genetic engineering into mammalian species and paved the way to the development of experimental tools that changed the way scientists approach the field of systems neuroscience. Importantly, the development of CRE-recombinase-based conditional expression methods[155], combined with knowledge of the complete mouse genome[156], has granted access to genetically identified cell groups. More recent optimisation of reporter lines now allows sufficient expression of fluorescent markers and functional proteins for monitoring and manipulating neural networks *in vivo.*

1.5.3 Genetic tools in murine system

We are now increasingly able of monitoring and perturbing the activity of genetically defined neural groups, as well as anatomically reconstructing their associated networks.

Viral tools. A first step in characterising how a genetically defined neuronal population contributes to network function is to assess their connectivity pattern within such network. Historically, molecular tracers such as wheat-germ agglutinin and biotinylated dextran amines were employed as neuroanatomical markers. However, some traditional tracers lack exclusivity in their labelling of antero- or retrograde projections; furthermore, the targeting of cells for tracing is intrinsically dependent on their location only. A number of recombinant viral tools are now commonly employed to selectively trace antero- or retrograde projections of neurons based on their genetic identity. Adeno-associated viruses (AAVs) have been extensively employed as anterograde tracers in light of their expression

stability, non-toxicity and excellent intracellular filling. These viruses can be easily genetically engineered to drive expression of fluorescent synaptic, membrane or cytoplasmatic markers under recombinase control; injections of such vectors *in vivo* allows visualisation of projections patterns and synaptic contacts of specific genetic classes of neurons[157]. Rabies viruses are instead intrinsically capable of trans-synaptic spreading, travelling retrogradely along neural networks. Similarly to AAVs, they can also be used to deliver expression of fluorescent markers to the infected cells[158]. However, if their trans-synaptic spreading is to be exploited experimentally to map pre-synaptic partners to a neuronal population of interest in the nervous system, it needs to be confined to a single retrograde "jump". Genetic manipulation of Rabies viruses led to the production of a replication-deficient strain, lacking the glycoprotein G (ΔG) necessary to induce propagation[159]; furthermore, the virus is pseudo-typed with the avian envelope protein EnvA, with the purpose of restricting infection to neurons that express the cognate tumour viral receptor A (TVA). The starting population of interest can be targeted with AAV constructs that provide expression of the TVA receptor and G protein; upon TVA-mediated infection, pseudo-rabies are then capable of travelling mono-synaptically and inducing expression of any associated fluorescent marker in the mono-synaptically connected input neurons only.

Optogenetics. When Nagel and Hegermann first established that the photosensitive proteins found in the green alga *Chlamydomonas* are light-gated cation channels, and named them Channelrhodopsin 1 and 2 (ChR1/2)[160,161], it was immediately clear they had stumbled upon a novel class of photoreceptive molecules. Unlike mammalian photoreceptors in the retina, channelrhodopsins produce a depolarizing effect in the cell upon blue light-mediated activation; additionally, their channel configuration confers much faster kinetics than previously known G-protein-coupled rhodopsins. As expected from these biophysical properties, expression of ChR2 in human kidney and other mammalian cell lines was shown to drive large light-induced membrane depolarisations[161]. The intuition of the experimental potential that lies in the application of channelrhodopsins to neuroscience is what opened the field of optogenetics. In 2005, Boyden and colleagues published the first report of neuronal manipulation using ChR2 in rat hippocampal cultures, demonstrating reliable control of spiking, as well as control of both inhibitory and excitatory transmission[162]. Based on its excitatory nature and high temporal resolution, ChR2 has since been widely employed for the manipulation of neural circuits *in vivo*. Whether it is via AAV infection or through genetically encoded expression under recombinase control, ChR2 can be delivered to genetically defined neurons with minor effects on their passive membrane properties and without significant concerns of toxicity. Following the successful application of ChR2 *in vivo*, it was reported that neurons expressing the light-activated chloride channel

halorhodopsin from *Natronomonas pharaonis* (NpHR) are hyperpolarized when exposed to yellow light[163], paving the way to the development of optogenetic inhibition of neural circuits. Given the difference in their excitation wavelengths, channelrhodopsins and halorhodopsins can be co-expressed in the same group of neurons to allow bidirectional control of cell firing.

Neurophysiology. Manipulation of circuit activity is often instrumental in determining what behaviour a given population of neurons *can* trigger, but it does not provide evidence of how the activity of such population is integrated during behaviour. The physiological recruitment of neurons can be monitored *in vivo* by electrophysiological or imaging tools, both of which present advantages and limitations. Optical imaging, using calcium or voltage indicators, can be used *in vivo* to simultaneously track the activity of many labelled cells, whose identity is often determined via genetic targeting. However, the low temporal resolution of optical imaging, together with its limited sensitivity to sub-threshold activity, constitutes a disadvantage compared to electrophysiological techniques. These limitations become even more apparent when the region of interest is too deep in the tissue to be visualised via two-photon (2P) imaging techniques, and microendoscopy with GRIN lenses[164] is adopted instead. On the contrary, electrophysiological recordings can yield high sensitivity and temporal resolution at any coordinate of intra-cerebral implantation. However, even with high-density silicon probes, such as Neuropixels[165], which have the potential to record large number of neurons at once, the spatial relationship between isolated units is difficult to reconstruct. Additionally, the genetic identity of the recorded neurons is unknown; while excitatory neurons and inhibitory interneurons can be discerned in the hippocampus and cortex based on their spike waveforms, subtypes within these classes cannot be identified by conventional physiology. Coupling optogenetic activation with electrophysiological recordings provides a meaningful strategy to assign identity to the recorded units while preserving access to their temporally precise activity pattern. This approach has been successfully applied *in vivo* to assign spikes to ChR2-expressing cells based on their firing delay following blue-light stimulation[166].

In summary, recent advances in molecular genetics have exponentially increased our ability to perform high-throughput genetic modifications in mammalian systems, so that we are now able to reconstruct the anatomical features and functional relevance of neuronal populations identified based on their gene expression patterns. This effectively provides a new starting point in the interrogation of the circuit design underlying complex behaviours and network computations, such as the emergence and organisation of motor representation is the SC.

1.6 Aims of the study

Over the last decades, the SC has emerged as a crucial player in the gaze-control network. While several lines of research in different model organisms have confirmed that the SC contributes to the initiation of orienting movements, how functionally distinct neuronal groups within the SC are organized to support the production of such motor outputs is poorly understood.

One of the reasons why the intrinsic circuit organization of the SC remains elusive is the lack of genetic characterization of the neuronal populations of the motor SC. In this thesis, I aim to apply a genetic strategy to the study of collicular circuits, identifying molecular markers for local subpopulations of neurons; secondly, I aim to characterise the anatomical properties of such genetically identified populations; finally, based on these anatomical observations, I aim to develop an appropriate functional paradigm to study the contribution of genetic classes of neurons to behaviour, with the expectation to unveil novel principles of circuit design underpinning SC function.

The remainder of this thesis is organised in the following sections to outline the experimental strategies adopted to address these goals, the results obtained and their interpretation:

- In Chapter 2, I present an overview of the experimental methodologies and statistical analysis employed in this study.
- Chapter 3 focuses on the application of transcriptomic tools to the study of collicular neuronal populations; in particular, I describe the identification of a novel molecular marker, Pitx2, which labels a functionally homogeneous subpopulation of glutamatergic neurons in the motor layers of the SC.
- In Chapter 4, I present the results obtained from the anatomical reconstruction of the pre- and post-synaptic partners of the Pitx2^{ON} population using viral tools.
- Chapter 5 summarises the experimental controls used to validate the application of a novel double-inertial-sensor system for tracking head motion in 3D.
- Chapter 6 presents the results of the application of optogenetic stimulation to the study of the functional significance of Pitx2^{ON} neurons in the control of SC-mediated head movements.
- In Chapter 7, I describe the topographical organisation of Pitx2^{ON} neurons-mediated head movement vectors in the SC.
- Chapter 8 presents a discussion of the main findings of this project and their implications, as well as an overview of the future experiments that could be performed to develop this line of research further.

2. Methods

2.1 Animal strains

Male mice aged between 8 and 12 weeks from of the following lines were used: C57BL/6 wild type (WT), *vGAT-CRE* (Jackson: Slc32a1tm2(cre)Lowl), *vGluT2-CRE* (Jackson: Slc17a6tm2(cre)Lowl), *Pitx2-CRE* (obtained from James Martin Lab), *Rosa-LoxP-STOP-LoxP-tdTomato* (Jackson: Gt(ROSA)26Sortm14(CAG tdTomato), *Tau-LoxP-STOP-LoxP-mGFP- IRES-nLacZ* (Jackson: 129OlaE14CB6(TAU-LSL-MGFP-INLA#18), *Rosa-LoxP-STOP-LoxP-ChR2-eYFP* (Jackson: B6.Cg-Gt(ROSA)26Sortm32(CAG- COP4*H134R/ EYFP)Hze/J), *Tau-LoxP-STOP-LoxP-FLPo-IRES-nLacZ* (obtained from Silvia Arber Lab).

All transgenic mice were isogenic in a C57BL/6 background, maintained in pathogen and opportunistic agents-free conditions and monitored quarterly. All procedures were conducted in accordance with the UK Animals (Scientific procedures) Act 1986 and European Community Council Directive on Animal Care. Animals were housed in a 12 hours light/dark cycle with food and water ad libitum.

2.2 *In vitro* electrophysiology

2.2.1 Recordings

For electrophysiological recordings *in vitro*, C57BL/6 wild type (WT), *vGluT2-CRE::Rosa-LoxP-STOP-LoxP-tdTomato, vGAT-CRE::Rosa-LoxP-STOP-LoxP-tdTomato, Pitx2-CRE::Rosa-LoxP-STOP-LoxP-tdTomato* and *Pitx2-CRE::Rosa-LoxP-STOP-LoxP-tdTomato*::*Rosa-LoxP-STOP-LoxP-ChR2-eYFP* mice were used.

Coronal collicular slices (300 μm) from 2 months old mice were prepared using a vibrating microtome (7000smz-2, Campden Instruments LTD, Loughborough, UK). Animals were anesthetized with 2% isoflurane, decapitated, the brain was extracted and immediately transferred in ice-cold solution (aCSF, in mM: 125 NaCl, 2.5 KCl, 2 $CaCl_2$, 1 $MgCl_2$, 25 glucose, pH 7.4 with 95% O_2, and 5% CO_2). Slices were cut in a potassium D-gluconate solution (in mM: 130 potassium gluconate, 15 KCl, 0.2 EGTA, 20 HEPES, 25 glucose, 2 kynurenic acid, to pH 7.4 with NaOH and maintained with 95% O_2, and 5% CO_2) and then kept for 1 minute in a D-mannitol based solution (in mM: 225 D-mannitol, 2.5 KCl, 1.25 NaH_2PO_4, 26 $NaHCO_3$, 25 glucose, 0.8 $CaCl_2$, 8 $MgCl_2$, 2 kynurenic acid with 95% O_2, and 5% CO_2) at room temperature (RT). Finally, slices were incubated in aCSF at 30 °C for 20 minutes and then maintained at RT for the entire duration of the experiment. Slices were individually transferred to the recording chamber and perfused with recording solution (in mM: 120 NaCl, 2.5 KCl, 1 NaH_2PO_4, 26 $NaHCO_3$, 1 $MgCl_2$, 2 $CaCl_2$, 10 glucose, pH 7.4 with 95% O_2 and 5% CO_2) at a flow rate of approximately 2 mL/min. Whole-cell patch-clamp recordings were obtained from SC neurons using 8-10 MΩ pipettes pulled from borosilicate glass capillaries (1.5 mm OD x 0.86 mm ID; Harvard Apparatus, Holliston, MA). Pipettes were filled with artificial intracellular solution containing (in mM): 145 potassium gluconate, 5 $MgCl_2$, 0.5 EGTA, 2 Na_2ATP, 0.2 Na_2GTP, 10 HEPES, to pH 7.2 with KOH, osmolarity 280 - 290 mOsm.

Single-cell recordings were performed in current-clamp configuration using an Axon Multiclamp 700B amplifier (Molecular Devices, Union City, CA). Signals were low-pass filtered at 2 kH and acquired at 5 kHz using a digitizer (Axon Digidata 1550A, Molecular Devices, Union City, CA, USA) on a PC running pClamp. Full-field photo-stimulation of ChR2-expressing neurons was done as follows: for continuous light stimulations, we used 0.25, 0.5, 1 or 2 s light pulses; for light pulse stimulations, we used 5 ms light pulses at 10, 20, 30, 40 or 50 Hz. Light-evoked responses were elicited using a 450-490 nm LED (pE-300 coolLED system, Scientifica Ltd, Uckfield, UK) through a 40X water immersion

objective (LUMPlan FI/IR 40X, 0.8NA, Olympus, Tokyo, Japan). Access resistance was monitored throughout the recordings and was between 16.66 and 42.22 MΩ.. Neurons that had a >15% change in access resistance were discarded. Recordings were analysed with Clampfit 10.3.

2.2.2 Analysis

The neuronal classification was obtained through Orange©, an open source machine learning interface available in Python. For each recorded neuron the following electrophysiological properties were used to compute the hierarchical clustering (dendrogram) and the distance map: passive membrane properties; access resistance (MΩ), resting membrane potential (mV), input resistance (MΩ), tau (ms), capacitance (pF); action potential properties; threshold (mV), amplitude (mV), width (ms), after-hyperpolarization amplitude (mV) and after-hyperpolarisation width (ms); firing profile (from 50 to 450 pA injected); frequency (Hz), frequency of adaptation (%), frequency between the first and third action potential (Hz), delay of the first action potential (ms), delay of the last action potential (ms). Distances were calculated using a Spearman correlation of the ranked variables. The dendogram obtained was cut at a height ratio of 60%.

2.3 Genetic screen

2.3.1 RNA extraction and cDNA library preparation

Five P7 mice were decapitated in two different days/batches (three mice in batch 1 and two in batch 2), the brains extracted and sectioned at a vibratome in ice-cold extracellular solution (see *2.2 In vitro electrophysiology*). Sensory (SZ, SGS and SO) and motor (SGI, SAI, SGP and SAP) domains were manually dissected from the slices and the tissue processed for total RNA extraction using an RNeasy Mini kit (Qiagen, Venlo, Netherlands). Four samples were obtained from each mouse: sensory anterior SC, sensory posterior SC, motor anterior SC and motor posterior SC. cDNA libraries were generated from total RNA using a TruSeq® Stranded Total RNA Library Prep Kit (Illumina, San Diego, CA) and sequenced on an Illumina HiSeq 4000 machine (single read, 50bp read length).

2.3.2 RNAseq data processing and analysis

Reads were trimmed using Trim Galore (version 0.4.2) with default parameters to remove the standard Illumina adapter sequence. Reads were mapped to the GRCm38 assembly using STAR version STAR_2.5.3a_modified[167]. Raw read counts per transcript were calculated using HTSeq version 0.9.1 on GRCm38.p5 gene set using directional counts. Differential analysis of gene expression was performed using the default settings in DESeq2[168]. Briefly, given that replicates were produced in two different batches, the statistical model was designed to take into account batch effects in the data by including two factors in the design formula: region in the superior colliculus (superficial vs. deep) and batch (batch1 vs. batch2). Normalized read counts for each gene were statistically compared according to these factors using a Wald test. The p values from this analysis were adjusted (p_{adj}) for multiple testing using the Benjamini-Hochberg procedure. This algorithm is designed to control the expected false discovery rate below a specified level given a list of independent p values. In this analysis, differentially expressed genes were called at $p_{adj} < 0.05$, so that the proportion of false positives we expect amongst our differentially expressed genes is 5%. Replicate SP_I for the sensory posterior SC was classified as an outlier and excluded from the analysis. Gene ontology enrichment analysis was carried using the custom-made analysis tool PEAT (available at: https://github.com/lmb-seq/PEAT).

2.4 Immunohistochemistry

For immuhistochemistry experiments, mice were anaesthetized with Euthatal (0.2 ml) and perfused with 20ml of ice cold phosphate buffered saline (PBS) followed by 20 ml of 4% paraformaldehyde (PFA) in PBS. Brains were incubated in PFA overnight at 4°C and then dehydrated for 48 hours in 30% sucrose in PBS at 4°C. The brains were frozen in O.C.T. compound (VWR, Radnor, PA) and sliced into 40 µm sections using a CM1950 cryostat (Leica, Wetzlar, Germany).

Free-floating sections were rinsed in PBS and incubated in blocking solution (1% bovine serum albumin and 0.3% Triton X-100 in PBS) containing primary antibodies for 24 hours at 4°C. Sections were washed with PBS four times at room temperature and incubated for 24 hours at 4°C in blocking solution with secondary antibodies. Immuno-labelled sections were washed four times with PBS at RT and mounted on glass slides (SuperFrost Plus, Thermo Scientific, Waltham, MA) using DAPI Fluoromount-G® (SouthernBiotech, Birmingham,

AL). Primary antibodies used in this study were: chicken anti-GFP (Aves Labs, GFP-1020, 1:2000), rabbit anti-RFP (Rockland, 600-401-379, 1:2000), mouse anti-NeuN (Millipore, MAB377, 1:1000) and chicken anti-β-Galactosidase (Abcam, ab9361, 1:2000). Secondary antibodies used were Alexa Fluor 488 donkey anti-chicken (Jackson ImmunoResearch, 703-545-155, 1:1000), Cy3 donkey anti-rabbit (Jackson ImmunoResearch, 711-165-152, 1:1000) and Cy5 donkey anti-mouse (Jackson ImmunoResearch, 715-175-150, 1:1000). Images were acquired using a Zeiss780 confocal miscroscope using a 20X/0.8NA air lens (Carl Zeiss AG, Jena, Germany). For quantification of the relative abundance of $Pitx2^{ON}$ neurons as a fraction of total neuronal population (marked by expression of NeuN) in the SGI, we sampled 9 coronal sections across different AP coordinates and counted the proportion of $Pitx2^{ON}$/NeuN only cells in the medial (x: 0-0.5), medial/lateral (x: 0.5-1.0) and lateral (x: 1.0-1.4) SGI. For the assessment of the distribution on $Pitx2^{ON}$ cells along the anteroposterior axis, we included cells located along the whole mediolateral extent of the SC in anterior (y: 3.3-3.64), central (y: 3.64-3.9) and posterior (y: 3.9-4.3) sections. For quantification of $Pitx2^{ON}$ neurons distribution across the brain, we counted $Pitx2^{ON}$ neurons in all thin sections obtained from three *Pitx2-CRE::Rosa-LSL-tdTomato* mice.

2.5 *In situ* hybridization

Pitx2-CRE::Rosa-LSL-tdTomato and WT mice were used in these experiments; brains were extracted, fresh frozen in O.C.T. and sliced into 15 μm sections at the cryostat. Brain sections were mounted on glass slides immediately after cryosectioning using an anti-roll blade and stored at -80°C for up to two weeks. On the day of the assay, sections were post-fixed for 30 minutes with ice-cold 4% PFA in PBS and then rinsed twice in PBS. Tissue pre-treatment and probe hybridisation were carried out using RNAscope® reagents and experimental protocols (Bio-Techne, Minneapolis, MN). Briefly, Protease IV was applied on the slides for 20 minutes at RT and the probes were warmed for 10 minutes at 40°C to ensure that the reagents were homogenised. Slides were rinsed twice in PBS and the target probes added to the slices and allowed to hybridise for 2 hours. The slides were rinsed twice in wash buffer and then underwent a series of hybridisation steps through which fluorescent signals were assigned to a specific probe channel (Amp 1-FL for 30 minutes, Amp 2-FL for 15 minutes, Amp 3-FL for 30 minutes, Amp 4-FL-Alt C for 15 minutes). All hybridization steps were performed in the HybEZ® oven at 40^0 C and were separated by washes in wash buffer. Slices were counterstained with DAPI for 30 s at RT and coverslipped with ProLong™ Gold Antifade mountant (Thermo Fisher Scientific, Waltham, MA). On the following day, sections were imaged using a Zeiss780 confocal microscope using a

63X/1.4NA oil lens (Carl Zeiss AG, Jena, Germany). The probes used in this study were: anti-vGluT2 (Mm-Slc17a6-C2, 319171-C2), anti-vGAT (Mm-Slc32a1, 319191), anti-tdTomato (tdTomato-C3, 317041-C3) and anti-Pitx2 (Mm-Pitx2-C2, 412841-C2). For quantification of the co-localisation of *Pitx2*-driven tdTomato with glutamatergic and GABAergic markers, we sampled 11 coronal sections across different AP coordinates. For the time course of *Pitx2* expression, we sampled three coronal sections for each time point considered.

2.6 Whole-brain clarification and imaging

2.6.1 Tissue preparation and image acquisition

Pitx2-CRE::Rosa-LSL-tdTomato mice were perfused and the brains fixed overnight as described in *Immunohistochemistry*. Brain clarification was carried out following the CUBIC protocol[169]. Briefly, the brains were immersed in 0.5x reagent-1A (10wt% Triton, 5wt% Quadrol, 10wt% Urea, 25mM NaCl in dH_2O, diluted in dH_2O) for 6 hours at RT and then 1x reagent-1A for two days at RT with shaking. Fresh reagent-1A was then replaced and the samples placed at 37°C with shaking; reagent-1A was replaced every other day for a total of 10 days of incubation. The brains were then washed in PBS at RT and incubated with 0.5x reagent-2 (25 wt% urea, 50 wt% sucrose, 10 wt% triethanolamine in dH_2O, diluted in PBS) for 24 hours at RT, followed by an incubation in 1x reagent-2 for 2 days at RT. Brains were allowed to equilibrate in a 50:50 silicon oil/mineral oil mix, then imaged in the same medium using an UltraMicroscope II light sheet microscope (LaVision Biotech, Bielefeld, Germany).

2.6.2 Analysis

Quantification of *Pitx2*-defined SGI periodicity was analysed by cropping a spherical cap in the 3D brain image using the G'MIC (gmic.eu) image-processing suite. Line where automatically detected using a custom-made code in Matlab (MathWorks, Natick, MA) as clusters of peaks in the Hough transform of the image segmented by thresholding the response of a difference of Gaussian filter.

2.7 Surgical procedures

All procedures using live animals were approved by the Home Office and the LMB Biosafety committee. Mice were anaesthetized with isoflurane delivered at a flow of 3% in 2 L/min of oxygen for the initial induction and then maintained at 1-2% in 2 L/min of oxygen. The anaesthetized animal was placed into a stereotaxic apparatus (David Kopf Instruments, Tujunga, CA) and Rimadyl (2 mg/kg body weight) was administered subcutaneously as anti-inflammatory. Both eyes were covered with Lubrithal eye gel (Dechra Pharmaceuticals, Northwich, UK) to prevent corneal desiccation during the surgery and the body temperature was maintained at 37°C through a CMA 450 Temperature Controller (Linton Instrumentation, Norfolk, UK) for whole duration of the surgical procedure. After skin removal, two sterile screws were inserted in the in the frontal part of the skull to give more stability to the implant. A craniotomy (1 mm diameter) was drilled to expose the area of interest and, after removal of the dura, we performed one of the following procedures: viral injection, optic fibre implantation, optetrode implantation or multi-fibre array implantation. For head restriction experiments, a head-plate was glued to the skull before drilling the craniotomy. For multi-fibre array implantation, a larger craniotomy (2 mm diameter) was drilled. The remaining exposed brain was then covered with sterile vaseline and the implant was sealed with RelyX^{TM} Unicem2 Self Adhesive Resin Cement (3M, Bracknell, UK). All mice were monitored after surgery and given at least one week to recover before recording.

2.8 Anatomical tracing

2.8.1 Viral injections

Viruses were injected using a 5 µl Hamilton syringe (Scientific Laboratory Supplies, Nottingham, UK) equipped with a 33G needle. The syringe was left in the brain for 5 min before being retracted. Up to a maximum of 500 nl of virus were injected in the SC (coordinates: x = -0.80, y = -3.80, z = 1.70). For anterograde tracing, the following viruses were co-injected: AAV(1)-CMV-FRT-TVAmCherry-2A-Gly (titer: $3.9x10^{12}$ genomic copies/ml) and AAV(9)-CMV-FRT-synGFP-WPRE (titer: $3.0x10^{12}$ genomic copies/ml). For retrograde tracing, AAV(1)-CMV-FRT-TVAmCherry-2A-Gly (titer: $3.9x10^{12}$ genomic copies/ml) was injected at day 0, followed by injection of virus EnvA-ΔG-Rabies^{GFP} (titer: $4.3x10^{8}$ infectious units/ml) at day 21 through the same craniotomy.

2.8.2 Analysis

Mice were perfused three weeks after viral injections of AAV constructs for anterograde tracing or one week after injection of Rabies virus for retrograde tracing. Brain tissue was processed as described in *Immunohistochemistry*. Images of mounted sections were automatically detected and acquired using a robot-assisted Nikon High Content Analysis microscope equipped with a 10X air objective (0.45NA) operated by NIS-Elements HC software (Nikon, Tokyo, Japan). The assignment of both input and output signals to specific brain areas was carried out manually aligning the acquired images to the Allen Mouse Brain Atlas. For quantification of synaptic density in anterograde tracing experiments, the average pixel intensity in a target region containing SynGFP punctae was calculated in ImageJ and the background was subtracted using an adjacent unlabelled region as reference.

2.9 3D tracking of head-over-body position

2.9.1 Sensor board setup and validation

We used sensor boards as described in Wilson et al., 2018 to track the position of freely moving animals in an open field Perspex arena (50x50 cm). In order to obtain the orientation of the mouse head relative to the body, we secured two inertial sensors on the head and the body of the animal using Mill-Max connectors and an elastic band respectively. The orientation of the head relative to the body was calculated as the difference between the head sensor and the body sensor outputs. All sensor data were acquired at 50 Hz. Prior to any recording session, we verified sensor alignment and recalibrated the boards if necessary as previously described[170].

The validity of the inertial sensor system for outputting reliable positional information was tested statically and while undergoing rotations at a range of velocities. To test for drift in the static regime, each sensor was fixed to a base plate in the recording arena and recorded for 10 minutes. Drift in the system was tested by determining the shift in the sensor output between each measurement (jitter) and the cumulative change in heading over the course of the 10 minutes recording (cumulative drift). To test their ability to track motion occurring at different velocities, the sensors were fixed to step-motor-controlled rotation table and their recordings compared to the expected motion pattern applied. The table was set to rotate at four speeds (28º/s, 40º/s, 56º/s and 80º/s), applied to both clockwise and counter-clockwise

directions. Recordings were carried out ten times for each direction and velocity. The expected angular displacement between each 50 Hz measurement (28º/s = 0.56º, 40º/s = 0.8, 56º/s = 1.12º and 80º/s = 1.6º) was then compared with the computed displacements between each temporal bin from the sensor output. The measurement of error was then transformed to give a measurement error per degree for each temporal bin.

2.9.2 Characterization of 3D head movements

Head motion events for each Eulerian component were defined as events in which the angular head velocity remained in a constant direction for at least five temporal bins (a total of 100 ms) at a speed of over 0.5° per bin (25°/s). This definition was further refined by searching backwards from the onset of the initially defined motion to the last temporal bin at which direction was the same as the defined motion; this was now defined as the onset of motion. A similar process was also carried out to define the offset of motion; the last temporal bin from the initially defined offset of motion to have the same direction as the defined motion was considered as the final offset of motion. From these values we retrieved the total extent of motion (the summation of the angular head velocity for a motion event) and the duration of motion for each motion event. This process was carried out separately for each Eulerian component.

Frequency histograms were created for the head displacements for each animal, taken from the light trial recordings. The computed head displacements were grouped into 36 10° bins and normalised based on the maximum sampling frequency for the creation of the frequency histograms. Gaussian curves were fit to the resulting distributions and the peak, mean and sigma of the fit were retrieved from fitted model.

2.10 Optogenetic stimulation in freely moving animals

2.10.1 Experimental design

For optogenetic manipulation experiments, *Pitx2-Cre::Rosa-LSL-ChR2-eYFP* mice were implanted with single optic fibres or custom-made optic fiber arrays (core = 100 μm, NA = 0.22; Doric Lenses, Québec, Canada) in the SGI. The design of the fibre array is presented in Figure 2.1. Implant coordinates for single fibres are presented in Appendix D; fibre arrays were implanted at x: 0.8, y: 3.3 and z: 1.8 from brain surface, measured from the central fibre in the array. WT mice were implanted as controls.

Light for optical stimulation was delivered by a 473 nm laser diode module coupled to a 100 µm multimode fibre (NA = 0.22) through a Schäfter + Kirchhoff fibre coupler (Cobolt, Solna, Sweden). For single-site stimulation experiments, light was delivered to the implanted optic fibre through a mono fiber-optic patchcord (core = 100 µm, NA = 0.22). For multi-fibre array stimulation, we used a custom-made optical fibre branching patchcord (core = 50 µm, NA = 0.22). All fibreoptic patchcords were from Doric Lenses, Québec, Canada. The laser power employed in all stimulation experiments was 3-5 mW at the tip of the fibre. We calculated the laser power delivered into the brain as a function of the distance from the fibre tip based on parameters of light diffraction in gray matter (Fig. 2.2a, b) and calculated the size of the relative illuminated area (Fig. 2.2c). Given that ChR2 is reported to require a power density in the range of 1-5 mW/mm^2 for activation[171] (at least 20% of our initial intensity), we estimated that sufficient illumination would be provided within a radius of ≈70 µm (highlighted in red in Fig. 2.2).

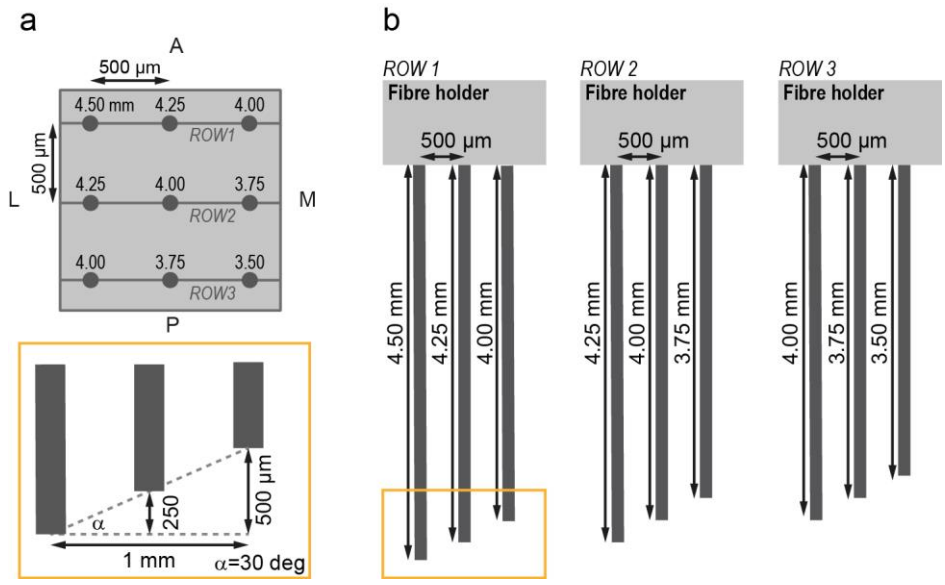

Figure 2.1 | Design of custom-made 3x3 optic fibre array.
a, **b**, Specifications of custom-made 3x3 optic fibre array and implant orientation with respect to mouse head; fibres are spaced at a distance of 500 µm along both the mediolateral and anteroposterior axes (**a**) and fibre length (reported in figure) is designed to accommodate for the spherical surface of the motor SC (**b**).

All optogenetic stimulation experiments were carried out in an open field arena; mice were acclimatised to the set up for 10 minutes before starting the recording sessions. Each recording session consisted of an initial 10 s during which no light stimulation was provided, followed by 10 repetitions of a 250 ms continuous light pulse every 10s. In the frequency modulation assay, the stimulus consisted of a train of 10 ms pulses presented at 10, 20, 30,

40 or 50 Hz lasting for 250 ms. In the duration modulation assay, the stimulus consisted of a continuous light pulse of 250, 500, 1000 or 2000 ms. For both assays, each recording session contained only one stimulation type presented 10 times. Each animal underwent at least 3 recording sessions per stimulation type.

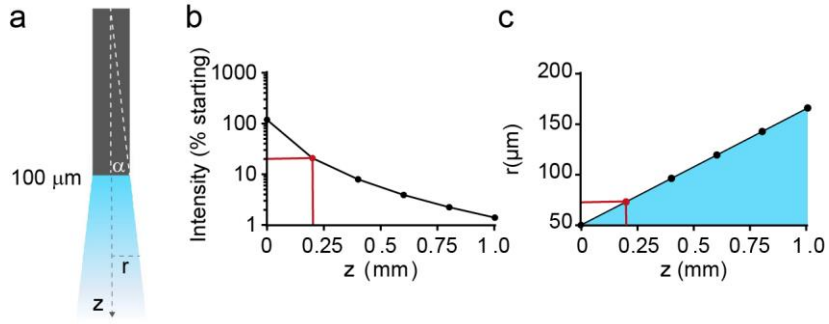

Figure 2.2 | Calculations on size of effective laser illumination for *in vivo* applications. **a**, Schematic of light diffusion from optic fibre used for optogenetic stimulation *in vivo*. **b**, **c**, Calculations of variation in light intensity (**b**) and radius (r) of light cone (**c**) as a function of the distance from fibre tip (z).

2.10.2 Analysis

Successful events were defined as episodes in which a motion event (see *2.9.2 Characterization of 3D head movements*) was detected within 2 s of light onset. Success rate for a given stimulation type was calculated as average success rate among sessions in which the same stimulation parameters were applied. The extent of the light-triggered motion was calculated as difference between the maximum head-over-body displacement observed within 2 s of light onset and the baseline head-over-body position (calculated as average position in the 1 s preceding light onset). Mean light-triggered head displacement was determined averaging successful events only.

Individual trials of optogenetic stimulation were baseline-subtracted and analysed for step-wise movements as follows. The velocity of head displacements was calculated as the derivative of the head position. We defined as movement onset the time when the head velocity exceeded 25°/s. This threshold was chosen in accordance with our definition of movement (see *2.9.2 Characterization of 3D head movements*). The termination of a movement was defined as the instant when the head velocity either inverted direction or reached a minimum between consecutive steps, or when the head position reached the maximum displacement attained during the trial. The amplitude of each motion step was defined as the difference between the head position at movement termination and the position at movement onset. For every light stimulation used, we

calculated the number of steps per trial, the fraction of trial presenting a given number of steps for progressively longer stimulation and the average step amplitude, duration and velocity.

2.10.3 Histologies

For histological confirmation of implant position, mice were perfused and their brain tissue processed and sectioned as described in *Immunohistochemistry*. Images of implant locations were referenced against the Allen Mouse Brain Atlas to estimate implant coordinates.

2.11 Optogenetic stimulation in head-restrained animals

2.11.1 Experimental design

For eye tracking experiments, *Pitx2-Cre::Rosa-LSL-ChR2-YFP* mice were implanted with two optic fibres (core = 100 μm, NA = 0.22; Doric Lenses, Québec, Canada), one in each hemisphere in the SGI, and a head plate. WT mice were implanted as controls. Light stimulation was provided by a solid-state 473 nm laser (Ikecool Coorporation, Los Angeles, CA). Awake mice were head-fixed and allowed to run on a wheel in dark conditions while their eyes were recorded using a DMK 23UM021 camera (Imaging Source, Bremen, Germany) equipped with MVL7000 lens with infrared illumination provided by a 850 nm Infrared LED array light source (Thorlabs, Newton, NJ). The camera was pointed at the centre of the eye, as gauged from the resting position of the pupil. Each recording session lasted 5 minutes; light pulses lasting 250 or 500 ms were repeatedly delivered every 10 s for the entire duration of the session for a total of 30 repetitions of light stimulation per session. Each animal underwent at least 2 recording sessions per stimulation type.

2.11.2 Analysis

Eye tracking movies were processed offline using a custom-made software in MATLAB (Mathworks, Natick, MA). Briefly, each frame was low-pass filtered to reduce noise and the pupil outline was detected by a level-crossing edge detector; the position and the area of the pupil were calculated from the ellipse fit to the pupil outline. The output of the algorithm was visually inspected and adjustments to the parameters (e.g., spatial filter strength, or

level-crossing threshold) were made where needed. The angular amplitude of eye movements relative to the resting position was estimated as:

$$\alpha = \arcsin\left(\frac{d}{r}\right)$$

where *d* is the distance travelled by the pupil centre and *r* is the radius of the eye, approximated to a sphere. Eye light-triggered average (LTA), movement amplitude and step-wise movement analysis were carried out as for head movements (see *2.12.3 Spike- and light-triggered average*).

2.12 *In vivo* electrophysiology

2.12.1 Optetrode recordings

Pitx2-CRE::Rosa-LSL-ChR2-eYFP mice were implanted with moveable 17 µm-diameter platinum-iridium (H-ML insulated) microelectrodes (California Fine Wire, US), configured as four tetrodes carried by 16-channel microdrives (Axona Ltd., St. Albans, UK). Tetrodes were platinum electroplated to an impedance of 100-250 kOhm using a Kohlraush/Gelatin (9:1, 0.5% gelatin) solution. In order to opto-tag Pitx2::ChR2 neurons, tetrodes were combined with an optic fibre (core = 100 µm, NA = 0.22; Doric Lenses, Québec, Canada). The resulting optetrodes were implanted just ventrally to the intermediate layers of the superior colliculus at co-ordinates 3.8-4.2 mm posterior from Bregma, 1.25 mm lateral of the midline and 1.3-1.5 mm ventral to the brain surface. Single-units were recorded as mice foraged a square Perspex arena (50x50 cm) for droplets of 30% diluted soya milk. Recording sessions consisted of eight five-minute foraging trials, four of which performed during blue light stimulation. The first and last trials occurred in light conditions and the second and third in darkness. The recording arena was situated within a Faraday cage containing stable polarising cues. Light trials were recorded with one door of the Faraday cage open, while the arena was completely enclosed during dark trials. During dark trials all other sources of light within the experimental room such as computer screens were switched off or covered.

Recordings were carried out using a multi-channel DacqUSB recording system (Axona Ltd., St Albans, UK). In order to record units, animals were connected to a pre-amplifier via a lightweight cable attached to the microdrive by a head-stage that modified the signal with AC-coupled, unity gain operational amplifiers. The signal was amplified ~12-20000 times

and bandpass filtered between 500 Hz and 7 kHz. Recording thresholds were set to ~70% above baseline activity levels, and data from spikes above the threshold from all channels were collected across a period spanning 200 µs preceding and 800 µs following the peak amplitude of a spike. The activity of channels from any given tetrode was referenced against the activity of a single channel from another tetrode, so as to increase the signal to noise ratio. Tetrodes were advanced ventrally into the brain by 50 µm after each recording session. The optic fibre was coupled with a blue diode pumped solid-state 473nm laser (Ikecool Coorporation, Los Angeles, CA) pulsed at 30 Hz with 5 ms pulse width and a 3-5 mW at the tip of the fibre at the tip of the fibre. Blue light-activated units were defined on the basis of the latency of the response to a pulse of light within a time window of 5 ms[166].

The inertial sensor was attached to the head-stage on the head of the mice using Mill-Max connectors. The signal from the sensor was passed through a lightweight cable via one Arduino for processing the signal and computing the DCM algorithm and a second for controlling synchronisation with the DacqUSB single unit recording system. The control Arduino was connected to the DacqUSB system using the system's Digital I/O port. A custom built BASIC script was written in DacqUSB to synchronise the start of single-unit recording and the start of the blue laser with the key-press initiation of inertial sensor recording (controlled using the Processing software sketchbook; processing.org).

2.12.2 Determination of motion tuning

The motion tuning of neurons was determined by calculating the spike-triggered average (STA) of head displacements. In order to do this, we first defined spike events, aligned corresponding head displacements to these events and compared the computed average displacement vectors with those drawn from a random distribution. Cells were only considered to be tuned to a given component if the motion vector of the cell for that component was above threshold and in the same direction in both light trials.

2.12.3 Spike- and light-triggered average

For STA of motion, the angular head velocity for the 50 (1 s) temporal bins preceding and 100 bins (2 s) following the onset of spike were computed for each Eulerian component. The direction of the head at the onset of each spike onset was normalised to zero for each Eulerian component. The calculated angular head velocities were cumulatively summated for each temporal bin to produce a head displacement for the 1 s preceding and 2 s following

the onset of spike. This was repeated for each spike. The mean and SEM of spike related head displacements were then calculated for each temporal bin to illustrate the tuning of neurons. Displacement vectors were calculated as the difference between the minimum and maximum of the computed displacement for each spike event, and the mean displacement vector for each Eulerian component was computed from each neuron's computed displacement vectors for the given component. The direction of the displacement vector was defined according to the temporal order of the minimum and maximum values of the computed displacement (i.e. if the minimum preceded the maximum value, the displacement was deemed to be positive). For LTA, the time of light onset was used in place of the spike onset.

2.12.4 Generation of shuffled data sets

For each cell, the spike-onset times were temporally shifted by 20-150 s (selected from a random distribution) in a wrap-around manner. This works to shift the relationship between the bursting times and the recorded heading directions of the animals while maintaining the temporal relationship between bursting events. Once these data were shifted, spike triggered analyses were carried out to determine the mean displacement vector of the temporally shifted data. This process was repeated 1000 times so as to produce a random distribution of mean displacement vectors.

2.13 Statistical methods

Data were tested for normality before statistical analysis. To assess the difference in distribution of Pitx2^{ON} cells in the SC, one-way ANOVAs were used to identify statistically significant difference in the number of Pitx2^{ON} cells among the mediolateral and anteroposterior portions of the SC, followed by Tukey's test for multiple comparisons with Bonferroni correction. For the measurement of sensor boards' error during motion, errors per temporal bin were compared using a two-way 4x2 factorial ANOVA. For the assessment of movement range in freely moving animals in our experimental setup, repeated measures ANOVA was used to compare standard deviations of the fit curves. For the analysis of the influence of stimulation duration and frequency on the amplitude and success rate of the movement produced, we used one-way ANOVA followed by Tukey's test for multiple comparisons with Bonferroni correction. For the analysis of step-wise kinematics, one-way ANOVA was used to compare amplitude, duration and velocity of individual steps within

full motion bouts. To assess the effect of stimulus duration on the head and eye movements, paired t-tests were used to compare amplitude of head and eye displacements following 250 and 500 ms light pulses. For optogenetic stimulation experiments with multi-fibre arrays, one-way ANOVA and Tukey's multiple comparison tests were used to assess the difference between the amplitude of displacement generated at various SC locations. In all STA and LTA analysis relative to *in vivo* recordings of Pitx2^{ON} units, a t-test was applied between the displacement vector and the mean displacement vector of the shuffled data with a threshold of 0.05. Neurons were considered to be motion tuned if the t-test determined a significant difference between the displacement vectors of the real and shuffled data. All results are presented as mean $\pm$ SEM. Results were considered statistically significant at $*p \leq 0.05$, $**p \leq 0.01$, $***p \leq 0.001$. Relevant *p*-values are reported in the figure legends. Data analysis in this paper was performed using MATLAB (R2014b), Python 2.7, GraphPad Prism7 and R.

3. Genetic dissection of pre-motor collicular circuits

Our current understanding of the network principles underlying collicular function is limited by our lack of knowledge regarding the contribution of distinct functional classes of neurons in sculpting collicular output. In order to overcome such limitations, we would need to be able to study each neuronal subpopulation in isolation, reconstructing its anatomical features, connectivity patterns and physiological recruitment, as well as selectively manipulating its activity to formulate hypothesis on their role in circuit function.

Genetic dissection of neural circuits confers the ability to target distinct classes of neurons within a region for their selective anatomical and functional examination. The mammalian S1 provides an exemplary case for the use of genetics in the study of neural networks. Cortical neurons divide into two main classes: excitatory glutamatergic principal cells encode specific features of the perceived sensory stimuli, sending extensive axonal projections to distribute signals within and among various stations; GABAergic interneurons form local connections among themselves and with principal cells, giving rise to a complex microcircuit organisation[172]. Without further refinement, the classification of cortical neurons into these two broad groups would give little insight into the computations that underlie the cortex's ability to process features regarding the incoming sensory flow. Over the last 20 years, the classification of interneuron types in subclasses based on their genetic identity has brought to the elucidation of the organizing principles of cortical networks. Parvalbumin-expressing interneurons receive strong excitatory inputs from the thalamus and cortex[173], and are capable of firing rapid trains of action potentials targeting the soma or initial axon segment of principal cells; as a consequence, they act to stabilize the activity of cortical networks and their absence leads to epileptic cortical states[174]. On the other hand,

somatostatin-expressing interneurons (SOMs) target the tuft dendrites of principal cells, partaking in processes of lateral inhibition and behaviour-dependent control of dendritic excitability[175]. Cells that express vasoactive intestinal peptide target SOMs, forming a disinhibitory circuit through which the primary motor cortex (M1) is capable of influencing sensory processing in S1[176]. The classification of cortical interneurons, as well as glutamatergic principal neurons, into additional subclasses is currently an active area of research, likely to further advance our understanding of cortical circuit design and operation.

Similarly, one can postulate that studying collicular neurons based on their genetic identity could provide a solid mean of interpretation of the vast functional heterogeneity in this midbrain region, leading ultimately to the elucidation of the organizing principles of motor representations.

3.1 *In vitro* electrophysiology highlights functional diversity within glutamatergic and GABAergic populations

The first step towards a genetic dissection of collicular motor circuits is the assessment of the degree of functional heterogeneity that exists among SGI neurons. In order to do this, we adopted a high-throughput, *in vitro* approach and performed whole-cell clamp recordings of SGI neurons in acute slices from WT mice, with the intention of classifying neurons based on their electrophysiological profile. Historically, neurons have been classified into electrophysiological groups based on the firing pattern they exhibit upon injection of steps of current, so that we refer to neurons as, for example, regular spiking, fast spiking or bursting. These response types are useful markers for the definition of broad functional categories; however, if the full spectrum of active (linked to ion-channel combinations) and passive properties (related to cellular morphology) of the neurons is taken into account, it is apparent that these classes often bring together physiologically heterogeneous neurons[177].

In order to provide an unbiased and comprehensive classification of SGI neurons into electrophysiological classes, we measured a number of electrophysiological parameters in SGI cells, including both passive and active membrane properties of the neurons, which are summarized in Appendix A. We then fed the extracted features into a hierarchical clustering algorithm in order to obtain an unbiased and quantitative picture of the intrinsic functional diversity of SGI neurons (see *2.2 In vitro electrophysiology*). First, electrophysiological parameters were normalized and all pairwise distances between cells calculated for each given feature using Spearman correlation. The average pairwise distance was then used to

draw a dendogram, describing the hierarchical relationship between SGI neurons based on the full spectrum of their electrophysiological parameters. This analysis revealed the existence of five broad functional classes of SGI neurons (Clusters I – V, Fig. 3.1a). Each one of these clusters was preferentially, although not exclusively, populated by neurons with a distinct firing profile (regular, Cluster I; fast spiking, Cluster II; late onset, Cluster III; stuttering, Cluster IV; inactivating, Cluster V; Fig. 3.1b).

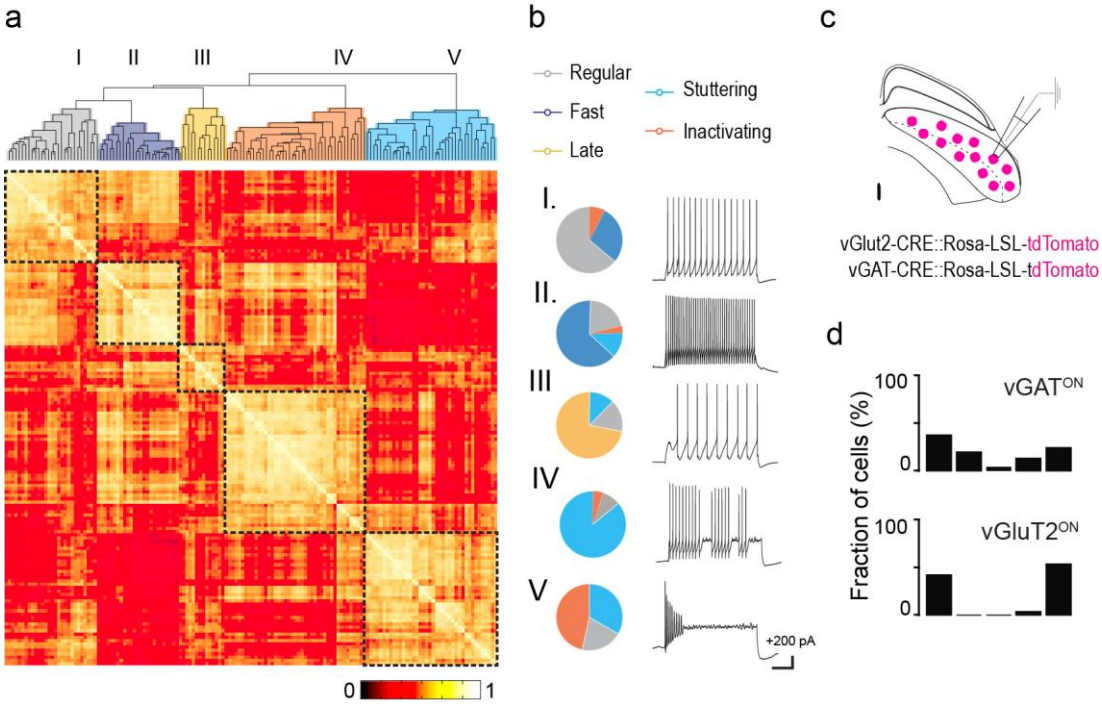

Figure 3.1 | Electrophysiological heterogeneity in glutamatergic and GABAergic collicular neurons.
a, Hierarchical clustering of SGI neurons based on electrophysiological parameters obtained from recordings of WT ($n_{NEURONS}$ = 64, n_{MICE} = 21), vGAT^{ON} ($n_{NEURONS}$ = 46, n_{MICE} = 17) and vGluT2^{ON} ($n_{NEURONS}$ = 26, n_{MICE} = 5). **b**, Relative distribution of firing profiles in each cluster in **a** (left) and representative traces of most prevalent firing profile in each cluster, recorded from WT animals (right, scale bars: 20 mV, 100 ms; 200 pA current injected). **c**, Schematic of whole-cell patch recordings of neurons expressing *tdTomato* in glutamatergic (vGluT2^{ON}) and GABAergic (vGAT^{ON}) populations. **d**, Relative distribution of vGAT^{ON} (top) and vGluT^{ON} (bottom) neurons in each cluster in **a**.

While far from being exhaustive, such an unbiased functional classification offers the opportunity to assess the degree to which genetic differences contribute to functional heterogeneity. Given that a primary determinant of functional diversity relates to the excitatory or inhibitory nature of the recorded neurons, we then assessed the distribution of glutamatergic and GABAergic neurons across our functional classes. Vescicular glutamate transporter 2 (vGluT2) is the predominant isoform for the neurotransmitter transporter expressed in glutamatergic neurons in the SC[178], hence providing a valid molecular marker for targeting the local excitatory neuronal population; the vescicular GABA transporter

(vGAT) instead localizes to synaptic vesicles in collicular GABAergic cells[179], so that its expression can be employed as a marker of inhibitory neurons. We therefore crossed *Rosa-LSL-tdTomato* reporter line to either *vGluT2-CRE* or *vGAT-CRE* mice, and selectively targeted excitatory or inhibitory neurons for recordings (Fig. 3.1c). Once added into the clustering algorithm, our analysis revealed that vGluT2^{ON} neurons predominantly populated Clusters I and V of the similarity matrix (Fig. 3.1d, bottom panel), whereas vGAT^{ON} neurons spread broadly throughout all clusters (Fig. 3.1d, top panel). A summary of passive and active membrane properties of vGluT2^{ON} and vGAT^{ON} neurons recorded in this study is provided in Appendix B. These findings indicate that, while excitatory and inhibitory neurons together broadly account for all characterized functional types, neither of them uniquely identifies a single class, highlighting the need for further refinement in characterizing the genetic diversity within the SGI.

3.2 *Pitx2* labels a subpopulation of glutamatergic neurons with common electrophysiological profile

In order to find genetic markers for specific subpopulations of neurons in the SGI, we screened local gene expression by extracting RNA from sensory and motor layers of the SC, manually dissected at post-natal day 7 (P7, Fig. 3.2a), and sequenced the derived cDNA libraries. We decided to carry out this genetic analysis at an early stage of development based on our speculation that genes most likely to display an orderly distribution along the laminar organization of the SC might be those related to developmental processes of, among others, sensorimotor alignment. Furthermore, we analyzed differential gene expression between the two functional domains of the SC with two aims: firstly, to identify genes enriched in the motor domain, providing possible markers for subpopulations of cells within the layer; secondly, through comparison of expression levels in the sensory domain, we intended to identify transcripts virtually exclusive to the motor layers, thus representing a convenient experimental tool for targeting *in vivo*.

We identified a total of 2,940 genes differentially expressed in the two SC domains during development (yellow dots, Fig. 3.2b). To investigate whether these differentially expressed genes were associated with particular biological processes, we carried out a gene ontology enrichment analysis based on the functional annotation of these genes. We found that a large number of our differentially expressed transcripts were indeed associated with nervous system development (p_{adj} = 3.88E-51), neurogenesis (p_{adj} = 3.33E-45) and neuron differentiation (p_{adj} = 2.96E-42). Two considerations can be made based on these

observations: on one hand, the abundance of developmental and neuronal-related transcript is in line with our predictions based on the age of the animals employed and the type of tissue studied, hence validating our sequencing dataset; additionally, it provides evidence for the assumption that developmental genetic factors themselves show differential distribution across SC domains, providing interesting candidates genes for labeling neuronal groups within the layer. To isolate candidate genetic markers, we focused on the 20 most significantly enriched genes in the motor vs. sensory domains (Fig. 3.2c, Appendix C). While being significantly differentially expressed, many of these genes (from Kif12 to Clec4f in the heatmap) showed low levels of enrichment in the motor domain, suggesting that the expression of these genes would be very sparse in the region. Higher levels of expression were instead recorded for Myelin-associated oligodendrocyte basic protein (Mobp), Transcription factor AP-2 Delta (Tfap2d), One Cut Homeobox 2 (Onecut2), Paired-like homeodomain transcription factor 2 (Pitx2) and One Cut Homeobox 3 (Onecut3).

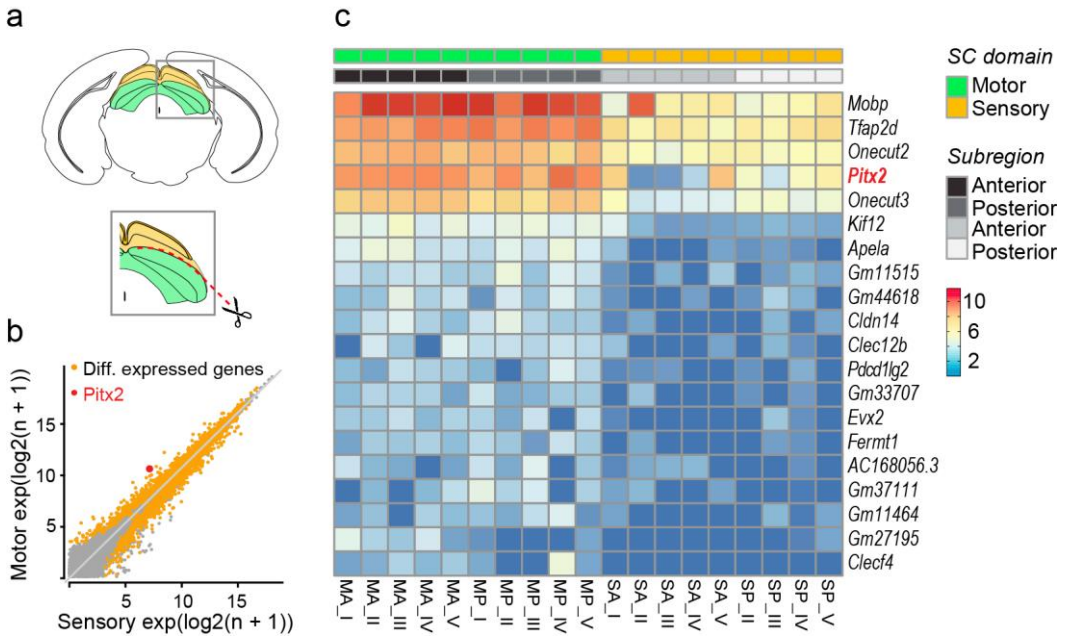

Figure 3.2 | RNAseq identifies markers for subpopulations of neurons in the SGI.
a, Schematic of SC dissection for RNA sequencing in P7 animals. **b**, Scatter plot of mean normalised read counts for each gene between sensory (superficial) and motor (deep) SC domains. Genes highlighted in yellow are significantly differentially expressed ($p_{adj} \leq 0.05$); *Pitx2* is highlighted in red. **c**, Heat map of 20 most significantly enriched genes in the motor vs. sensory domain of the SC, with levels of expression assessed in sensory and motor SC domain fractions (anterior and posterior) across replicates ($n_{MICE} = 5$).

While its differential expression is an interesting finding that corroborates the validity of our manual dissection of SC domains along alternating layers of white and gray matter, Mobp is unlikely to represent a valid candidate for our labeling of distinct groups of neurons in the SGI. Additionally, despite being significantly enriched in the motor SC domain, Tfap2d,

Onecut2 and Onecut3 were detected to relatively high levels in the sensory domain as well. Interestingly, the mRNA encoding for Pitx2 was instead selectively enriched in the SGI and virtually absent from more superficial layers of the SC ($Log_2FoldChange$ = 2.8, p_{adj} = 7.477E-04), therefore providing an interesting candidate gene for our genetic dissection of SGI circuits.

In order to validate our sequencing data, we crossed *Pitx2-CRE* mice with a *Rosa-LSL-tdTomato* reporter line and studied the distribution of Pitx2^{ON} cells in the SC (Fig 3.3a). We found that Pitx2^{ON} neurons were indeed excluded from the superficial layers of the SC and solely present in the SGI, where they account for 23 ± 2% of all neurons (Fig. 3.3c). Pitx2^{ON} cells spanned the entire SC, along both the mediolateral and anteroposterior axes (Fig. 3.3b), with a larger proportion of cells concentrated in the lateral portions of the SC.

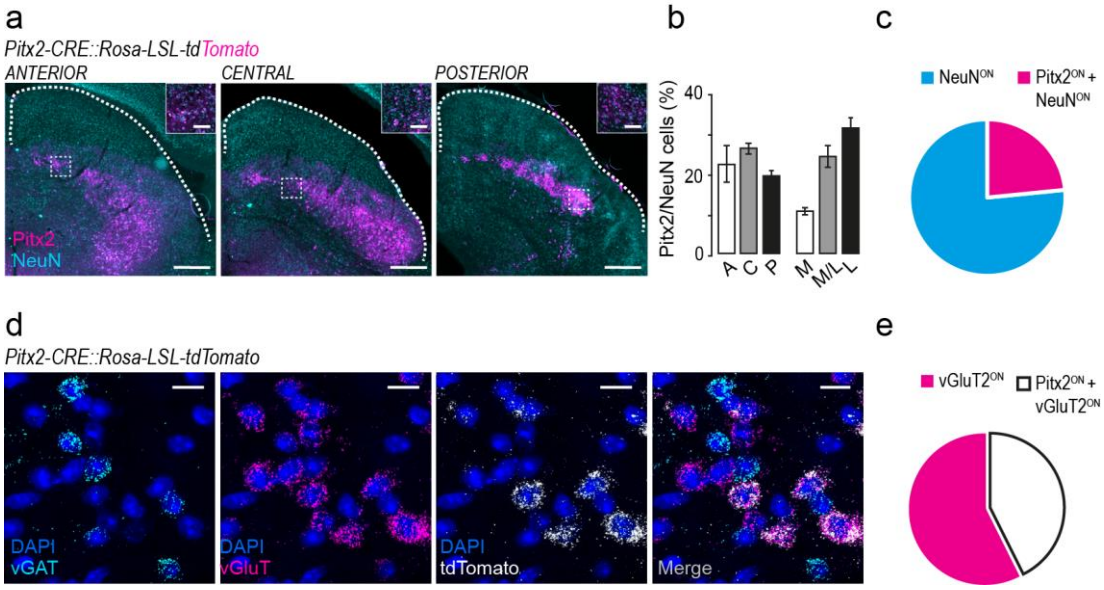

Figure 3.3 | *Pitx2* labels a subpopulation of glutamatergic neurons in the motor SC.
a, Distribution of Pitx2^{ON} neurons in the anterior (left panel), central (middle panel) and posterior (right panel) portions of the SGI of *Pitx2Cre::Rosa-LSL-tdTomato* mice (scale bars: 250 µm, inset 50 µm). **b**, Distribution of Pitx2^{ON} cells across the anteroposterior and mediolateral extents of the SGI, expressed as proportion of total number of neurons in the region. **c**, Proportion of neurons in the SC expressing *tdTomato* under Pitx2-CRE control ($n_{NEURONS}$ = 16,184 for NeuN^{ON}, 3,793 for Pitx2^{ON}+ NeuN^{ON}; n_{SLICES} = 9). **d**, Triple *in situ* hybridization in *Pitx2Cre::Rosa-LSL-tdTomato* mice, with *tdTomato*, *vGAT* and *vGluT2* probes (scale bar: 20 µm). **e**, Proportion of glutamatergic neurons in the SC expressing *tdTomato* under Pitx2-CRE control ($n_{NEURONS}$ = 4,630 vGluT2^{ON}, 1,973 Pitx2^{ON}+ vGluT2^{ON}; n_{SLICES} = 12). Statistical parameters relative to b are: $p_{AP\ axis}$ = 0.2609 and $p_{ML\ axis}$ < 0.0001; statistically significant comparisons are: Mvs.M/L (p = 0.0006) and Mvs.L (p < 0.0001).

We then characterized additional cellular phenotypes of Pitx2^{ON} neurons to test whether the expression of this gene is indeed a valid marker for the identification of a homogeneous class

of neurons. In order to determine the neurostransmitter identity of Pitx2^{ON} neurons, we favoured multiplex fluorescent *in situ* hybridization (FISH) over immunohistochemistry techniques in light of the high levels of myelination in the SGI, which in our experience often leads to low signal-to-noise ratio when detecting non-genetically encoded proteins in the tissue using antibodies. We used t*dTomato*, *vGluT2* and *vGAT* probes in *Pitx2-CRE::Rosa-LSL-tdTomato* mice, revealing that Pitx2^{ON} neurons express *vGluT2* RNA (Fig. 3.3d), representing about half of the excitatory population in the SGI (44 ± 3%, Fig.3.3e).

Having established that the expression of *Pitx2* labels exclusively a glutamatergic subpopulation of neurons in the SGI, we then asked whether this genetically identified neuronal population also shares unique physiological features. Firstly, we performed electrophysiological recordings of *Pitx2-CRE::Rosa-LSL-tdTomato* neurons in acute slice preparation (Fig. 3.4a). Upon a first qualitative observation, Pitx2^{ON} neurons appeared to share an inactivating electrophysiological profile (Fig. 3.4b, c); indeed, when we fed their electrophysiological parameters into the clustering algorithm described in Section 3.1, they populated a single cluster in the similarity matrix (Cluster V, Fig. 3.4d). Compatibly with previous observations from electrophysiological recordings of glutamatergic neurons, we concluded that Pitx2^{ON} neurons represent a physiologically homogeneous subgroup within the glutamatergic SGI population, corroborating the validity of our genetic approach in the functional dissection of collicular circuits.

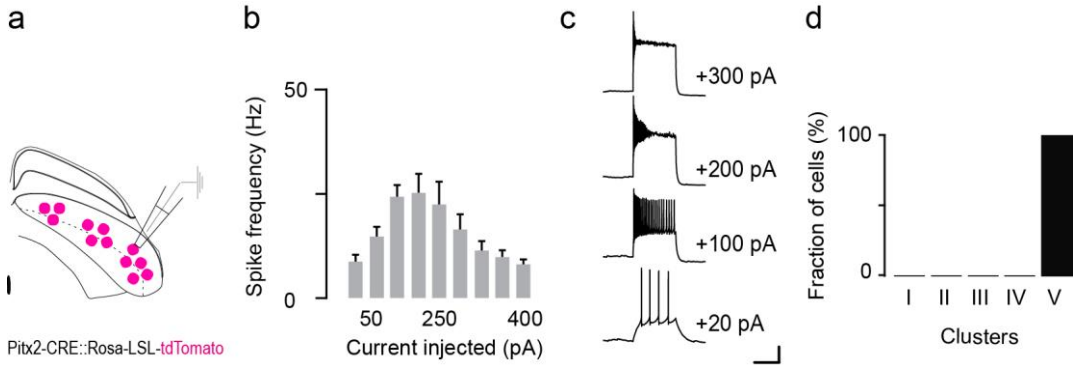

Figure 3.4 | Pitx2^{ON} neurons share a homogenous electrophysiological profile.
a, Schematic of whole-cell patch clamp recordings of *Pitx2-CRE::Rosa-LSL-tdTomato* neurons. **b**, Membrane potential response to steps of increasing positive current (20-400 pA) in Pitx2^{ON} neurons. **c**, Representative traces of firing pattern displayed by Pitx2::tdTomato neurons upon injection of steps of current of different intensity (scale bar: 20 mV, 500 ms). **d**, Distribution of Pitx2^{ON} neurons in similarity clusters defined in Section 3.1 ($n_{NEURONS}$ = 16, n_{MICE} = 5).

3.3 Location and time course of *Pitx2* expression

As previously described, *Pitx2* expression within the SC is strictly confined to its motor domain. However, we wanted to further investigate the abundance of Pitx2^{ON} neurons across the brain to estimate its potential as an experimental tool to functionally manipulate and anatomically reconstruct neural circuits. In particular, it was important for us to assess the levels of expression of *Pitx2* in neighbouring brain regions to the SGI; this would shape our future experimental design, both in terms of restricting the injection size for viral targeting of the population and in assessing the feasibility of adopting genetically encoded functional molecules for its selective manipulation. Additionally, considering whether any known input region to the SGI contains a high abundance of Pitx2^{ON} neurons is also key; indeed, if using a genetically encoded ChR2 targeted to Pitx2^{ON} cells, the presence of Pitx2::ChR2 axons of passage in the region might lead to the concomitant activation of these axons[180] and ultimately the erroneous interpretation of the role of collicular Pitx2^{ON} neurons. We therefore built an atlas of *Pitx2* expression across the mouse brain using *Pitx2-CRE::Rosa-LSL-tdTomato* mice. We observed that the expression of our genetic marker was very sparse in the brain; only a limited number of subcortical areas, most notably the motor layers of the SC (42 ± 1%) and the mammillary nucleus (MM, 18 ± 2%), contained Pitx2^{ON} neurons (Fig. 3.5).

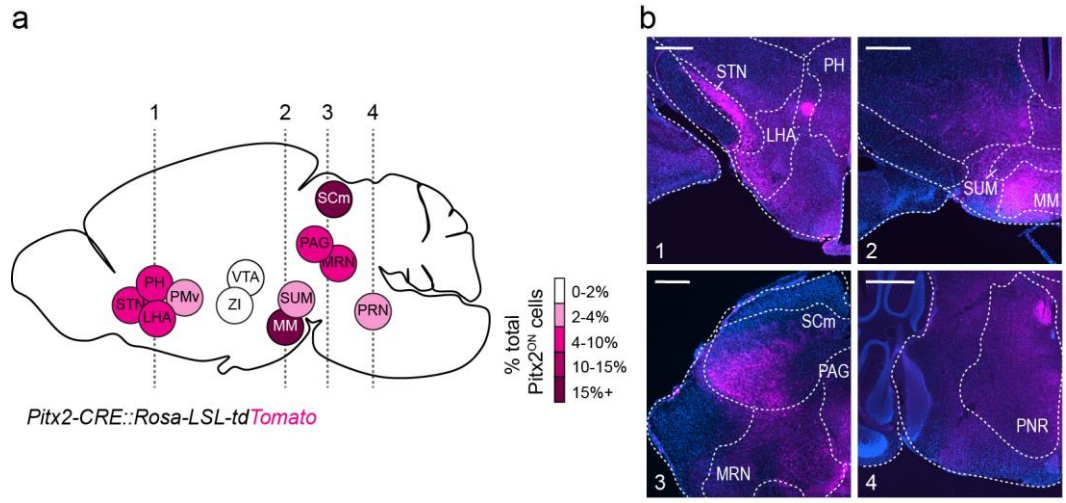

Figure 3.5 | Atlas of Pitx2^{ON} neurons distribution in the murine brain.
a, Schematic representation of the brain regions containing Pitx2^{ON} cells studied in the *Pitx2-CRE::Rosa-LSL-tdTomato* line, quantified as fraction of total Pitx2^{ON} neurons in the brain (n_{MICE} = 3). **b**, Representative histologies highlighting presence of Pitx2^{ON} cells in coronal sections marked with dashed lines in **a** (scale bars: 500 µm). Areas containing Pitx2^{ON} cells are: Lateral hypothalamic area, LHA; Mammillary nucleus, MM; Midbrain reticular nucleus, MRN; Periacqueductal gray, PAG; Posterior hypothalamic nucleus, PH; Ventral premammillary nucleus, PMv; Pontine reticular nucleus, PRN; Superior colliculus, motor related, SCm; Subthalamic nucleus, STN; Supramammillary nucleus, SUM; Ventral tegmental area, VTA; Zona incerta, ZI.

In terms of proximity to other *Pitx2*-expressing regions, we found that SGI Pitx2^{ON} neurons were sufficiently segregated from expressing neurons in neighbouring areas. The closest Pitx2^{ON} cells were detected in the MRN and PAG; in both cases however the cells were positioned far enough from the border with the SC (Fig. 3.5b, bottom left panel) to allow for specific viral targeting and optogenetic manipulation of Pitx2^{ON} cells in the SGI. Together with the ZI, the MRN and PAG also represent examples of the previously characterized input regions to the SC; however, the distribution of Pitx2^{ON} cells in these areas was very sparse along the anteroposterior axis and the absolute number of cells sufficiently low (Pitx2^{ON} cells in ZI = 450 ± 10; in MRN = 1732 ± 29; in PAG = 1328 ± 42) to be able to discard that any significant innervation to the SGI from this region would result from the contribution of Pitx2^{ON} cells.

Having assessed *where* in the brain Pitx2 is expressed, we further investigated *when* the transcription of this gene can be detected, with particular focus on the patterns of temporal expression in the SGI. Going back to our gene set enrichment analysis, we found that *Pitx2* was listed in a number of gene sets relating to nervous system development, cellular development and neurogenesis. Based on these findings and its nature as a transcription factor, we speculated that the expression of *Pitx2* might be confined to a specific temporal window during development. Using FISH, we carried out a histological assay to define the time course of *Pitx2* expression in the SGI, sampling collicular sections at P2, P7, P14, P21 and two months of age (Fig. 3.6). Contrary to our expectations, we found that active transcription of the gene could be detected after our sampling point for RNAseq (P7); in fact, *Pitx2* appears to be expressed in adult mice as well, consistently displaying a pattern of distribution comparable to what previously described in the *Pitx2-CRE::Rosa-LSL-tdTomato* line.

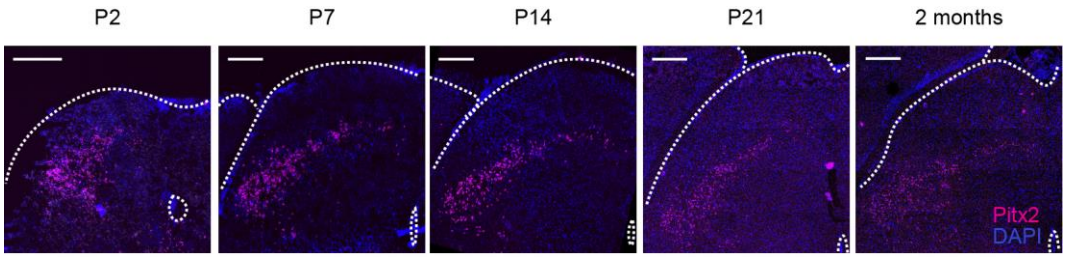

Figure 3.6 | Time course of *Pitx2* expression in the SGI.
In situ hybridization in WT mice with *Pitx2* probe displaying active expression of *Pitx2* in the SGI throughout development, sampled at P2, P7, P14, P21 and 2 months of age (scale bars: 250 µm).

In summary, our histological experiments suggest that the transcription factor Pitx2 is expressed in a restricted number of subcortical brain regions. With the exception of the SCm and MM, where high concentrations of Pitx2^{ON} cells were detected, the distribution of Pitx2^{ON} neurons is very sparse within the identified region, suggesting that this genetic marker might provide a convenient experimental tool for the selective manipulation of neural circuits *in vivo.* While Pitx2 is a transcription factor implicated in developmental processes, its expression is sustained throughout adulthood in the SC according to a precise spatial pattern.

3.4 Pitx2^{ON} neurons define anatomical modularity in the SGI

While gathering the histological data summarized so far in *Pitx2-CRE::Rosa-LSL-tdTomato* mice, we observed that the distribution of Pitx2^{ON} cell bodies was non-homogeneous within the motor domain of the SC (Fig. 3.3a). This was more evident in certain portions of the SC, suggesting that perhaps our sectioning of the region along the coronal plane was not best suited for the study of this feature. This prompted us to look for alternative ways to analyse in greater detail the anatomical distribution and morphological features of Pitx2^{ON} neurons within the SGI. In order to minimize sectioning bias, we clarified whole brains of *Pitx2-CRE::Rosa-LSL-tdTomato* mice and acquired 3D images of the SC using light-sheet fluorescence microscopy (Fig. 3.7).

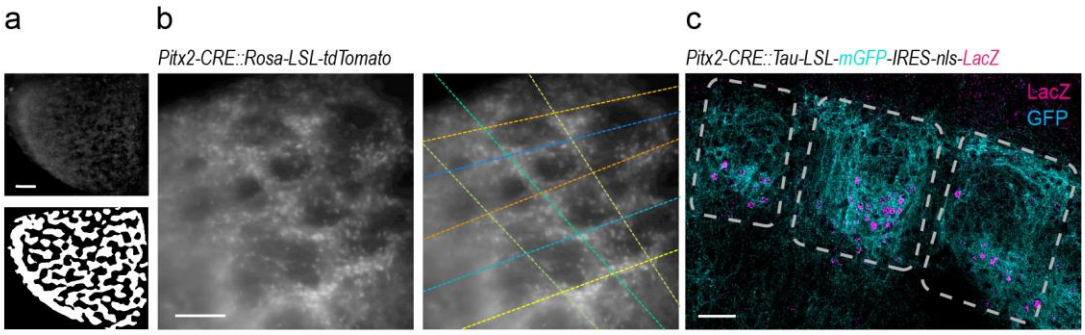

Figure 3.7 | Pitx2^{ON} neurons are organized in discrete anatomical modules.
a, Projection of top SC view in clarified brain of *Pitx2-CRE::Rosa-LSL-tdTomato* (top) and image segmentation (bottom) (scale bar: 300 µm). **b**, Magnified top view of SC (left) with automatically fitted lines (right), highlighting grid-like organisation of SGI by Pitx2^{ON} population (scale bar: 300 µm). **c**, Modular organization of Pitx2^{ON} neurons dendrites (*cyan*, mGFP) and cell bodies (*magenta*, LacZ) from a coronal section of *Pitx2-CRE::Tau-LSL-mGFP-IRES-nls-LacZ* mice (scale bar: 100 µm).

At first glance, it was apparent that indeed the cell bodies of Pitx2^{ON} neurons were not randomly distributed across the motor domain (Fig. 3.7b). Following image processing to segment the 3D stack accounting for the spherical nature of the SGI surface (see *2.6.2 Analysis*), we automatically fitted lines along the areas of higher *Pitx2*-dependent signal to extract features of this organisation (Fig. 3.7a, b). Pitx2^{ON} neurons were distributed in a patchy organisation in the SGI, delineating a grid-like structure spanning the entire layer (periodicity along AP axis: 275.76 ± 20.94 μm; ML axis: 326.67 ± 34.89; Fig. 3.7a, b). Furthermore, analysis of the expression pattern of membrane-bound GFP in *Pitx2-CRE::Tau-LSL-mGFP* animals in thin slices showed that this modular pattern extends to the organisation of dendritic arbors of Pitx2^{ON} neurons (Fig. 3.7c), suggesting that such modularity could be exploited by incoming inputs. The modularity of Pitx2^{ON} neurons bears a striking resemblance to canonical cortical modular structures, such as the barrel cortex[181]; however, in the SGI, modularity cannot be explained by a mere variation in cell density (see NeuN staining in Fig. 3.3a) and it is only visible through the lens of genetics. These observations suggest that the genetic approach to circuit study is not only instrumental in dissecting functionally homogeneous groups of neurons, but can also reveal principles of circuit design that would not be otherwise appreciated.

3.5 Summary

In this chapter, we adopted an *in vitro* approach to illustrate the wide physiological diversity among neurons that populate the murine SGI. While excitatory and inhibitory neurons together account for all electrophysiological types in the SC, neither population represents exclusively one physiological class. Through a genetic screen, we identify *Pitx2* as a marker for a glutamatergic subpopulation of neurons in the SC characterized by a homogeneous, inactivating electrophysiological profile, suggesting that the genetic approach can grant access to neuronal groups characterized by uniform physiological properties. Furthermore, *Pitx2* expression is strictly confined to the SGI, together with a limited number of subcortical regions outside the SC, making it a useful genetic tool for targeting specific neuronal populations. Strikingly, we found that Pitx2^{ON} neurons show a unique anatomical arrangement within the motor layers of the SC, delineating a modular grid-like structure with the distribution of both their cell bodies and dendritic arborisations. As this anatomical feature is not the result of changes in cell density across the SGI, our results suggest that genetic analysis of circuits can uncover underlying principles of circuit design.

4. Pitx2^{ON} population in the head-orienting control network

The grid-like organisation of Pitx2^{ON} units is reminiscent of modular structures observed in other subcortical and cortical regions. In the case of the barrel cortex, for example, modularity is instrumental for mapping discrete somatotopic features onto appropriate cortical microdomains[182]; clustered striosomes have been implicated in context-sensitive processes of reinforcement learning[183]; finally, anatomically distinct glomeruli in the olfactory bulb form the site of convergence of sensory neurons that share expression of given odour receptors[184-186].

We therefore wondered about the underlying logic of SGI modularity, and what features might me mapped onto Pitx2^{ON} modules. A first step to take in formulating a hypothesis regarding their functional relevance is to anatomically reconstruct their associated pre- and post-synaptic populations, revealing their position within the collicular gaze control network.

4.1 Pitx2^{ON} neurons project along the tecto-thalamic and cephalomotor pathways

Given the excitatory nature of Pitx2^{ON} neurons, we first considered whether they are part of the projecting network of the SGI. Using recombinase-dependent viral anterograde tracers allowed us to target selectively Pitx2^{ON} neurons in the SGI and reconstruct their projection patterns. In order to discard the eventuality of fluctuations in the levels of expression of

Pitx2 over time, we first crossed *Pitx2-CRE* with *Tau-LSL-FLPo-INLA* mice. This leads to permanent expression of a FLP recombinase in neurons that expressed *Pitx2* at any point in their development, hence ensuring we were virally targeting the entire population of neurons previously analysed anatomically using our *Pitx2-CRE::Rosa-LSL-tdTomato* strain. We then co-injected two FLP-dependent AAV constructs expressing a synaptic and a membrane marker respectively, AAV(1)-CMV-FRT-TVAmCherry-2A-Gly and AAV(9)-CMV-FRT-synGFP-WPRE, in the SGI of adult male mice (Fig. 4.1a, b). We then quantified downstream connectivity based on the intensity of the synaptic marker SynGFP signal measured in thin brain sections (Fig. 4.1c-e).

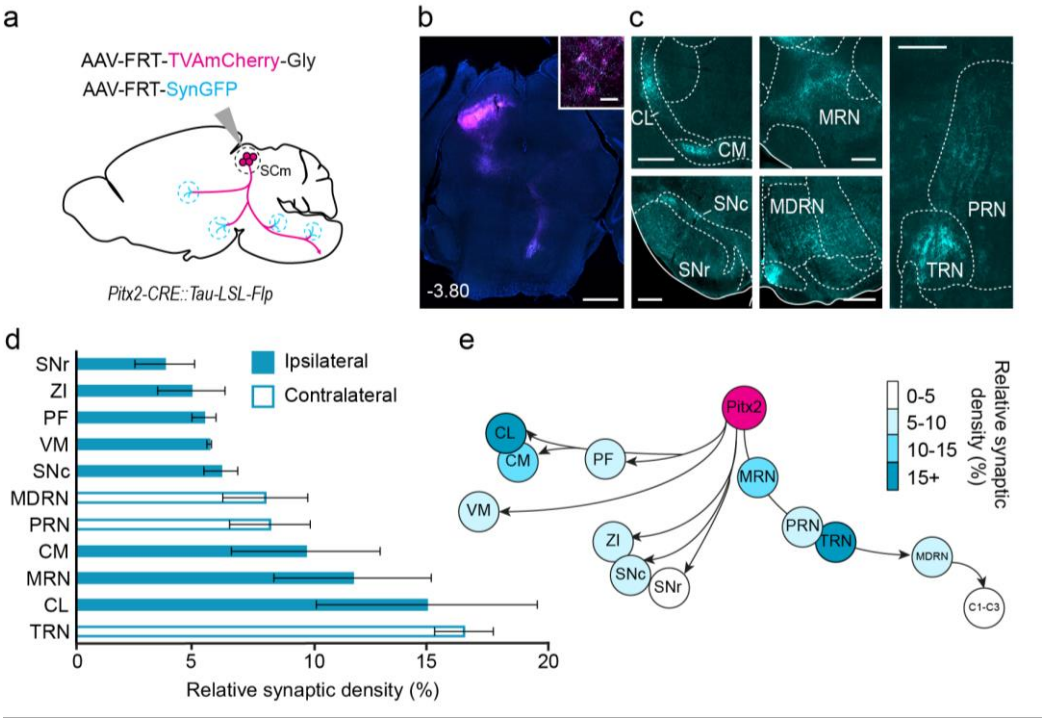

Figure 4.1 | Pitx2^{ON} neurons are an output population of the motor SC.
a, Projections of Pitx2^{ON} neurons in *Pitx2-CRE::Tau-LSL-FLPo-INLA* mice targeted via FLP-dependent AAVs expressing synaptic (*cyan*, SynGFP) and membrane (*magenta*, TVAmCherry) markers. **b**, **c**, Overview of infected neurons (scale bar: 1 mm, inset: 50 µm) (**b**) and their extra-collicular targets (scale bars: 300 µm) (**c**). **d**, **e**, Quantification (**d**) and schematic representation (**e**) of relative synaptic density of Pitx2^{ON} neurons terminals in target areas (Central lateral nucleus of the thalamus, CL; Central medial nucleus of the thalamus, CM; Ventral medial nucleus of the thalamus, VM; Parafascicular nucleus, PF; Zona incerta, ZI; Substantia nigra pars compacta, SNc; Substantia nigra pars reticulata, SNr; Midbrain reticular nucleus, MRN; Pontine reticular nucleus, PRN; Tegmental reticular nucleus, TRN; Medullary reticular nucleus, MDRN; Spinal cord, cervical segments C1-C3; $n_{MICE} = 3$).

Our results show that the Pitx2^{ON} population forms long-range connections with nuclei outside the SC, targeting both the ipsi- and contralateral hemispheres relative to the injection site. Interestingly, Pitx2^{ON} neurons seem to contribute to both ascending and descending outputs of the motor SC. In terms of ascending outputs, we observed a prominent projection to the ipsilateral thalamus, notably the central lateral (CL, 16 ± 5%) and central medial (CM, 10 ± 3%) thalamic nuclei. Pitx2^{ON} fibres also contact the ipsilateral basal ganglia, terminating most prominently in the substantia nigra pars compacta (SNc, 7 ± 1%); additional fibre terminals are observed in the neighbouring hypothalamic ZI (5 ± 2%).

On the other hand, Pitx2^{ON} descending fibres follow the tecto-spinal tract, synapsing onto neurons in motor-related centres of the midbrain (MRN, 12 ± 4%), pons (Pontine reticular nucleus, PRN, 9 ± 2%; Tegmental reticular nucleus, TRN, 17 ± 1%) and medulla (MDRN, 9 ± 2%). Synaptic contacts could also be detected in the cervical segments of the spinal cord, but they were too sparse to be quantified following the same strategy. With the exception of MRN connections, all Pitx2^{ON} descending fibres contact pre-motor nuclei in the contralateral hemisphere.

In summary, the analysis of Pitx2^{ON} synaptic terminals identified three main projection pathways: the most modest connections were to the basal ganglia, which together with the hypothalamus received 16 ± 1% of total Pix2^{ON} neurons outptut. A more substantial projection was that to thalamic nuclei, accounting for 38 ± 2% of the total. The most prominent projection route was however down the tecto-spinal tract (47 ± 2%), suggesting Pitx2^{ON} neurons are a premotor population in the SC that might play an important role in the orchestration of neural activity along the cephalomotor pathway.

4.2 Cortical and subcortical inputs converge onto Pitx2^{ON} neurons

The anatomical modularity of Pitx2^{ON} neuronal cell bodies and dendrites, together with their connection to movement execution centres, seems uniquely suited to ensure coherent spatial-motor integration of incoming inputs. For this reason, we sought to establish the source of inputs to Pitx2^{ON} neurons by performing trans-synaptic retrograde tracing using monosynaptically restricted Rabies virus. We first injected an FLP-dependent virus expressing Rabies-G protein and TVA receptor, AAV(1)-FRT-TVAmCherry-2A-Gly, in the SGI of *Pitx2-CRE::Tau-LSL-FLPo-INLA* mice, followed by injection of EnvA-ΔG-RabiesGFP to selectively target TVA-expressing Pitx2^{ON} neurons (Fig. 4.2a). We were then

able to identify input cells to the Pitx2^{ON} population in thin brain sections, marked by the expression of GFP, and discern them from our starting cells, which express both mCherry (fused to the TVA receptor) and GFP markers (Fig. 4.2b, c).

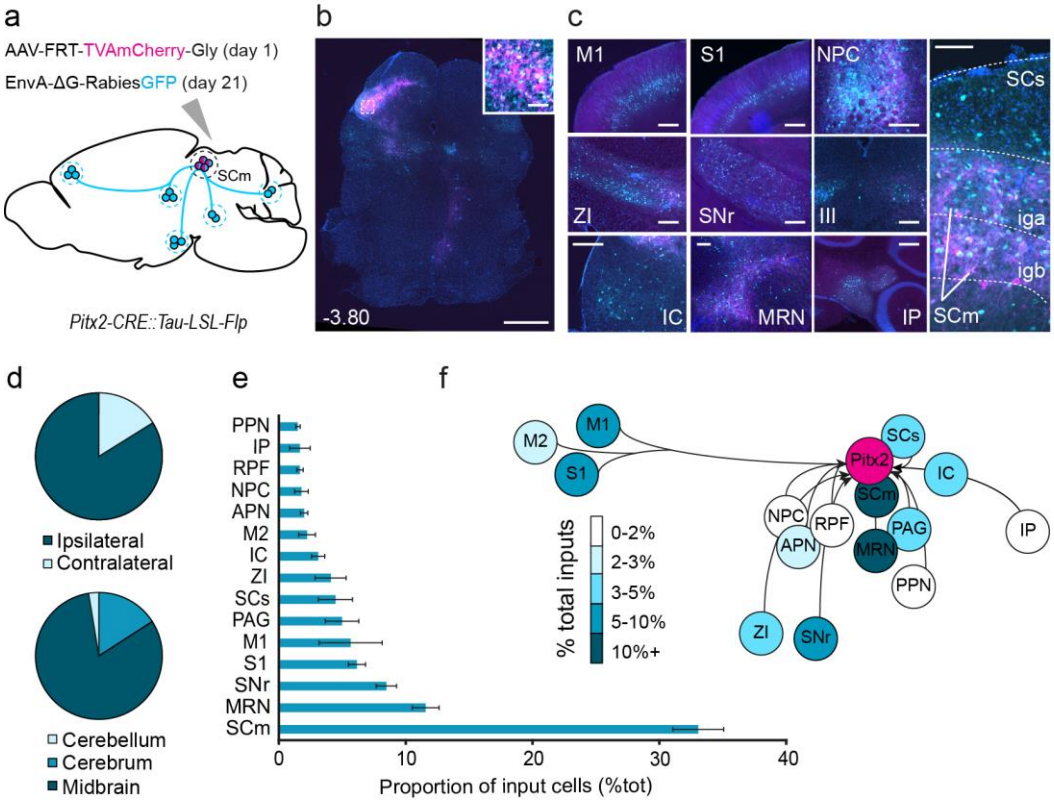

Figure 4.2 | Input convergence on Pitx2^{ON} neurons.
a, Brain-wide pre-synaptic input to Pitx2^{ON} neurons in *Pitx2-CRE::Tau-LSL-FLPo-INLA* mice revealed through the selective targeting of Pitx2^{ON} neurons via an FLP-dependent AAV expressing TVA-Gly (*magenta*, TVAmCherry) followed by EnvA-ΔG-Rabies^{GFP} (*cyan*, GFP) injection. **b, c**, Overview of targeted neurons (**b**, scale bar: 1mm, inset: 100 µm) and their presynaptic cortical and subcortical partners (**c**, scale bars: 250 µm). **d**, Distribution of pre-synaptic partners of Pitx2^{ON} neurons in ipsi- and contralateral hemispheres to injection site (top) and across brain divisions (bottom). **e**, **f**, Quantification (**e**) and schematic representation (**f**) of top 15 input regions to Pitx2^{ON} neurons across both hemispheres (n_{MICE} = 3). Input areas are: Primary motor cortex, M1; Secondary motor cortex, M2; Primary somatosensory cortex, S1; Zona incerta, ZI; Nucleus of the posterior commissure, NPC; Anterior pretectal nucleus, APN; Substantia nigra pars reticulata, SNr; Retroparafascicular nucleus, RPF; Superior colliculus, sensory related, SCs; Superior colliculus, motor related, SCm (with relative subdivisions: Intermediate gray a, iga; Intermediate gray b, igb); Midbrain reticular nucleus, MRN; Periaqueductal gray, PAG; Peduncolopontine nucleus, PPN; Inferior colliculus, IC; Interposed nucleus, IP.

This approach revealed a diverse range of inputs to Pitx2^{ON} neurons, with presynaptic partners located in cortical and subcortical structures, in both ipsi- and contralateral

hemipsheres to the injection site. The vast majority of inputs generated in the ipsilateral hemisphere (84 ± 3%), and midbrain nuclei provided 75 ± 1% of the total input to these cells (Fig. 4.2d). Panels 4.2e and 4.2f report a quantification and graphical representation of the 15 most abundant sources of inputs to Pitx2^{ON} neurons respectively. In order to provide a more exhaustive picture of the Pitx2^{ON} population pre-synaptic network, Figure 4.3 presents instead the contribution of each of the identified input regions, expressed as a percentage of the total inputs from their relative brain subdivision.

Our findings suggest a high level of convergence of inputs to Pitx2^{ON} neurons from within the motor domain of the SC itself, with local cells representing 33 ± 2% of the total pre-synaptic partners identified. The superficial layers of the SC also contribute a large percentage of total inputs (SCs, 6 ± 1%), potentially relaying information regarding the visual scene. The somatosensory cortex (S1, 6 ± 1%) provides the major source of cortical input; interestingly, the portions of S1 providing inputs to Pitx2^{ON} cells are those related to facial structures, including barrel fields (S1 BF), mouth (S1 M) and nose (S1 N), or upper limb (S1 UL) (Fig. 4.3b). Among the most prevalent input regions is the inferior colliculus (IC, 3 ± 1%), a critical integration center of the auditory pathway, and a smaller proportion of cells in the primary auditory cortex (AUD1, 0.3 ± 0.3%) also contact Pitx2^{ON} neurons (Fig. 4.3b). Taken together, these observations suggest a degree of multisensory convergence exists on Pitx2^{ON} neurons directly, which might be instrumental to the generation of spatially appropriate motor commands.

A number of motor-related regions were also identified in our retrograde tracing study; both ipsilateral and contralateral MRN provide inputs to Pitx2^{ON} neurons, collectively 12 ± 1% of the total, suggesting a reciprocal connection exists between the two populations. The ipsilateral M1 also sends projections onto Pitx2^{ON} cells (6 ± 3%), as do deep cerebellar nuclei, such as the interposed nucleus (IP, 2 ± 1%). Furthermore, we found that the basal ganglia provide a substantial direct input to the Pitx2^{ON} population through the SNr (9 ± 1%); while our experimental design does not allow to draw this conclusion definitely, we could speculate that such connections exert inhibitory control over the premotor Pitx2^{ON} cells, again reinforcing the hypothesis that they might be crucial in the control of movement initiation.

Lastly, our results suggest that Pitx2^{ON} neurons are targeted by neuromodulatory systems, given they receive input from PPN cells (2 ± 0.2%); as mentioned in the introduction, the PPN is one of the two sources of cholinergic innervation in the SC and it is thought to

modulate attentional states, suggesting Pitx2^{ON} neurons might participate in the integration of multisensory, motor and cognitive functions to coordinate SC output.

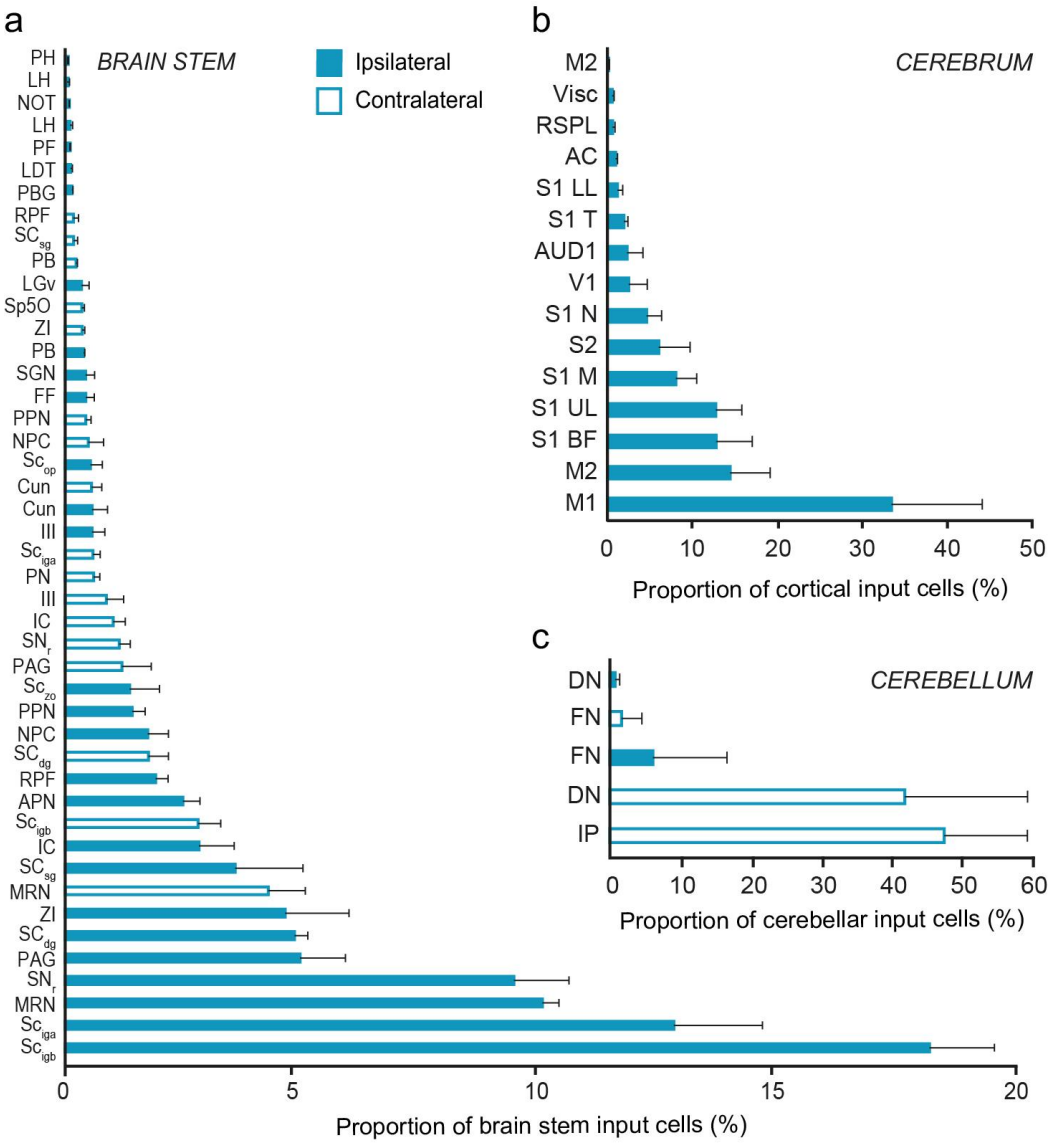

Figure 4.3 | Complete list of pre-synaptic partners to the Pitx2^{ON} population.
a-c, Distribution of input cells in brain stem (**a**), cerebral (**b**) and cerebellar nuclei (**c**), expressed as percentage of total input cells in relative brain division (n_{MICE} = 3). A full list of the abbreviations adopted in this figure is available in the preface.

4.3 Summary

In this chapter we reconstructed the pre- and post-synaptic networks of Pitx2^{ON} neurons using viral tracing tools. We find that Pitx2^{ON} neurons are an output population of the SC that projects down the cephalomotor pathway along the tecto-spinal tract, synapsing onto

neurons in motor-related centres of the midbrain (MRN), hindbrain (TRN and PRN) and medulla (MDRN); further connections are made with nuclei in the thalamus and the basal ganglia. Retrograde tracing identified a number of cortical, mainly somatosensory and motor in nature, and subcortical input areas for Pitx2^{ON} neurons. These cells appear to be direct recipients of information from the sensory and motor domains of the SC, as well as being targeted by motor-related centres in the midbrain, such as MRN and SNr. Notably, structures previously known to provide patchwork innervation to the SGI, such as the SNr and the PPN [119,187], directly synapse onto Pitx2^{ON} neurons, revealing a matching modular design at both the pre- and post-synaptic levels.

Altogether, this connectivity data suggests a role for Pitx2^{ON} neurons as recipients of a vast array of sensory information and motor commands; their projection pattern suggests they might be directly involved in implementing motor plans for head displacement based on coherent integration of internal motor commands and external sensory inputs.

5. Studying 3D head movements in freely moving mice

Based on their projections along the cephalomotor pathway described in Chapter 4, we sought to investigate whether direct activation of Pitx2^{ON} neurons could drive motor output, specifically head displacement. Given their modular organisation, we also aimed to characterise the precise metric of such displacement with the ultimate intention of assigning functional significance to this anatomical feature. The first necessary step to take was to develop an experimental system to reliably track head displacements in a freely moving animal. Video tracking techniques have been widely employed in neuroscience to study innate behaviours[188,189], locomotion[190] and even fine motor control[191] in unrestrained mice. However, working with video files presents the intrinsic limitation of bidimensionality, which constitutes a major drawback for our intention to extract the metric of a motion that is performed in 3D. Previous work in the lab brought to the development of an inertial-based system for monitoring head rotations along the three Eulerian components, yaw (horizontal), pitch (vertical) and roll (torsional)[170]. Using this as a starting point for our work, we further refined this approach to allow for precise reconstruction of head-over-body dynamics.

5.1 Dual inertial sensor approach can be used to compute head-over-body displacement

When attempting to reconstruct the precise metric of head motion associated with a given pattern of neural activity or following exogenous stimulation, being able to subtract from a

single head sensor readings any rotational component associated with body displacement seems like a fundamental experimental requirement.

In order to obtain information regarding the orientation of the mouse head relative to the body, we implemented a dual inertial-sensor-based system, which allows for simultaneous recording of head and body positions in 3D. Before applying our system *in vivo*, we verified two essential requirements in our sensor boards: firstly, sensor board readings have to be stable over time and accumulate negligible drift angles given our intention to apply this system to long recording sessions *in vivo*. Secondly, sensors need to be able to output positional information reliably at a wide range of displacement velocities in light of the high physiological speed of head rotations observed in rodents.

We started by recording independently and in a static regime the output of two sensor boards that we intended on using for measuring head and body positions. We recorded the output of the sensors at 50 Hz for 10 minutes and measured drift in the system for each Eulerian component (Fig 5.1a). This was tested determining: the shift in the sensor output between each measurement (jitter, Fig. 5.1b) and the cumulative change in heading over the course of the 10 minutes recording (cumulative drift, Fig. 5.1c). For both head and body sensors, jitter values appeared to never exceed ±1° along yaw, pitch and roll. Similarly, the cumulative drift in each sensor was within ±1.5° along all Eulerian components, suggesting our experimental system is suitable for tracking positional information for a prolonged period of time.

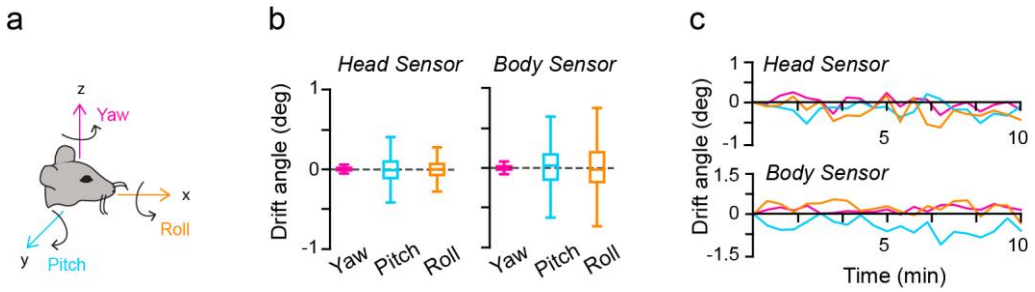

Figure 5.1 | Stability of sensor readings in static regime.
a, Schematic of the colour-coded axes of rotation: yaw (*magenta*), pitch (*blue*) and roll (*orange*). **b**, Box and whisker plots showing the jitter in the sensors during static regime for each Eulerian dimension. **c**, Cumulative drift of the two sensors over 10 minute recordings in static regime.

We then tested the ability of the sensors to track motion occurring at different velocities. To this end, the sensors were fixed to a step-motor-controlled rotation table and their output compared to the motion trace expected from the pattern applied. Trajectories were analysed as difference between the readings of the two sensors; for analysis of head sensor in-motion reliability, the body sensor was maintained fixed throughout the recording while the head sensor was rotating at four fixed speeds (28, 40, 56 and 80°/s; Fig. 5.2a, left panel). The opposite conformation was adopted to study body sensor reliability in this dynamic regime (Fig. 5.2a, right panel). Plotting the sensors' readings over the expected trajectories gives an indication of their ability to reliably track high-speed movements. In order to provide a more quantitative assessment, we computed the difference between sensor readings for each pair of subsequent 20 ms temporal bins and subtracted these values from the expected angular displacement between each 50 Hz measurements (28°/s = 0.56°, 40°/s = 0.8, 56°/s = 1.12 and 80°/s = 1.6°). This was carried out separately for the two sensors, at each speed and direction tested. The average difference between expected travel per bin and the relative measured value is considered to be the characteristic error for each motion protocol applied (Fig. 5.2b). Neither of the two sensors reported significant errors in motion tracking at any speed and direction tested, suggesting that our dual sensor approach is a valid strategy to reliably track head-over-body displacements at a wide range of velocities.

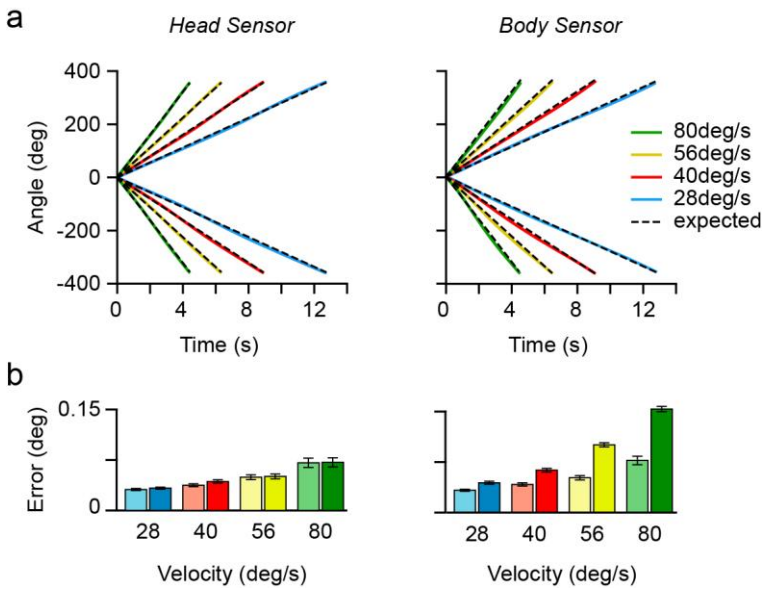

Figure 5.2 | Stability of sensor readings in dynamic regime.
a, Output of head (left) and body (right) sensors recorded during step-motor-driven rotations over 360° at four different speeds and two directions (coloured lines) plotted against the expected trajectory (black dashed line). **b**, Bar plots showing the error of the head (left) and body (right) sensor for each direction of rotation, at each speed tested (light shades for clockwise rotations and dark shades for counter-clockwise rotations; $p = 0.08$).

5.2 Quantification of naturalistic behaviour in mice

We then applied our system *in vivo* by securing the two inertial sensors on the head and on the body of the animal using Mill-Max connectors and an elastic band respectively (Fig. 5.3a). Head-over-body displacements, estimated as the difference between the readings from the two sensors, were then recorded along the three rotation axes while the animals were freely moving in an open field arena. Our results indicate that angular head displacements showed a bimodal distribution along all axes of rotation, particularly evident for the yaw component of head movement (Fig. 5.3b). While this seems to suggest that mice perform head rotations of smaller amplitudes (±10°) at a lower frequency than ±10-20° movements, this effect can be most likely explained as an underestimation of motion events of the former type due to our definition of movement. We then fitted a Gaussian to the head movement frequency histograms to estimate the range of movement amplitude in each dimension of rotation. We observed that yaw movements are associated with the widest range ($mean_{yaw}$ = 0.82, σ_{yaw} = 27.2), while a smaller range of movements was recorded in pitch and roll ($mean_{pitch}$ = 1.00, σ_{pitch} = 19.5; $mean_{roll}$ = 0.97, σ_{roll} = 21.0) (Fig. 5.3c).

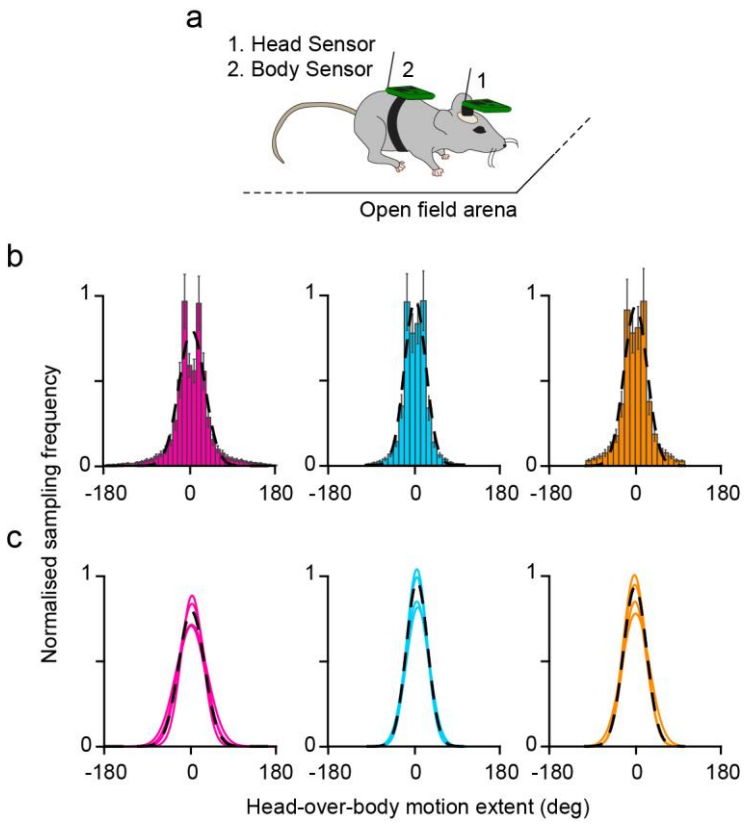

Figure 5.3 | Head-over-body movement kinematics in freely moving mice.
a, Schematic of the *in vivo* head motion recording setup with two sensor boards secured on the head and body of the mouse. **b**, Average head-over-body displacement for yaw (left, *magenta*), pitch (centre, *blue*) and roll (right, *orange*) recorded from freely moving animals, normalised to the maximum displacement produced. **c**, Single animal average (solid lines) and population average (dashed line) of the Gaussian curve fitted to the histogram of head-over-body displacements (n_{MICE} = 5).

These results indicate that under our experimental conditions, mice are able to perform a wide range of head-over-body rotations along three Eulerian axes within their physiological motor range, suggesting that our setup does not pose particular restrictions on the freedom of movement of the mice.

However, studies in primates[192] have revealed that the head is not routinely rotated relative to the body using all possible combinations of vectorial components. This dimensionality reduction, described formally by Donder's law[192], originates in primates from constraints on the use of the torsional component of motion. Understanding whether any rotational components of the head movement co-vary with each other in our animal model is an important requirement to interpret any potential neural correlates of head rotations isolated in neurophysiological experiments. In order to characterize the conjunctive nature of these 3D head movements (Fig. 5.4), two-dimensional head-displacement scatter plots were constructed from the analysis of all motion bouts (Fig. 5.4a). Linear regression analysis revealed that there was no particular correlation between yaw and pitch (R^2 = 0.001) or between pitch and roll displacements (R^2 = 5.551e-06), indicating that there is very little covariance between yaw and pitch, and between pitch and roll rotations. A significant covariance was instead found for conjunctive yaw and roll movements (R^2 = 0.764), so that rightwards yaw movements were almost exclusively performed in concomitance with counter-clockwise roll movements, and vice versa.

This analysis suggests that a level of constraint exists in the way 3D head rotations are performed by mice. To directly address the issue of Donders' law conformity and compare our observed constraints on head motion with those previously described for head rotations in primates[192], we replicated our analysis of the fit in 3D space as it has been traditionally used in primate studies. We fit the following second order surface equation to our data:

$$z = a + b \cdot x + c \cdot y$$

where a, b and c were the variable parameters to be determined to optimize the fit, x represents yaw, y is pitch and z represents roll. This process is fundamentally equivalent to fitting a curve to two-dimensional data, but allowed us to extract values of torsional standard deviation (TSD), which represents the SD of the data from the surface fit along the torsional axis of this space. Obedience to the Donders' law would constrain the tips of the vectors on the surface fit; as a consequence, lower TSD values are representative of a good fit and adherence to Donder's law, while high TSD values would represent a deviation from the surface and a divergence from Donder's law. Across all animals tested, we calculated an

average TSD value of 10.92 ± 1.21, lower than what previously calculated for primates (TSD = 15 ± 11). This analysis corroborates our previous observations of movement constraint in 2D datasets and suggests that dimensionality reduction in mice is even more pronounced than in primates.

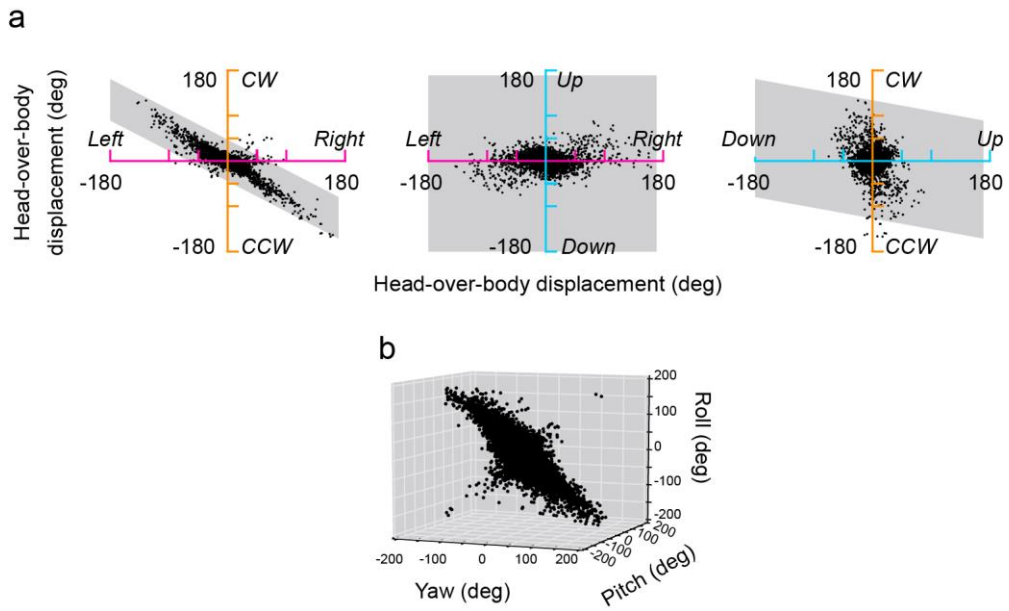

Figure 5.4 | Analysis of conjunctive movements in freely moving mice.
a, **b**, Eulerian representation of conjunctive motion from one representative mouse (**a**) and 3D representation of yaw, pitch and roll displacements for all mice (**b**) (n_{MICE} = 5).

5.3 Summary

In this chapter, we implemented the use of a dual inertial sensor approach to study head-over-body displacements in freely moving mice. Having assessed the stability of the sensors' readings over time at a range of velocities, we show that mice are able to perform their full repertoire of head rotations under our experimental conditions. Working with three-dimensional data sets, we observed that the horizontal and torsional components of rotation are tightly linked in mice, while the vertical component of the movement vectors is independent of either one of the other rotation components. This observation is instrumental in the interpretation of motor-related activity in the SC, particularly when reconstructing the logic underlying local motor representations.

6. Role of Pitx2^{ON} population in the control of head movement

Equipped with a validated experimental strategy to study three-dimensional head rotations in freely moving mice, we moved on to assess the involvement of Pitx2^{ON} neurons in the generation of head movements. To the present date, few studies have investigated SC physiology in unrestrained rodents; their experimental observations have provided evidence of SC contribution to left-right choices during goal-directed locomotion[193] and its involvement in visual orienting responses[194]. Additionally, micro-stimulations of the rat SC demonstrated that activation of collicular circuits is sufficient to produce circling behaviors[195]. However, none of these studies characterized the existence of a spatial metric for the production of SC-mediated motor behavior, specifically head movements. Recent work from the lab provided the first evidence of the existence of premotor neurons in the murine SC that are tuned for 3D vectors of head rotation[170], suggesting that collicular circuits in rodents contain premotor units that display tuning to particular motor plans for orienting, similarly to higher mammals. Here, by applying our sensor-based, three-dimensional motion tracking technology to the study of our modular Pitx2^{ON} populations, we aimed to define their contribution to such motor encoding through optogenetic means.

6.1 *In vitro* electrophysiological recordings of Pitx2::ChR2 units

Given the restricted distribution of Pitx2^{ON} neurons to the SGI, we decided to employ genetically encoded ChR2 in our optogenetic studies. We started by verifying the validity of

our experimental conditions, testing the ability of our genetically encoded ChR2 to drive the generation of action potentials in Pitx2^{ON} neurons upon blue light stimulation. Additionally, we aimed to characterize the responses of Pitx2::ChR2 neurons to different light stimulation protocols before proceding to *in vivo* applications. To this end, we used *Pitx2-CRE::Rosa-LSL-ChR2-eYFP::Rosa-LSL-tdTomato* mice to confine the expression of ChR2 to our Pitx2^{ON} population; the cytoplasmatic marker tdTomato was added to our population of interest to guide visual identification of the cells in slices (Fig. 6.1a, b). We performed whole-cell patch recordings of Pitx2^{ON} neurons and recorded their electrophysiological firing profiles; in line with our previous findings reported in Chapter 3, we observed that all Pitx2^{ON} neurons recorded displayed an inactivating firing profile (Fig. 6.1c).

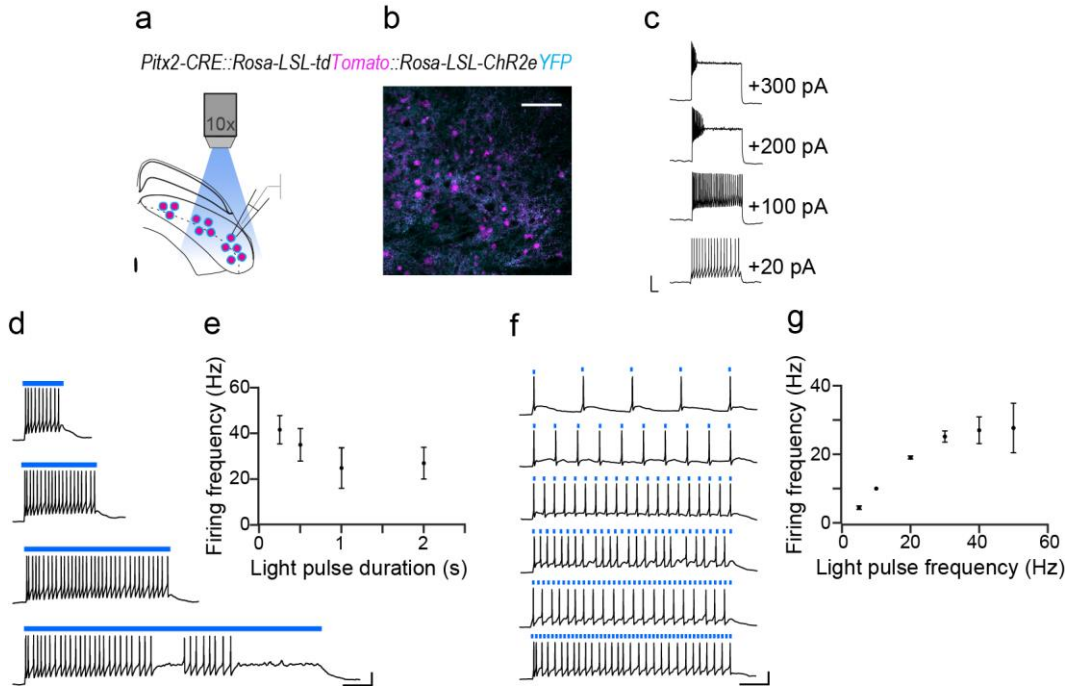

Figure 6.1 | *In vitro* responses of ChR2-expressing Pitx2^{ON} neurons to various regimes of optical stimulation.
a, **b**, Schematic of recording setup (**a**) and visual targeting of Pitx2^{ON} neurons in *Pitx2-CRE::Rosa-LSL-tdTomato::Rosa-LSL-ChR2-eYFP* mice (**b**, scale bar: 100 µm). **c**, Membrane potential response to steps of increasing positive current (20-300 pA current injected; scale bars: 100 ms, 20 pA). **d**, **e**, Changes in membrane potential (**d**) and firing frequency (**e**) in response to blue light pulses of increasing duration. **f**, **g**, Changes in membrane potential (**f**) and firing frequency (**g**) in response to 5 ms blue light pulses delivered at increasing frequency (5-50 Hz) (scale bar: 20 ms, 20 pA; $n_{NEURONS}$ = 7, n_{MICE} = 2).

We then applied different light stimulation protocols to study the active membrane properties of Pitx2::ChR2 neurons during optogenetic stimulation. We first tested the changes in

membrane voltage induced in Pitx2^{ON} neurons by application of pulses of continuous light of varying duration. As a first qualitative assessment, we observed that Pitx2^{ON} neurons were able to fire continuous trains of action potentials upon application of 0.25, 0.5 and 1 s light pulses, while some stuttering membrane responses were observed for stimuli of 2s duration (Fig. 6.1d). The firing frequency reached by Pitx2^{ON} neurons stimulated with continuous light was maximal during 0.25 s light pulses, reaching 42 ± 6 Hz; longer stimulations showed an overall decrease in firing rate along the duration of the pulse, down to 27 ± 7 Hz for 2 s light stimulations (Fig. 6.1e).

Additionally, we assessed the ability of Pitx2::ChR2 units to follow a pattern of 5 ms light pulses delivered at various frequencies for 1 s. Our results indicate that Pitx2^{ON} units under optogenetic control are able to reliably follow stimulation frequencies of 5, 10, 20 and 30 Hz; however, upon stimulation at 40 and 50 Hz, we observed a loss in fidelity of spiking and recorded a maximum firing frequency of 28 ± 7 Hz with a 50 Hz light stimulation (Fig. 6.1f, g). Our findings indicate that our genetically encoded ChR2 is a valid tool to induce Pitx2^{ON} cell spiking. Furthermore, our *in vitro* work suggests that Pitx2^{ON} cells are able to sustain firing at around 30 Hz during prolonged light stimulation; similarly, these cells are able to reliably follow optogenetic patterns of stimulation up to a maximum frequency of 30 Hz. While these findings may not be directly relevant to Pitx2^{ON} activation *in vivo* due to the limited conservation of inputs in our slice preparation, notably the long-range inhibitory connections from SNr, they are indicative of the intrinsic firing capabilities of these cells, which is instrumental for the design and interpretation of *in vivo* experiments.

6.2 Optogenetic activation of Pitx2^{ON} neurons triggers head displacement of fixed metric

Having validated our genetically encoded ChR2 system, we tested the effects of optogenetic stimulation of Pitx2^{ON} neurons in freely moving mice while monitoring head-over-body kinematics. *Pitx2-CRE::Rosa-LSL-ChR2-eYFP* mice were implanted with single optic fibres in the SGI and their head displacements tracked using the dual inertial-sensor based approach previously described (Fig. 6.2a, b). Based on our calculations of light diffraction in gray matter, we estimated that sufficient light illumination would be provided in a circular area characterized by a diamater of around 150 μm (see *2.10.1 Experimental design*); this is compatible with our measurements of the periodicity defined by *Pitx2* expression in the SGI, suggesting that the results of our optogenetic stimulation could be approximated to the activation of one to two Pitx2^{ON} modules.

We found that activation of Pitx2^{ON} neurons *in vivo* through delivery of 250 ms pulses of continuous light generated robust and precise displacements of the head relative to the body around all three main Eulerian axes of rotation (yaw, pitch and roll; Fig. 6.2c), whose metric was consistent from trial to trial. The 3D scatter plot in Figure 6.2d provides a visual representation of the consistency in the metric of movement generated following the applied light stimulation.

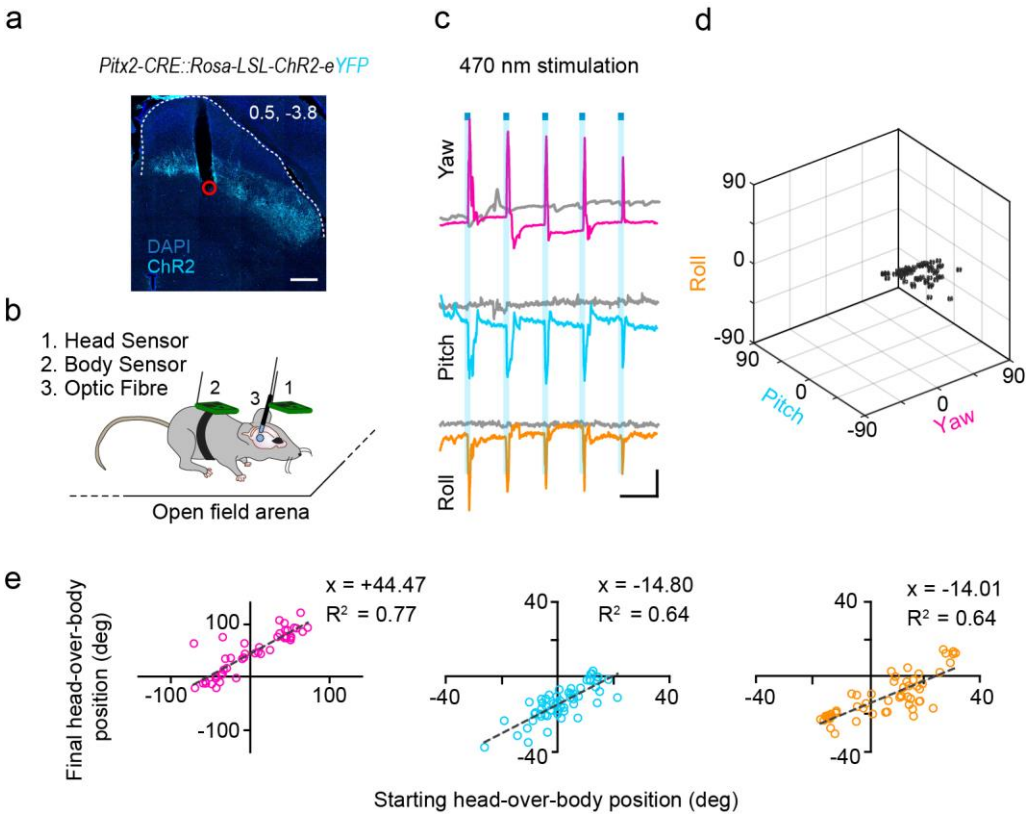

Figure 6.2 | Optogenetic activation of Pitx2^{ON} neurons drives head motion.
a, Representative SC coronal section of an implanted *Pitx2-CRE::Rosa-LSL-ChR2-eYFP* mouse with implant coordinates (x, y; scale bar: 250 µm). **b**, Schematic representation of optic fibre implant and sensor boards placement on head and body. **c**, Light-driven three-dimensional head displacements (250 ms light pulses, blue squares) in yaw (*magenta*), pitch (*blue*) and roll (*orange*) from a representative *Pitx2-CRE::Rosa-LSL-Chr2-eYFP*; grey traces represent head displacements along the same Eulerian axis in an implanted control animal exposed to the same optogenetic protocol in absence of ChR2 expression (scale bars: 10 s, 20 deg). **d**, 3D plot showing trial-by-trial reproducibility of light-driven head displacements; black spheres indicate final head-over-body position following the stimulation ($n_{TRIALS/MOUSE}$ = 60). **e**, Linear correlation between starting and final head position following optogenetic stimulation for 250 ms ($n_{TRIALS/MOUSE}$ = 60).

Having determined that optogenetic activation of Pitx2^{ON} neurons is sufficient to trigger head displacements, we sought to investigate the nature of the produced motion further. We

observed a high degree of correlation between initial and final head-over-body positions following optogenetic stimulation (yaw, R^2 = 0.77; pitch, R^2 = 0.64; roll, R^2 = 0.64), suggesting that activation of Pitx2^{ON} neurons produces a fixed motor program rather than displacements towards a fixed position in space (Fig. 6.2e).

We also asked what dictates the exact metric of the produced displacements. To this aim, we assessed the effect of the rate or duration of the optogenetic stimulation of Pitx2^{ON} neurons on the metric of the elicited head displacements. Systematic variation of the stimulation frequency between 10 and 50 Hz, delivered for a total of 250 ms, had no significant impact on the metric of the output vector produced (Fig. 6.3a). This indicates a rate-independent coding of head motions driven by Pitx2^{ON} neurons, in agreement with previous findings on the coding of the metric of head displacements by SGI neurons in mice[170]. The success rate of observed displacements was however affected through modulation of the stimulation frequency; while continuous light stimulation and stimulations at a frequency $\geq$ 30Hz produced displacements around all axes of head rotation in the large majority of trials, success rate dropped drastically when stimulation Pitx2^{ON} neurons at 10 or 20 Hz (Fig. 6.3b). With reference to our findings of direct inputs of SNr onto Pitx2^{ON} cells reported in Chapter 4, these observations are compatible with the idea that the Pitx2^{ON} population might be subject to tonic inhibition, which is only effectively overcome by the higher stimulation frequencies tested. Furthermore, our *in vitro* data suggest that upon optogenetic activation Pitx2^{ON} neurons can reliably sustain firing rates of up to around 30Hz, suggesting that higher stimulation frequencies (or continuous light) might produce comparable firing patterns in Pitx2::ChR2 cells.

We then analyzed the impact of the duration of stimulation (0.25 - 2 s) on the metric of motion produced. The amplitude of the displacements produced appeared to increase with stimulus duration (Fig. 6.3c). For all durations tested, we recorded success rates above casuality (Fig. 6.3d). Wild-type mice implanted with optic fibres and stimulated under the same experimental condition did not display any head rotation linked to the blue light pattern delivered (Fig. 6.2c and Fig 6.3b, d); this allowed us to exclude the possibility that the motor behaviour observed in *Pitx2-CRE::Rosa-LSL-ChR2-eYFP* mice upon optogenetic stimulation is a simple reflex response due to the presentation of light above the animals' heads.

Taken together, these results suggest that activation of Pitx2^{ON} neurons is sufficient to elicit fixed motor programs for head rotations in 3D. The metric of such displacements is

unaffected by the frequency of stimulation employed, but their amplitude instead increases with stimulus duration.

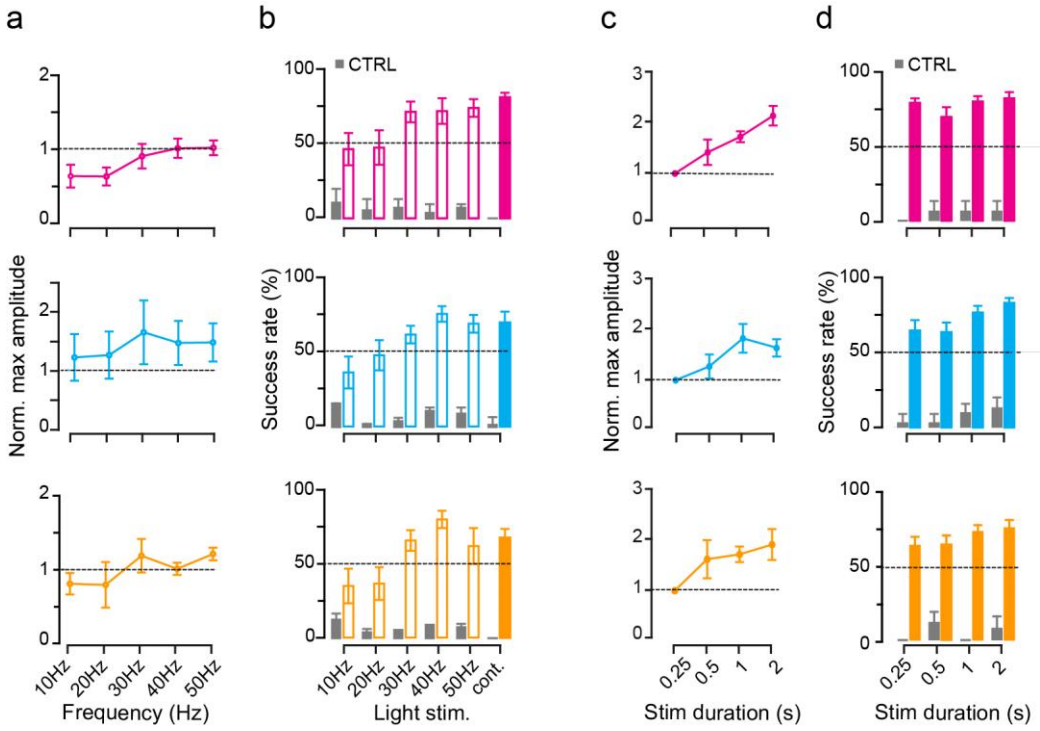

Figure 6.3 | Effect of parameters of optical stimulation on head movement metric.
a, **b**, Effect of stimulation frequency on the head displacement angle (**a**) and on the probability of executing a head movement bout for yaw (*magenta*), pitch (*blue*) and roll (*orange*) (**b**). For all frequencies tested, the stimulation duration was kept at 250 ms. For each animal, angles are normalised to the characteristic vector obtained with a 250 ms continuous light pulse (n_{MICE} = 7, $n_{TRIALS/MOUSE}$ = 60). **c**, **d**, Effect of stimulation duration on the head displacement angle (**c**) and the probability of executing a head movement bout (**d**) for yaw, pitch and roll (n_{MICE} = 12, $n_{TRIALS/MOUSE}$ = 60) normalised to the characteristic vector obtained with a 250 ms continuous light pulse. Grey bars represent the success rate of the stimulation in control mice in absence of ChR2 expression (n_{MICE} = 3, $n_{TRIALS/MOUSE}$ = 30). Statistical values relative to **a** are: p_{yaw} = 0.1056; p_{pitch} = 0.9515; p_{roll} = 0.3481. Statistical values relative to **b** are: p_{yaw} = 0.0794; p_{pitch} = 0.0072; p_{roll} = 0.0139. Statistical values relative to **c** are: p_{yaw} = 0.0002; p_{pitch} = 0.0292; p_{roll} = 0.0806. Statistical values relative to **d** are: p_{yaw} = 0.2113; p_{pitch} = 0.0412; p_{roll} = 0.3552. Statistically significant comparisons are: for pitch values in **b**, 40 Hz vs. 10 Hz (p = 0.0085) and 50 Hz vs. 10 Hz (p = 0.047); for roll values in **b**, 40 Hz vs. 10 Hz (p = 0.027) and 40 Hz vs. 20 Hz (p = 0.0443); for yaw values in **c**, 0.25 s vs. 1 s (p = 0.019), 0.25 s vs. 2 s (p = 0.0001) and 0.5 s vs. 2 s (p = 0.0198); for pitch values in **c**, 0.25 s vs. 1 s (p = 0.0314).

6.3 Pitx2^{ON} neurons activation generates staircase-like head displacements for longer stimulations

Our observations regarding the effect of stimulus duration on the head motion produced are in contrast with previous observations on the fixed tuning of premotor units in the SGI for particular angles of head displacements[170]. To study this phenomenon in more detail, we analyzed motion traces generated by long stimulations, paying particular attention to the trajectories described by the head-over-body rotations. We noticed that for progressively longer stimulations, deflection points could be detected along the kinematics trajectory (Fig. 6.4a). Such deflection points represented brief interruptions in the ongoing motion, appearing as reset points that divide the motion trace into "steps".

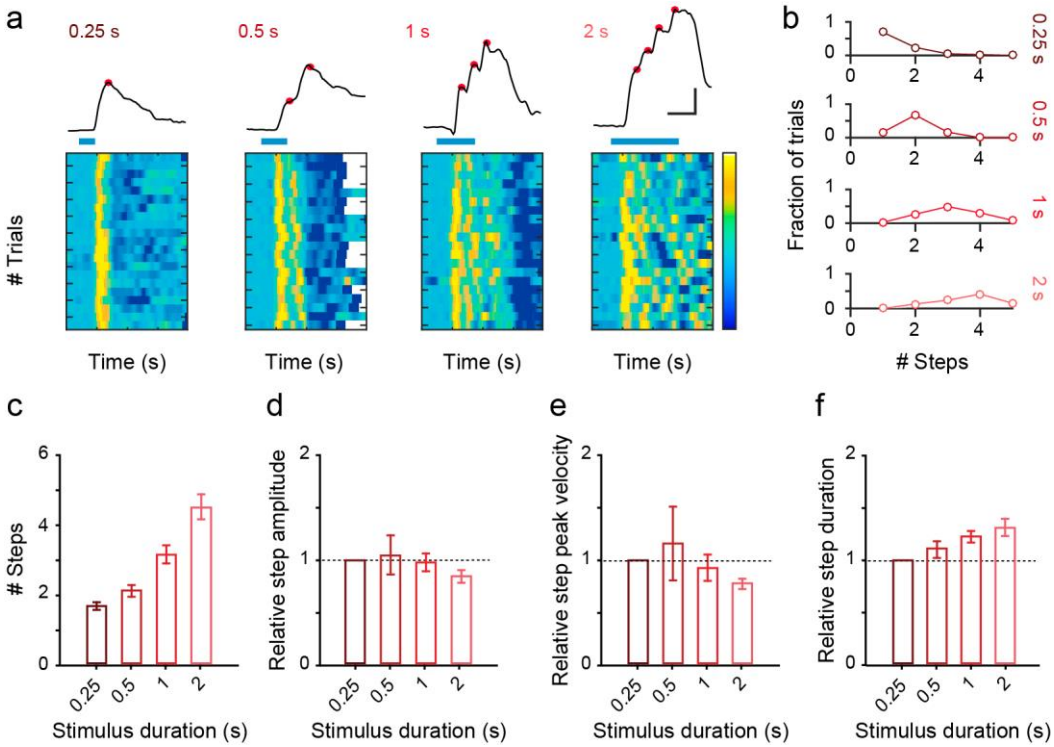

Figure 6.4 | Quantal nature of Pitx2^{ON} neurons-driven head motion.
a, Kinematics of head displacements in the yaw dimension for increasing duration of blue-light stimulation (0.25, 0.5, 1 and 2 s); note the step-wise trajectories for prolonged stimulations (top). Trial-by-trial identification of the deflection points giving origin to the step-wise kinematic was carried out in derivative space (bottom). High values (yellow colours) indicate sudden acceleration marking the onset of a head motion bout. **b**, Fraction of trials presenting a given number of steps for progressively longer stimulus duration (data shown in **a** and **b** represent examples from one animal, shown in Fig. 6.2). **c-f**, Average number of steps (**c**), step amplitude (**d**), velocity (**e**) and duration (**f**) for increasing stimulus duration across all animals relative to their characteristic vector generated with a 250 ms light stimulus ($n_{TRIALS/MOUSE}$ = 60; n_{MICE} = 12; $p_{AMPLITUDE}$ = 0.60; $p_{VELOCITY}$ = 0.58; $p_{DURATION}$ = 0.06).

The average number of steps detected in the motion traces increased with stimulation duration (Fig. 6.4b, c); the shortest stimulus (0.25 s) produced single-step head displacements, which we refer to as *characteristic vector* for a given stimulation site. The longest stimulation tested (2 s) produced instead an average of 4.5 ± 0.4 steps. Analyzed across all trials and animals tested, the average amplitude, duration and consequently velocity of these composing steps remained fairly constant among stimulus durations (Fig. 6.4d, e).

Taken together, these results support the view that the physiological motor output of individual Pitx2^{ON} modules is characterized by a fixed metric; when longer activation periods are imposed to a given module, the overall amplitude of movement produced is indeed greater, but this occurs through the production of a concatenated series of characteristic head movement vectors. The biological substrate of such "quantal" output of Pitx2^{ON} modules, with respect to head movements, is examined in greater detail in the *Discussion*.

6.4 Pitx2^{ON} neurons activation leads to small-amplitude, monotonic eye movements

Such stepwise kinematics closely resemble the "staircase" of identical saccades elicited by the electrical stimulation of the SGI in primates[56,63-65]. Hence, we assessed whether stimulation of Pitx2^{ON} neurons could also elicit eye movements. In order to do so, we implanted a head plate and two optic fibres in the SGI of *Pitx2-CRE::Rosa-LSL-ChR2-eYFP* mice, one in each hemisphere. We then recorded the right eye of the head-fixed animals using an infrared camera, while stimulating the contralateral (left) or ipsilateral (right) SGI (Fig. 6.5a, b). Indeed, stimulating Pitx2^{ON} neurons with a 250 ms continuous light pulse led to the execution of rapid, low-amplitude (< 5°) eye movements when applied to both the contralateral (Fig. 6.5c) and the ipsilateral hemisphere (Fig. 6.5d), suggesting a role of Pitx2^{ON} neurons in the full control of gaze shifts (combined head and eye movement). Concomitant pupil dilation was also recorded, indicating an increase in arousal in the animals upon Pitx2^{ON} neurons activation. Wild-type animals recorded under the same experimental conditions did not display similar light-triggered eye movements, proving that the application of laser stimulation on the animal's head does not lead to a reflexive eye rotation *per se* (Fig. 6.5e, f).

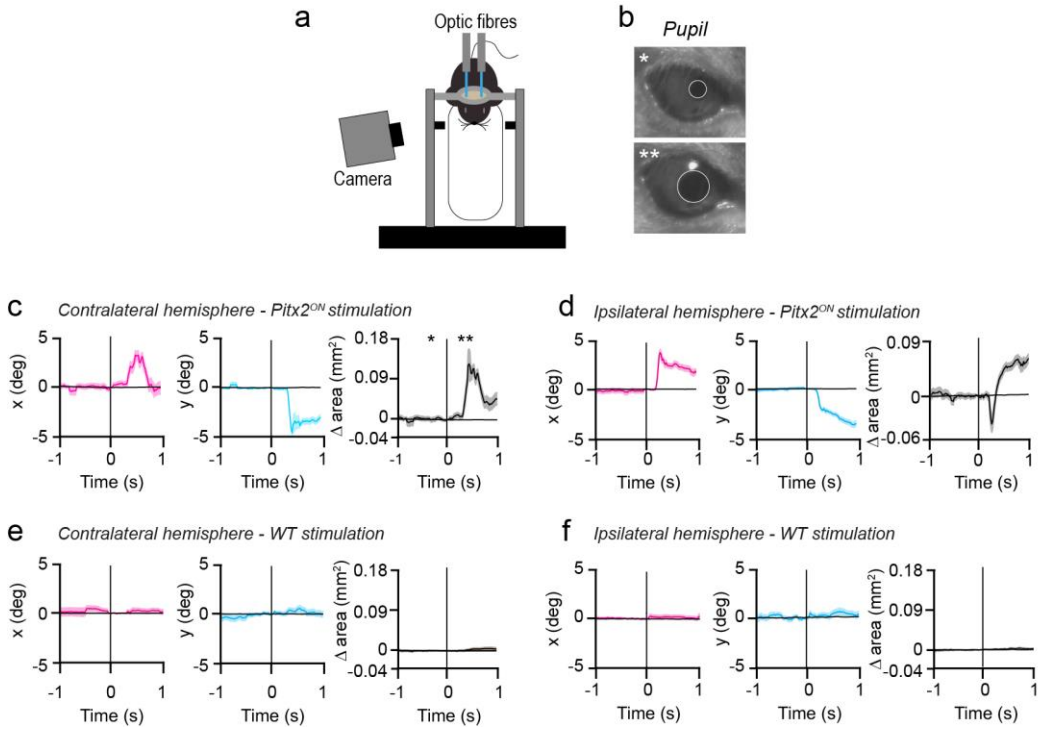

Figure 6.5 | Eye movements elicited by optogenetic stimulations of Pitx2^{ON} neurons.
a, Schematic of experimental setup for eye tracking in head-restrained *Pitx2-CRE::Rosa-LSL-ChR2-eYFP* animals. Two optic fibres were implanted: one in the left and one in the right hemisphere to record movements evoked by a contra- or ipsi-lateral SC stimulation with respect to the monitored eye (right eye). **b**, Frames from the eye camera showing changes in pupil dilatation (see panel **c**) taken before (one asterisk) and after (two asterisks) 250 ms blue light stimulation, with fitted ellipses (*white*). **c**, Examples of LTA of eye movements along the x (*magenta*) and y (*blue*) components, and of the pupil area (*grey*), calculated for blue light stimulation of 250 ms in the left hemisphere of a *Pitx2-CRE::Rosa-LSL-ChR2-eYFP* animal. **d**, Same as in **c** for the right hemisphere. **d**, LTA of eye position and pupil area, calculated for blue light stimulation of 250 ms in the left hemisphere of a control animal. **f**, Same as in **e** for the right hemisphere. (n_{MICE} = 3 for Pitx2::ChR2, n_{MICE} = 3 for controls, $n_{TRIALS/MOUSE}$ = 30).

Given our previous observations regarding head displacements, we wondered whether a step-wise increase in eye movement amplitude could be elicited through prolonged stimulation of Pitx2^{ON} neurons. Unlike what previously described for our study of head movements, here we tested only two durations of stimulation, namely 250 and 500 ms. This is because we assumed that, under our head-restrained conditions, mice would still be induced to produce fast, high-amplitude head rotations upon Pitx2^{ON} neurons stimulation; therefore, we ruled that longer stimulations might lead to an excessive level of stress in the animals. Additionally, stimulations of 500 ms were consistently efficient in revealing step-wise kinematics of head rotation in our open field setup (Fig. 6.4a), suggesting this stimulation protocol should be sufficient to reveal the existence of a similar control of eye movements. Indeed, when we tested our eye-tracking mice in the open field arena and optogenetically activated Pitx2^{ON} neurons, we observed the characteristic quantal nature of

light-triggered head rotations (Fig. 6.6a) and the increase in overall displacement amplitude along both yaw (Fig. 6.6b) and pitch (Fig. 6.6c) axes.

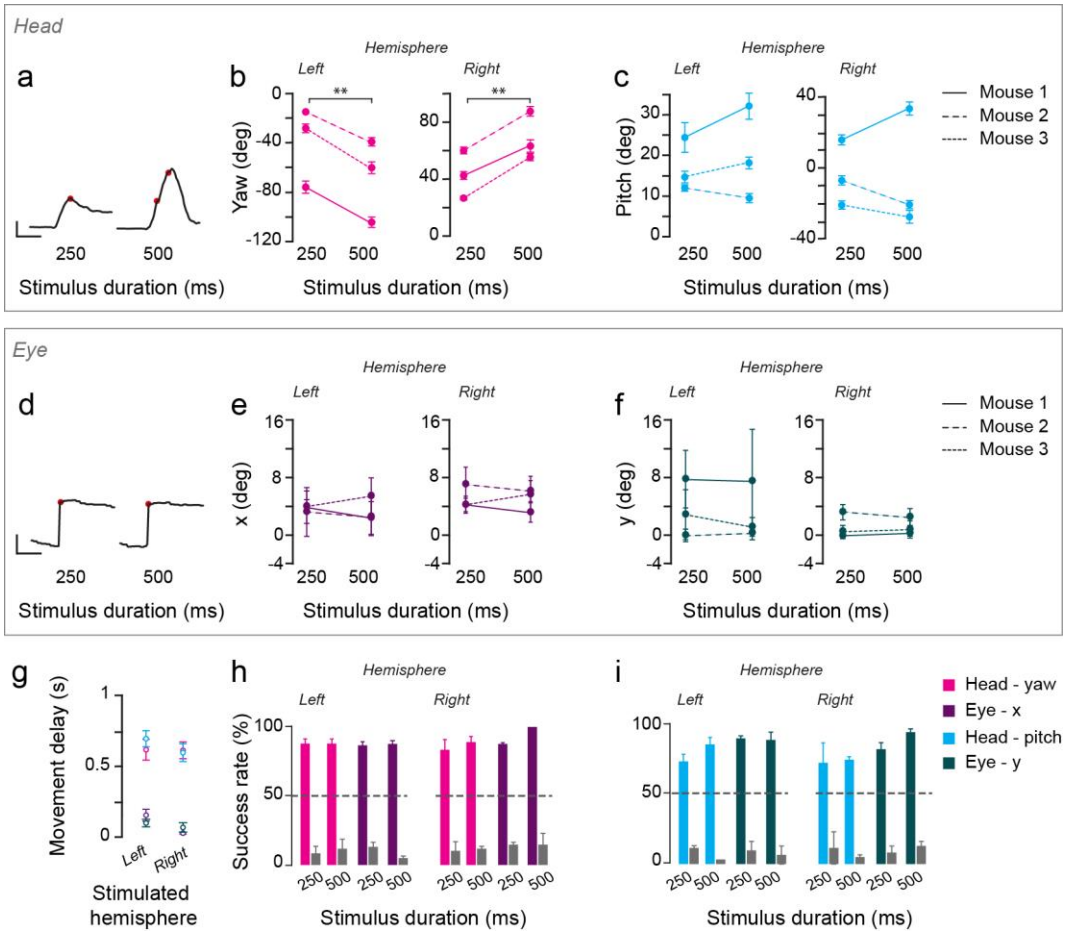

Figure 6.6 | Comparison of light-triggered eye and head movements.
a, Representative traces for yaw component of the head movement after 250 (left) or 500 ms (right) of blue light stimulation of the left SGI. Red dots mark a change in velocity for the head (scale bar: 20 deg, 1 s). **b,** Effect of stimulus duration on the head displacement angle for yaw after stimulation of the SGI in the left or right hemisphere (n_{MOUSE} = *3;* $n_{TRIALS/MOUSE}$ = 30; $p_{LEFT,YAW}$ = 0.008, $p_{RIGHT,YAW}$ = 0.006). **c,** Same as **b** for pitch movements (n_{MOUSE} = *3;* $n_{TRIALS/MOUSE}$ = 30; $p_{LEFT,PITCH}$ = 0.9334, $p_{RIGHT,PITCH}$ = 0.4251). **d**, Representative traces for x component of the eye movement after 250 (left) or 500 ms (right) of blue light stimulation of the left SGI. Red dots mark a change in velocity for the eye (scale bar: 2 deg, 1 s). **e**, Effect of stimulus duration on the eye movement in x after stimulation of the SGI in the left or right hemisphere (n_{MOUSE} = *3;* $n_{TRIALS/MOUSE}$ = 30; $p_{LEFT,X}$ = 0.11, $p_{RIGHT,X}$ = 0.0712). **f**, Same as **e** for y movements (n_{MOUSE} = *3;* $n_{TRIALS/MOUSE}$ = 30; $p_{LEFT,Y}$ = 0.4367, $p_{RIGHT,Y}$ = 0.72). **g**, Time of onset of motion after blue light stimulation for yaw (*magenta*) and pitch (*blue*) and for x (*purple*) and y (*dark green*) (n_{MOUSE} = *3;* $n_{TRIALS/MOUSE}$ = 30). **h**, Effect of stimulus duration on the probability of executing a head movement bout in yaw (*magenta*) and eye movement in x (*purple*) after the stimulation of the SGI in the left or right hemisphere. Grey bars for the effect of the stimulation in control mice in absence of ChR2 expression (n_{MICE} = 3, $n_{TRIALS/MOUSE}$ = 30). **i**, Effect of stimulus duration on the probability of executing a head movement bout in pitch (*blue*) and eye movement in y (*dark green*) after the stimulation of the SGI in the left or right hemisphere. Grey bars for the effect of the stimulation in control mice in absence of ChR2 expression (n_{MICE} = 3, $n_{TRIALS/MOUSE}$ = 30).

However, prolonged stimulations of Pitx2^{ON} neurons failed to elicit a staircase of saccadic eye movement in the same animals recorded in head-restrained conditions, driving instead monotonic eye movements whose amplitude remained constant with increased stimulation time (Fig. 6.6d-f). These eye movements were characterized by a much smaller delay from stimulus presentation compared to the head displacements elicited via stimulation of the same site (Fig. 6.6g), and were reliably generated along both horizontal and vertical components (Fig. 6.6h, i). These results are compatible with the hypothesis that Pitx2^{ON} neurons-mediated eye movements might be characterized by a stronger reflexive nature than the saccadic eye movements observed in primates.

6.5 Summary

This chapter summarizes our findings regarding the causative role of Pitx2^{ON} neurons in the generation of head movements. Using our double inertial sensor board to track head displacements in 3D in freely moving animals, we demonstrated that optogenetic activation of Pitx2^{ON} neurons is sufficient to reliably drive the execution of fixed motor plans for head rotations along all three Eulerian components. While we reported that longer light stimuli produce ampler head displacements, we show that this occurs via the summation of smaller events of similar amplitude, suggesting that indeed the motor output of Pitx2^{ON} modules obeys a fixed metric. As discussed in the *Introduction*, such staircase-like motion has been associated with saccades evoked by prolonged SC stimulation in primates and cats, suggesting that premotor groups in the SC produce motor commands characterized by a conserved quantal nature. However, sustained activation of Pitx2^{ON} neurons by optogenetic means in mice fails to elicit similar staircase-like movements of the eye, leading instead to small monotonic displacements. Taken together, our data suggest that Pitx2^{ON} neurons-mediated head displacements alone are a valid motor readout to understand principles of motor space encoding in rodents.

7. Topography of Pitx2^{ON} neurons-dependent movement vectors

Given that the metric of head motion produced appears to be an intrinsic feature of Pitx2^{ON} modules, produced via rate-independent coding, we next asked how the Pitx2^{ON} population is able to drive the execution of head movement along distinct vectors. As discussed in the *Introduction*, the existence of a topographic representation of saccadic eye movements in the motor layers of the SC has been described through micro-stimulation studies in higher mammals[59]. Because of the ethological relevance of such movements in rodents, we hypothesized that Pitx2^{ON} neurons might participate in the encoding of topographically organized head, rather than eye, displacements in mice. With this in mind, we investigated whether the positional identity of the activated Pitx2^{ON} module was the key determinant of the head movement metric and assessed the relationship between the produced head displacement vectors and the topography of Pitx2^{ON} modules.

7.1 Characteristic vectors of head movement vary across SC locations

To gain a preliminary indication of whether this speculation was corroborated by our experimental data, we performed a qualitative assessment of the distribution of head movement vectors in the SC based on the single optic fibre experiments reported in Chapter 6. We confirmed the coordinates of the implant site for each of the 12 mice used in this study (Appendix D, Panel a) and then plotted the characteristic vector for each mouse based on

these coordinates (Fig. 7.1). We were able to observe that the angles of displacement produced varied among animals in a way that seemed to correlate with the site of stimulation in the SC, and hence Pitx2^{ON} module, activated. More posterior implant sites were often associated with ampler displacement angles in yaw, together with the tightly coupled roll dimension (see Mouse 2, 5 and 6), than anterior sites (see Mouse 3, 4, 11 and 12). The representation of pitch movements also appeared to vary across stimulated SC locations; while in the majority of animals we observed a downward head displacement, optogenetic stimulation in the anteromedial portions of the colliculus led to upward movements instead (see Mouse 3, 4, 7, 11 and 12).

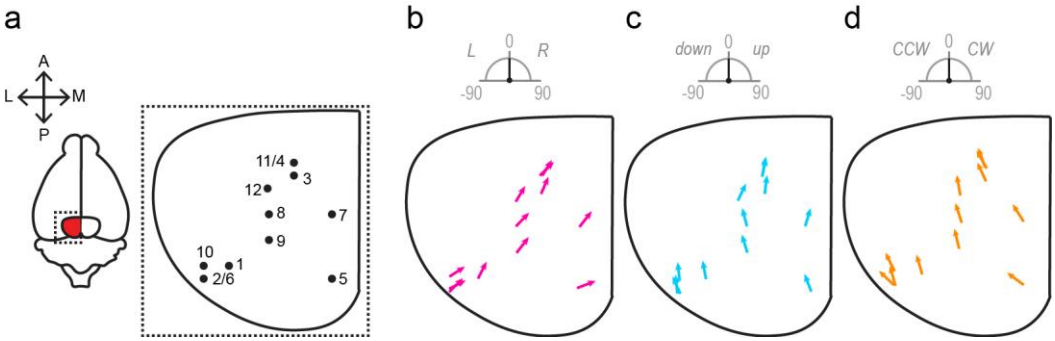

Figure 7.1 | Head displacement vectors vary across SC locations.
a, Top view summary of implant locations (numbers correspond to those shown in Appendix D). **b-d**, Characteristic movement vectors produced at any given implant site, decomposed in their yaw (**b**), pitch (**c**) and roll (**d**) components.

These qualitative observations suggest that indeed the metric of the head movements produced might be correlated to the coordinate of SC stimulation. However, by comparing motor responses across different animals, our interpretation of this topography is limited by our ability to faithfully assign precise implant coordinates to a given animal.

7.2 Multi-fibre array recordings reveal *Pitx2*-defined motor map in the SGI

One strategy to overcome these limitations is to individually stimulate multiple SC locations within the same animal and subsequently study the relationship among the motion kinematics produced. To this end, we implanted a custom-made 3x3 multi fibre array in the SGI, which allowed us to individually address nine SC locations for optogenetic stimulation (Fig. 7.2a-c, see *2.10.1 Experimental design*). We then applied a light stimulation pattern

consisting of repeating 250 ms pulses through one of the fibres in the array at a time. As mentioned in Chapter 6, we estimate that the resulting light stimulation would be sufficient to activate approximately one Pitx2^{ON} module, hence revealing whether the identity of the module is a key determinant of the metric of motion produced.

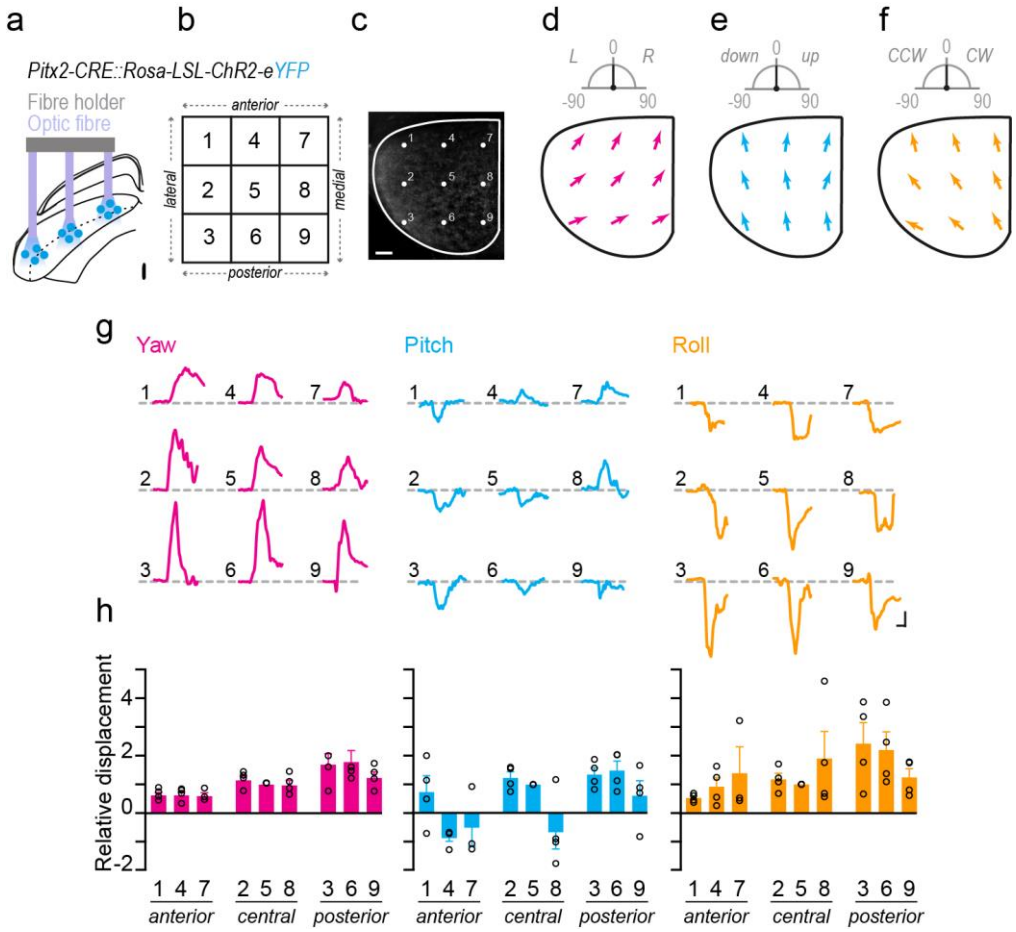

Figure 7.2 | Topography of Pitx2^{ON} neurons-driven motor plans.
a, **b**, Schematic of the optic fibre array (**a**) with fibre reference numbers (**b**). **c**, Schematic representation of array placement in the SC (top view) in a *Pitx2-CRE::Rosa-LSL-tdTomato* clarified brain (scale bar: 250 µm). **d-f**, Average movement vector produced in yaw (**d**), pitch (**e**) and roll (**f**) by light stimulation of nine SC locations from one representative animal. **g** Representative traces of the light-triggered three-dimensional head movement for each site shown in **d-f**, decomposed in yaw (*magenta*), pitch (*blue*) and roll (*orange*) components,. **h**, Average amplitude of the light-driven displacement for each site and each Eulerian component, relative to the amplitude of head displacement generated at position 5 within each array ($n_{TRIALS/POSITION}$ = 40*;* n_{MICE} = 4). Statistically significant comparisons are: Pos1-3 (p = 0.0005), Pos1-6 (p = 0.0006), Pos2-3 (p = 0.009), Pos2-6 (p = 0.0102); Pos3-4 (p < 0.0001), Pos3-5 (p = 0.0018), Pos3-7 (p = 0.0001), Pos3-8 (p < 0.0001), Pos3-9 (p = 0.0085), Pos4-6 (p < 0.0001), Pos5-6 (p = 0.0021), Pos6-7 (p = 0.0002), Pos6-8 (p < 0.0001), Pos6-9 (p = 0.0096).

We found that the head movement vector produced varied across different stimulation locations in the same animal. We observed that all elicited movements were strictly

contralateral to the site of stimulation; in yaw and roll, their amplitudes increased from anterior to posterior sites, while remaining relatively constant along the mediolateral axis. Both upward and downward pitch directions were mapped on the hemi-lateral SC, with upward pitch being represented in the anteromedial portions of the SC and downward pitch in the posterior-lateral region (Fig. 7.2 d-h).

Overall, these experiments confirm the topographical nature of the SGI motor vector map for head movements in mice and provide further support to the hypothesis of the module dependence of this motor representation. However, none of the data reported so far provides evidence of the tuning of individual Pitx2^{ON} neurons within a module for a particular angle of displacement; additionally, while these findings indicate that Pitx2^{ON} neurons are capable of driving head motion on exogenous stimulation, they do not clarify whether they are recruited physiologically during spontaneous directional head movements.

7.3 Single Pitx2^{ON} units display motion tuning coherent with module output

We further investigated whether spontaneous activity of individual Pitx2^{ON} neurons was predictive of the onset and metric of subsequent head displacements. To do so, we recorded Pitx2^{ON} neurons activity using optetrodes implanted in *Pitx2-Cre::Rosa-LSL-ChR2-eYFP* mice (Fig. 7.3a).

Following application of a light stimulus pattern consisting of 5 ms pulses presented at 30 Hz, we were able to isolate Pitx2^{ON} units from our extracellular recordings on the basis of the latencies of their responses to light stimulations (< 5 ms, Fig. 7.3b).

We then tracked the activity of Pitx2^{ON} cells during a naturalistic foraging task while simultaneously monitoring head kinematics in an open field arena. Our results show that Pitx2^{ON} neurons activity was highly correlated to, and predictive of, the metric of the produced head displacements (Fig. 7.4b, c); their firing activity preceded the onset of motion, as demonstrated by the z-score of neural activity significantly increasing prior to motion onset (Fig. 7.4f, g), suggesting that Pitx2^{ON} neurons are indeed involved in the initiation of motor plans of a fixed metric.

.

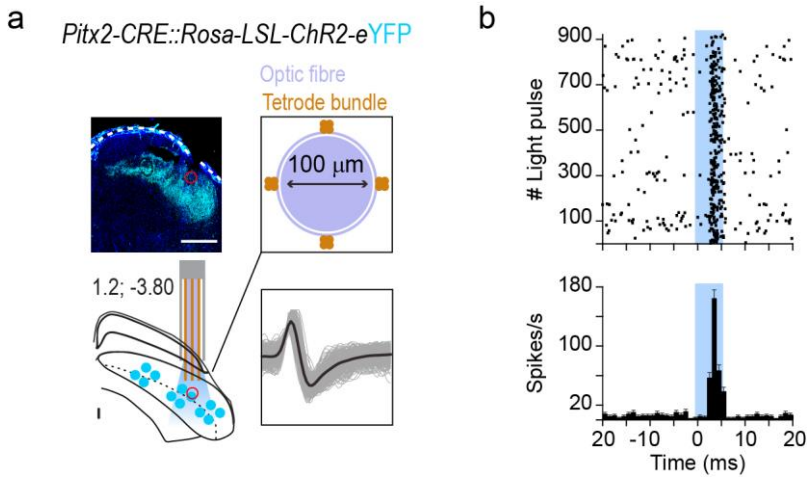

Figure 7.3 | Optetrode design and Pitx2^{ON} units isolation.
a, Optetrode targeted to the SGI of a *Pitx2-CRE::Rosa-LSL-ChR2-eYFP* mouse, with relative histological confirmation of implant position (left panels, scale bar: 500 µm). Optetrode design (top right): four tetrode bundles (*gold*) are attached around the fibre optic core (*blue*). Example of spike-sorted waveform of an isolated unit expressing ChR2 (bottom right). **b**, Raster plot (top) and peri-stimulus histogram (bottom) for the single unit in **a** during multiple trials of blue light stimulation (5 ms, *shaded area*).

Moreover, the optetrode approach also allowed us to compare directly, within the same animal and recording site, the metric of motion following the onset of Pitx2^{ON} neurons activity (STA, Fig. 7.4e), with the metric of head movements produced by the optogenetic stimulation of the area (LTA, Fig. 7.4d). We observed that LTA and STA values were always in the same direction and presented closely matching metrics. This suggests that the activity of single Pitx2^{ON} neurons within one module is predictive of the motor output of the module as a whole.

Overall, these findings indicate a physiological role for Pitx2^{ON} neurons in dictating the execution of head movements, as well as encoding their precise metric. While this electrophysiological approach does not allow us to study population dynamics, hence providing conclusive evidence regarding the coherent firing preference of neurons within a module, for most neurons recorded we observed a correlation between STA and LTA values. This is compatible with the hypothesis that individual neurons within a single module display tuning to head displacements that correspond to the motor output of the module.

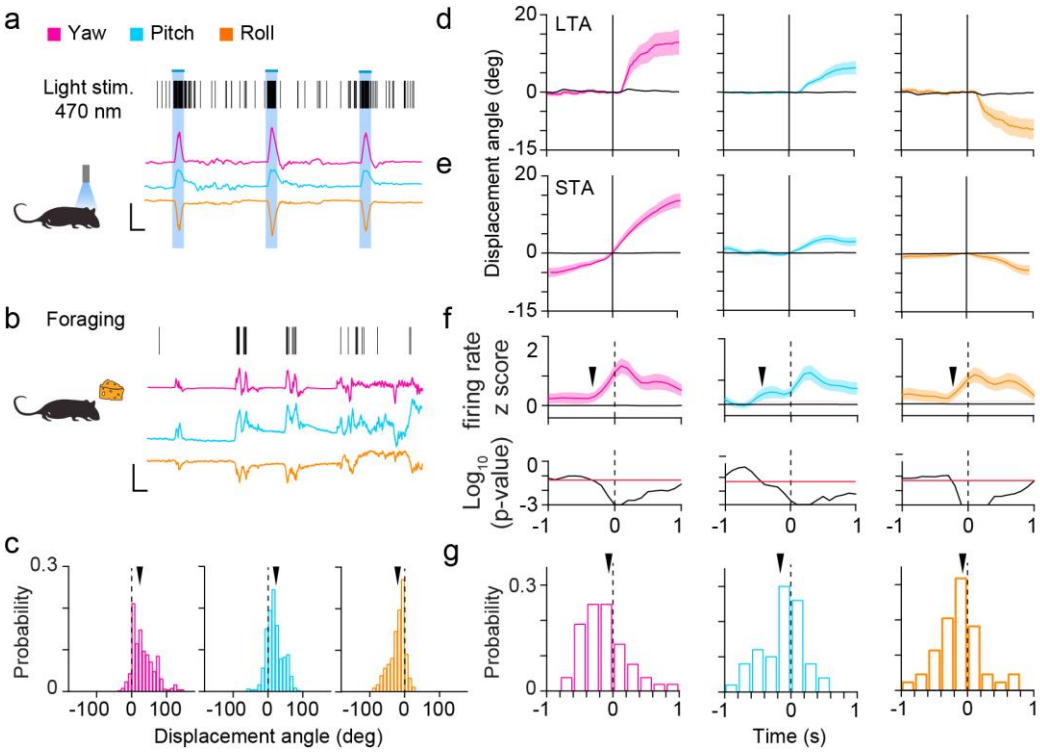

Figure 7.4 | Physiological recruitment of Pitx2^{ON} neurons for head displacements during foraging.
a, Example spiking activity from an optotagged unit upon blue light stimulation during open field explorative behaviour, aligned to the simultaneously recorded head displacements in yaw (*magenta*), pitch (*blue*) and roll (*orange*) components (scale bars: 250 ms, 20 deg). **b**, Same as in **a**, for the same unit recorded during foraging behaviour in the absence of blue light stimulation. **c**, Distribution of yaw, pitch and roll head movements following spiking activity of an example optotagged unit. The characteristic angle for each unit was measured as the mean of these distributions (black arrowheads). **d-e**, Light-triggered average (LTA, **d**) and spike-triggered average (STA, **e**) of head movements in the yaw (*magenta*), pitch (*blue*) and roll (*orange*) components calculated for the optotagged neuron in **c**. LTA and STA were tested for significance against shuffled data (grey curves). **f**, Top panel: z score of firing rate for the optotagged neuron in **e** around the onset of head movement (dashed line), calculated separately for yaw, pitch and roll displacements. The z score is derived from firing rate and provides a normalised measure of cell activity; it is calculated at each timepoint as: [(instant firing rate – average firing rate in recording session) / standard deviation of firing rate in recording session]. The time of firing onset (black arrowheads) was identified by comparison against null distributions obtained from shuffled data. Bottom panel: statistical parameters relative to z score values around head movement onset (dashed line), expressed as Log_{10} of p-values obtained from comparison within each time bin of z score against null distribution plotted in top panel. Red line represents significance threshold. **g**, Distribution of firing onset across optotagged units with respect to the onset of yaw, pitch and roll movements. Arrowheads mark the mean value (n_{UNITS} = 13, n_{MICE} = 2).

7.4 Summary

In this chapter, we provide evidence of the topographical organization of Pitx2^{ON} neurons-dependent head movement vectors in the murine SC. Using multi-fibre arrays for optogenetic stimulation, we show that exogenous activation of distinct Pitx2^{ON} modules leads to the execution of different motor plans. These movement vectors appear to be arranged in a motor map reminiscent of those organizing saccades in the SGI of primates and cats. We used *in vivo* electrophysiology to study the physiological role of Pitx2^{ON} units during foraging tasks; we observed that the activity of Pitx2^{ON} neurons precedes the initiation of movements of a fixed metric. Our preliminary results suggest that neurons within a module might share similar motion tuning, which presents matching metric to the motor output of the module itself.

Altogether, our results are compatible with the existence of a discrete representation of motor space for head displacements in the murine SC; we hypothesize that the modularity highlighted by *Pitx2* expression represent the physical substrate for this map, whereby each Pitx2^{ON} module encodes head displacements along a fixed movement vector.

8. Discussion

While decades of neurophysiological research in higher mammals have implicated the SC in the control of orienting behaviour, the precise network organisation and associated computations that govern its sensorimotor integration function are yet to be elucidated. We propose that adopting a genetic approach can represent a meaningful strategy to isolate individual layers of this network, identify their associated pre- and post-synaptic partners and investigate their relevance to collicular output. Following this strategy, we identified a physiologically homogeneous glutamatergic population in the murine SGI, characterized by the expression of the transcription factor Pitx2, which provides a modular representation of motor space for head rotations.

In this chapter, I will discuss our findings regarding the Pitx2^{ON} population, both in terms of their connectivity and functional properties, as well as the implications that such modular representation of space might have on current models of collicular function.

8.1 Considerations on genetic strategies

Collicular circuits are known to contain a wide array of different neuronal types, most of which have been defined in light of their morphological features; the large majority of the characterized populations are relevant to the superficial visual layers. Based solely on their anatomical properties reported by numerous Golgi studies and intracellular stainings in

slices, SGS neurons have been categorized into horizontal cells, vertical cells (further divided into narrow and wide field type based on the distribution of their dendritic arbors), stellate cells and marginal cells[97]. In light of their specific morphology, various speculations have been formulated regarding the type of information that might be processed by each of these classes; however, at present there is very little indication of the correlation between structural and functional characteristics of collicular neurons. Some evidence is provided by experiments that combined intracellular recording *in vivo* and horseradish peroxidase staining, which suggested there is a significant correlation between receptor field types and cell morphology[196]. Nevertheless, we are still far from fully appreciating how different neuronal types operate together to interpret the incoming sensory flow and convey this information in a meaningful manner to the motor domain. Neuronal classification is even more obscure for the intermediate layers of the SC; the SGI contains several types multipolar cells, which in cats and primates have been subdivided in two main classes: larger X-cells are located more ventrally in the layer and project to contralateral brain stem nuclei, sending few collaterals within the SGI itself; T-cells preferentially populate the more dorsal aspect of the motor SC domain and send extensive collateral fibres to the contralateral SC, as well as projecting to both contralateral and ipsilateral brain stem via the predorsal bundle[197]. An indication of the distinct functional relevance of these two morphological classes comes from physiological studies in monkeys, which have revealed a correlation between the activity of T-cells, but not X-cells, and the occurrence of spontaneous saccades[198]. Again, these observations yield little insight into the organizing principles of collicular circuits for sensorimotor integration and their associated computations.

8.1.1 Molecular identity of neurons as a key to circuit function

We started from the assumption that assigning molecular identity to cells in the SC might provide a previously unexplored potential to isolate functional cell types in collicular networks; these neuronal groups would probably correlate to an extent to the morphological classes described so far, but the genetic approach would additionally grant selective access to these groups for their *in vivo* characterization.

In order to assess the degree to which the genetic identity of neurons can explain their cellular phenotype, we initially provided a classification of SGI cells based on their electrophysiological, rather than morphological, profiles. The physiological profile of a cell is intrinsically linked to some of its anatomical features, which more precisely affect its passive membrane properties, as well as providing an indication of the combinations of ion channels they express, reflected in their firing profile properties. Using electrophysiological

parameters obtained from *in vitro* recordings as classifiers of neuronal diversity provided a high-throughput and comprehensive approach for the assessment of functional heterogeneity that exists among SGI neurons. Employing an automatic clustering algorithm, we identified five functional groups of neurons in the layer based on their passive and active membrane properties (Fig. 3.1a, b), which correlate with previously identified electrophysiological types in the area[199]. We found that both glutamatergic and GABAergic SGI neurons were spread across multiple of the functional classes we identified, albeit following different distribution patterns (Fig. 3.1d). The physiological diversity of GABAergic neurons is largely recognized, especially in light of the well-characterized contribution of individual functional groups to cortical computations[200]; the heterogeineity of glutamatergic neurons is instead often under-represented in the literature, so that we commonly think of excitatory neurons across diverse brain regions as the principal encoders and distributors of the information to which the area is dedicated. Our *in vitr*o recordings suggest that the expression of glutamatergic markers, vGluT2 in this instance, is associated with cells displaying distinct electrophysiological profiles, possibly representing neurons that cover different roles within the collicular network. Through an RNAseq screen designed to identify genetic elements enriched in the motor layers of the SC compared to the sensory domain, we identified a molecular marker, *Pitx2*, which labels exclusively a physiologically homogeneous portion of the glutamatergic population of the SGI (around 44% of vGluT2^{ON} neurons, Fig. 3.3). Additionally, we observed that Pitx2^{ON} neurons are non-homogenously distributed in the layer, defining instead anatomical clusters along the medio-lateral and anterior-posterior axis of the SC (Fig. 3.7). These findings indicate that genetic dissection of neural circuits is not only instrumental for the isolation of distinct functional classes of neurons, but can also reveal principles of circuit design to which other experimental strategies remain oblivious.

In this study, we have focused our attention on the characterization of the connectivity pattern and functional relevance of the Pitx2^{ON} population, formulating hypotheses on the structure-function relationship of the observed modularity. The question remains as to what network function the remaining glutamatergic population is responsible for; are they an output population involved in the orchestration of additional motor plans? Or are they instead local interneurons, whose study might provide interesting insights in the organisation and computations of intracollicular networks? We have implemented an experimental strategy that would allow us to target genetically this Pitx2^{OFF}::vGluT2^{ON} population; we generated a double recombinase line by crossing Pitx2-CRE and vGluT2-FLP mice, and designed an FRT-not-FLEX AAV construct that would drive the expression of fluorescent markers or functional molecules in cells that contain a FLP recombinase, but have no

detectable levels of CRE. With this viral approach, we will be able to replicate the line of work described here for Pitx2^{ON} neurons and present a full picture of the role of glutamatergic neurons of the SGI in collicular function.

Additionally, our RNAseq screen identified a large number of plausible candidates for the labeling of subgroups of neurons in the motor domain of the SC (Fig. 3.2). Using multiplex FISH, we could perform a high-throughput assay to validate the results of the genetic screen and identify transcripts with interesting histological features. Many of our top hits, including Tfap2d, Onecut2 and Onecut3, were transcription factors, potentially involved in the specification of cell identity and differentiation during development. As a consequence, many of these transcripts hold the potential to be valid markers for neurons with distinctive physiological properties and connectivity patterns, providing additional entry points for the functional dissection of collicular networks.

8.1.2 *Pitx2* gene: beyond cell labeling

Throughout this study, we have referred to the expression of *Pitx2* as a mere marker for targeting a select population of neurons in the SGI. Little attention has been paid instead to the molecular role this transcription factor covers in the expressing cells. While we demonstrated the Pitx2^{ON} cells are sparsely distributed in the brain outside the SGI and MM (Fig. 3.5), expression of *Pitx2* is extremely ubiquitous during development in a variety of tissue types and organs, most prominently in skeletal muscle, urinary bladder and pituitary gland[201-203], which suggests that Pitx2 might lead to the establishment of distinct cellular phenotypes according to the combination of additional transcription factors with which it is expressed. Even within the nervous system, Pitx2 appears to be related to heterogenous cellular interactions; while cross-species approaches have suggested a conserved function for Pitx2 in controlling GABAergic differentiation as homologous of the nematode *unc-30*[204], cholinergic identity has been associated with spinal Pitx2^{ON} interneurons[205,206]. Adding further to this complexity, our results suggest that, at least in the adult tissue, Pitx2^{ON} neurons have a glutamatergic phenotype in the SC (Fig. 3.3d). Altogether, we can speculate that *Pitx2* expression *per se* is not a good predictor of the neurotransmitter identity that neurons will adopt in the mature stage of their lives. An interesting observation of our study is that *Pitx2* expression is maintained in adult SGI (Fig. 3.6), which is somewhat unexpected of a transcription factor conventionally considered to be involved in neural development, neurogenesis and cell differentiation (as confirmed by our gene ontology analysis). While its presence might be not be linked to a universal transcriptional programme across the brain,

we could speculate that in the SC Pitx2 is a key player in the definition of the cell identity of the expressing cells, as well as being necessary for its post-developmental maintenance. Pitx2 might therefore drive the expression of gene sets necessary for the function of this modular population. A fascinating hypothesis is that this transcription factor might coordinate the expression of a set of membrane channels that confer Pitx2^{ON} neurons their unique and homogeneous electrophysiological profile, perhaps ideal for their operation as sensorimotor integration units. Alternatively, Pitx2 might be important to promote the expression of transmembrane receptors (eg. nicotinic and muscarinic ACh receptors[207], D2 receptors[208]) to make this population exclusively capable of interpreting incoming inputs from neuromodulatory systems.

8.2 Circuits for motion and attention

The prominent role of the SC in processes of sensorimotor integration is bound to be the result of coherent integration of sensory, motor- and internal state-related inputs. A large number of anatomical studies in several model organisms, summarized in the *Introduction*, have contributed to our understanding of where sensory and motor information is conveyed to the SGI. Strikingly, many collicular inputs terminate in patches in the intermediate layers of the SC; by studying the anatomical relationships among these afferent compartments, Illing and Graybiel hypothesized the existence of motor domains in the SGI, consisting of the constellation of AChE-rich patches and their inputs from SNr, PPN and the prefrontal cortex[119]. They speculated that AChE-poor zones would represent instead sensory domains of the SGI, receiving inputs from the inferior colliculus and the somatosensory and visual association cortices[121]. However, being unable to target specifically collicular neurons that populate these putative functional domains within the SGI, Illing and Graybiel could not precisely reconstruct the anatomical convergence of inputs of different sensory and motor modalities onto distinct neuronal groups, nor study their associated projection patterns.

8.2.1 Pitx2^{ON} modules as sensory-motor integrator units

Through our genetic approach, we have reconstructed the presynaptic network of the patchy Pitx2^{ON} population, revealing interesting principles of input convergence in the SGI. Pitx2^{ON} neurons are the direct recipients of synaptic input from previously characterized patchy afferents to the SC, importantly SNr and PPN (Fig. 4.2). Additional histological evidence from the lab not shown in this thesis confirms that indeed Pitx2^{ON} modules are juxtaposed to

the characteristic cholinergic patches of the SGI. Combined with the experimental support for the causative role of Pitx2^{ON} neurons activation in generating head movements presented in this study (Fig. 6.2), we can conclude that Pitx2^{ON} modules most closely resemble the motor domains described by Illing and Graybiel. We observed that the vast majority of inputs to Pitx2^{ON} cells were generated from within the SGI itself, with many of the input cells located between Pitx2^{ON} zones. With reference to Illing and Graybiel's model, this suggests that a significant axis of communication ought to exist between sensory and motor SGI domains, although the nature of these horizontal interactions cannot be extrapolated from our tracing data. While studies of collicular pre-synaptic networks have been interpreted in favour of a clearly segregated organisation of motor and sensory functional areas in the intermediate layers of the SC, our data suggest that, at least in the murine SGI, premotor units resident in putative motor domains are direct recipients of sensory information as well. In particular Pitx2^{ON} neurons receive abundant synaptic input from pyramidal neurons located in layer 5 of S1 (Fig. 4.2), suggesting that sensory information can also be relayed directly onto premotor units of the SC. Based on existing evidence in support of the columnar organisation of interlaminar connections from *in vitro* studies, visual information is also probably conveyed to Pitx2^{ON} neurons from cells in the overlaying portions of the SGS, where we reported a substantial concentration of input cells (Fig. 4.2). Finally, the IC provides a major source of input, most likely related to the auditory sensory modality, to Pitx2^{ON} cells, together with a more modest contribution directly from AUD1 (Fig. 4.2, 3).

Our findings are obviously in line with the previously proposed modular organisation of collicular networks, although they challenge the hypothesis that such modularity might be instrumental in defining sensory and motor domains in the SC. Rather, Pitx2^{ON} modules appear to be the site of convergence of multiple cortical and subcortical inputs, conveying both sensory and motor-related information. In light of the topographical representation of visual, auditory and somatosensory information in the SC, these modules may act as direct integrators of sensory inputs of various modalities relative to a given spatial location, creating a local representation of portions of space as sampled through multiple sensory strategies. Hence, modularity of the premotor Pitx2^{ON} neurons gives origin to a spatial-motor register addressable by cortical and subcortical inputs for the execution of accurate and precise voluntary actions towards desired positions in space.

If the full spectrum of sensorimotor representations is indeed relayed directly on Pitx2^{ON} modules, then what is found in the Pitx2^{OFF} gaps? The Pitx2^{ON} population represents only around a fourth of the total neuronal population of the SGI, and under half of its

glutamatergic one. It is reasonable to imagine that many of the Pitx2^{OFF} cells in the SGI might be local interneurons. An important consideration to make is that in our study we have never considered the exclusivity of the characterized input areas for the Pitx2^{ON} population. In fact, it may be plausible that both motor and sensory patchy inputs would also be distributed onto local interneurons within the dendritic arborisations of Pitx2^{ON} modules, and then relayed to our genetically defined population (in line with our observation of extensive input from SC_{iga}, Fig. 4.2, 3), providing an additional level of integration. Furthermore, the functional output of Pitx2^{ON} neurons is strictly correlated to the role that the SC plays in orienting, but we were not able to trigger any innate behaviour upon optogenetic activation of Pitx2^{ON} neurons, a function also largely associated with collicular circuits[189,209-211]. Anatomical studies in rats have suggested that segregated anatomical inputs to sub-regions of the SGI are associated with approach and defense responses[212]; these observations suggest that different neuronal groups in the SGI, with their unique associated connectivity patterns, might account for different aspects of collicular function.

8.2.2 Links between attention and motor performance

In this study, the relevance of collicular Pitx2^{ON} neurons activity in behavioural performance has been studied in light of its prominent efferent projections along the cephalomotor pathway, hence with a strong focus on their orchestration of orienting movements of the head. Nonetheless, it should be discussed that a large proportion of Pitx2^{ON} fibres originating in the SGI terminate in thalamic nuclei (Fig. 4.1) and are unlikely to be directly involved in the execution of head rotations. Instead, inputs to the thalamic nuclei are probably involved in attentional processes described in the *Introduction*. The experimental design that we adopted in our anterograde tracing does not allow us to determine whether individual Pitx2^{ON} neurons contribute to both ascending and descending projections through collateral decussation, or if rather different subgroups within the Pitx2^{ON} population provide separate streams of information along the two pathways. Demonstrating which of these hypotheses is a faithful representation of the organisation of collicular networks would be achievable injecting retro-AAVs[213] with distinct fluorescent markers in the thalamic nuclei and in a relevant nucleus of the reticular formation (eg. MDRF), and then look at the levels of co-expression of the markers in cell bodies of origin in the SGI. Without this experimental evidence, we could maintain the assumption that the expression of *Pitx2* defines a highly homogenous neuronal population, also in terms of connectivity patterns. This would imply that upon activation, Pitx2^{ON} cells would send motor commands down the cephalomotor pathway to initiate head rotations, and concomitantly influence thalamic nuclei in control of attention. At first, it might seem difficult to envision a role for premotor neurons for goal-

oriented movements in shaping processes of attention; in fact, the current thinking about attention is that of a causal agent, a "zoom lens" that can influence processes of sensorimotor integration by acting as a filter on the incoming sensory influx[214]. This view of attention has been corroborated by a large number of neurophysiological studies that have demonstrated that, for example, neurons in sensory cortices modify their firing according to how attention is allocated during perception[215]; this modulation is the result of cortical computations that implement a competitive mechanism, resulting in the enhanced representation of some signals at the expense of others[135,216,217], consistent with the filter-like properties of attention. This model proposes that representation competition would be further refined by feedback "priority" signals produced at later stages of processing, provided by frontal and parietal cortex[218], as well as the SC[219]. This model is of course compatible with our anatomical observations, so there is no *a priori* reason to exclude that Pitx2^{ON} neurons might be ultimately affecting cortical representations.

However, we could also envision an alternative model for how the SC shapes this higher cognitive function. In an opinion article published in 2014, Krauzlis and colleagues propose a very different way of thinking about attention, suggesting it may be an effect of the interpretation of sensory and other data regarding our internal state, rather than its cause[220]. The article presents an eloquent argumentation for this model, as well as substantial experimental evidence in favour of this novel framework. For the purposes of this discussion, it is perhaps sufficient to describe the key features of this framework and how they would be compatible with our anatomical data. Krauzlis and colleagues criticize the current model of attention as the zoom lens that guides sensory perception as it appears to demand for what they refer to as a "homunculus" to aim the spotlight; they argue that instead we should be able to define the circuit properties that underlie attention without ever using the word. They start by considering that good decision-making relies ultimately on the identification of the current state of an organism, which is the result of the integration of inputs regarding external sensory cues, the internal state of an animal and their on-going needs. A subject can create many templates for possible states, each of which would differ in the weights it assigns to the various inputs. The template that provides the best match would therefore be selected as the system's interpretation of current state. According to Krauzlis and colleagues, attention can be explained as the competition between possible states, rather than for the representation of sensory information.

If state estimation is the key computation underlying attention, then it is reasonable to presume that the basal ganglia would assume a central role in this cognitive feature in light of their involvement in value-based motor and non-motor decision-making[221]. In the context

of SC-mediated visual attention, this provides an attractive model since several lines of evidence suggesting that collicular influence on attention is not mediated by the visual cortex[96] have left us looking for alternative pathways through which this modulation might occur. Indeed, the SGI forms both direct and indirect connections to the basal ganglia[97]; Pitx2^{ON} neurons themselves contribute indirectly to basal ganglia innervation through their connection to the PF (Fig. 4.1), which constitutes the primary source of thalamic input to both the direct and indirect pathway of the striatum[222], and directly by contacting SNc neurons, possibly providing information regarding the detection of salient sensory events[223]. Conceptually, providing feedback regarding a process of goal-oriented movement selection and initiation seems better suited to support competition for the definition of current state, rather than to shape sensory perception. Knowledge of the genetic identity of SGI neurons contributing to this line of communication from the SC to the basal ganglia opens new avenues for the investigation of this novel model of attention.

8.3 Mapping gaze in the SC

8.3.1 Optogenetic investigation of collicular motor output

In this study, we used optogenetics tools coupled with a sensor board-based technology to study the effects of Pitx2^{ON} neurons activation on head-over-body rotations in 3D. We found that short (250 ms) pulses of light were sufficient to trigger precise movements of the head relative to the body at a high success rate, along all axes of rotation (Fig. 6.2). Using optetrodes, we were also able to investigate the physiological recruitment of Pitx2^{ON} neurons while mice were foraging in an open field arena. This complementary experiment revealed that indeed Pitx2^{ON} units are motor-related in nature (Fig. 7.4); with their activity preceding the onset of head motion, we deemed that these neurons would be driving movement initiation. Furthermore, Pitx2^{ON} units appeared to display fixed tuning for particular vectors of head rotations. A preliminary analysis of this small dataset of isolated units suggested that STA (angle for which the cell is tuned) and LTA values (angle produced by the optogenetic activation of the module) were correlated, suggesting that individual Pitx2^{ON} neurons within a module might encode angles of displacement similar to the motor output of the module as a whole. Possible experimental strategies to investigate this preliminary observation further are discussed later (see *8.5.1 How does the Pitx2^{ON} module operate as a unit?*).

Consistently with this hypothesis of fixed motor tuning of Pitx2^{ON} neurons, we reported that the metric of the motion produced by optogenetic stimulation of Pitx2^{ON} neurons could not be modified according to the rate of stimulation applied; we observed that short light pulses delivered at 30, 40 or 50 Hz for 250 ms produced the same extent of motion as a continuous step of light of the same duration (Fig. 6.3). In our *in vitro* characterization of optogenetically induced cell firing in Pitx2::ChR2 units, we observed that with higher stimulation frequencies or during continuous optical stimulation, Pitx2^{ON} cells would only reach around 30 Hz of firing frequency (Fig. 6.1), which would provide a simple explanation for this apparent lack of effect of stimulation frequency on the metric of movement produced. However, it would be inaccurate to assume that the observed pattern of optogenetically induced firing *in vitro* would provide a direct indication of the behaviour of Pitx2^{ON} cells i*n vivo*, as many anatomical features of the network are lost in slices. In fact, based on previous reports on the frequency of burst firing displayed by motor-related cells in the murine SGI[170], as well as our recording of their firing profile upon injection of current *in vitro* (Fig. 3.4), our prediction would be that Pitx2^{ON} units can indeed fire at rates higher than 30 Hz *in vivo*. Perhaps the non-linear correlation of firing and optogenetic stimulation frequency is more indicative of a limitation in ChR2 kinetics[224], than informative of the intrinsic firing capabilities of Pitx2^{ON} cells. To provide more conclusive evidence of the rate-independent coding of Pitx2^{ON} neurons, we should rather exploit our optetrode recordings to assess the physiological firing rates of Pitx2^{ON} cells, as well as their supra-threshold membrane responses to the various light patterns imposed. Although it is very likely that the different light patterns we imposed on Pitx2^{ON} modules are triggering distinct firing frequency in the affected neurons, this approach would elucidate the relationship between stimulation parameters and cell response, reinforcing our hypothesis of rate-independent coding.

Our experiments indicated that the motor output of a given Pitx2^{ON} module could instead be clearly modulated by the duration of the optical stimulation applied (Fig. 6.3), although we reported that this happens via the repetitive execution of the characteristic vector that the module encodes for (Fig. 6.4). At present, we cannot provide a definitive explanation as to what circuit mechanisms are leading to such behaviour. Are longer stimulations leading to non-physiological repetitions of bursts of activity in individual Pitx2^{ON} neurons? Or is it rather the effect of a gating mechanism occurring downstream of collicular regions? Again, our optetrode approach could provide significant insight into this question; recording the activity of isolated Pitx2^{ON} units during prolonged optogenetic stimulation, we should be able to temporally correlate the firing pattern of isolated units to the individual steps of the

staircase-like movement performed by the animal and rule in favour of one of the proposed hypotheses.

All the experimental evidence summarized above supports the view that the metric of the produced head motion is a fixed property of Pitx2^{ON} modules, suggesting that different modules are able to trigger movements along different vectors. We therefore tested the effects of optical stimulation in different collicular locations, hence activating different Pitx2^{ON} modules, with the intention to extrapolate organizing principles of the representation of motor space in the SGI. When characterizing naturalistic head-over-body displacements in freely moving animals, we observed that the torsional component of head rotations co-varies with yaw movements (Fig. 5.4a), possibly representing a simple anatomical constraint linked to the execution of left-right displacements. For this reason, we concentrated our analysis of the representation of movement in the SGI solely on the observed vertical and horizontal components of rotation. We found that the representation of such motor plans is topographical in the SGI (Fig. 7.2); the amplitude of contralateral left-right head rotations represented along the mediolateral axis remains unchanged, increasing instead when moving from anterior to posterior locations for stimulation. An important observation that should be made here is that the uniformity of motor plans represented on the medio-lateral axis, along which we reported a significant difference in Pitx2^{ON} neurons distribution (Fig. 3.3b), provides evidence of the independence of the metric of the executed motor plan from the absolute number of premotor cells involved in its execution. The vertical component of head displacements is also topographically mapped in the SC, so that the anteromedial portions of the SC contain representations for upward pitch and the posterior-lateral portions downward movements instead. Of course, our experimental system only allowed us to reconstruct the displacements associated with nine collicular locations, so only sampling around nine Pitx2^{ON} modules, at a time, leading to quite an approximative estimation of Pitx2^{ON} neurons-dependent topography. Nevertheless, in all animals analysed we recorded a similar trend for the distribution of movement vectors across the SGI, suggesting that indeed movement vectors might be organized along the anatomical axes described above, summarized in Figure 8.1.

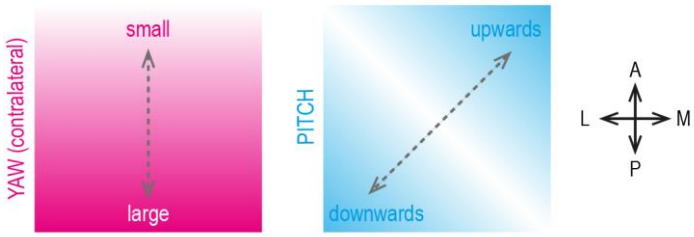

Figure 8.1 | Proposed organisation of yaw and pitch movements along anatomical axes in the SC.
Contralateral yaw displacements are mapped along the antero-posterior axis of the SC, with movements of smaller amplitude represented anteriorly and bigger displacements mapped posteriorly (left). Pitch movements are instead organized along a diagonal anatomical axis, so that upward motor plans are represented in the antero-medial portion of the SC and downwards movements in the lateral-posterior region (right). As a consequence of this mismatch between the two described axes, upward pitch is most oflen encoded with small amplitude movements in yaw; conversely, larger displacements in yaw are predominantly coupled to downward component in pitch.

If this model were correct, it would carry an important implication: not all yaw-pitch combinations of head rotations are represented by the Pitx2^{ON} population, or at least not to the same extent. Instead, upward pitch would be mainly associated with smaller displacements along the horizontal axis, while downward pitch would instead be preferentially represented with ampler rotations in yaw. Because we did not record any particular correlation between the metric of yaw and pitch movement in freely moving mice (Fig. 5.4), we can conclude that the selective motor representation in the SGI finds no parallel in the physiological range of movements performed by the animals. Rather, it would suggest that the representation of certain motor plans is favoured at the expenses of others, similarly to what has been described for the representation of visual features in the SGS[225]. The significance of this coding strategy will be discussed in further detail in *8.4 Functional modularity in collicular networks*.

8.3.2 Universality of SC goal representations

In this study, we focused our efforts to reconstruct the metric of motion encoded in the SC on the characterization of head displacements, which we deemed to be the main ethological orienting behaviour for goal-oriented plans in rodents. Using head rotations as a motor readout of collicular coding strategies, we were indeed able to describe some fundamental principles of motor representation in the murine SC. On the contrary, our results on Pitx2^{ON} neurons-dependent eye movements are not equally informative of the topography of movement vectors in the SGI, nor did they shed light on the fixed tuning of distinct modules

for particular angles of displacement. Instead, we observed very low-amplitude eye movements (< 5°) for every stimulation parameter applied (Fig. 6.5, 6), at every site stimulated in all the mice tested. The head movement associated with stimulations through the same fibre implants varied across sites and, most notably, showed a dependency on the duration of the stimulation protocol applied (Fig. 6.6). While we did not carry out a systematic study of the distribution of movement vectors relative to eye rotations using a multi-fibre array, these observations led us to conclude that Pitx2^{ON} collicular circuits for orienting might not orchestrate goal-oriented eye movements. Perhaps the glutamatergic Pitx2^{OFF} SGI population might be involved in this additional orienting behaviour. Yet, our description of the representation of Pitx2^{ON}-neurons dependent head rotations strongly mirrors prior observations of the nature of saccadic movement coding in the SC of primates and cats (ie. fixed motor tuning of premotor units, topography of movement vectors, staircase-like motor behaviour[55]). As a consequence, we rather interpret these results as evidence that collicular circuits have evolved to encode gaze in a way that is most ethologically relevant; in the case of rodent species, which possess afoveated eyes, gaze is entirely the product of head rotations and hence collicular circuits might prioritise the representation of these motor plans for orienting. As described in the *Introduction*, monkeys meaningfully employ coordinated rotation of structures of the head in goal-directed actions; here, the activity of SC premotor units is more closely correlated to the direction and amplitude of a gaze shift produced by a combination of head and eye displacements, rather than to either component considered in isolation[66]. Hence, collicular circuits would be most accurately defined as encoder of goals, rather than the motor plans that underlie them. Further support for this hypothesis comes from a study by Walton and colleagues, who reported that activity in a portion of SC premotor neurons in macaques is modulated during head-only movements[226]. Interestingly, the authors reported substantial differences between SC neurons that respond during head-only movements and those that are active prior to gaze shifts. While this small group of head-only neurons increased their frequency of firing while the animals were performing a behavioural test designed to dissociate head and eye movements, their maximal firing rates were an order of magnitude lower than the high-frequency bursts observed for head-restrained saccades and head-unrestrained gaze shifts. Head-only cells displayed no strong preference for any given motion metric and hence they do not display a topographical organization relative to head amplitude or direction.

Taken together, these observations suggest that our Pitx2^{ON} population is most likely to be homologous to the premotor network in control of gaze shifts in higher mammals, rather than providing a separate motor map for the selective representation of head-only movements. As a consequence, our results point to the existence of a large degree of

universality across species in the way that the SC represents goals for successful interaction with the environment, preferentially conserved over the motor plans through which they are achieved.

8.4 Functional modularity in collicular networks

8.4.1 General considerations

There is no *a priori* reason for which motor space should be mapped in functional clusters in the CNS. With respect to the modularity of the organization of movement vectors in the SGI described here, it is noteworthy that it mirrors the clustered organization of orientation- and direction-selective neurons in the visual layers of the murine SC[225,227], suggesting the existence of a shared design for the anatomical grouping of either perceptual or motor features in the SC according to a spatial logic.

Interestingly, it has been shown that only a relatively small range of orientations are represented in the functional columns observed in the visual SC in mice[225]. Likewise, given the finite numbers of Pitx2^{ON} modules and the quantal nature of the elicited motor output (Fig. 6.4), the motor space does not appear to be immediately fully represented in the SGI. A solution to the problem of this seemingly low-dimensional spatial-motor representation comes from considering Pitx2^{ON} modules not as point-to-point representations of the motor space, but rather as cardinal spatial-motor primitives[228] that could be combined downstream to the SC to generate the full metric of the spatial-motor repertoire of an animal.

As mentioned earlier in this *Discussion*, we additionally hypothesize that the Pitx2^{ON} population encodes only a limited number of combinations of yaw and pitch displacements. This observation adds a possible mean of interpretation of the finite nature of motor representations in the modular network just discussed; rather than providing a low resolution representation of movement which require further integration downstream to generate spatially accurate orienting actions, the SGI might favour representations of the most meaningful plans for interactions with the environment. Indeed, the motor map in the primate SC also contains a non-homogeneous representation of saccadic eye movement space that favors upward locations[229]. According to this alternative system, Pitx2^{ON} modules might be recruited in isolation, as they would be able to produce independently the full spectrum of meaningful motor plans for head rotation. While the optogenetic approach

described in this study has proven a valid strategy to elucidate some principle of motor representation in the SGI, it holds more limited potential in addressing questions regarding the rule governing the operation of the Pitx2^{ON} population as a whole. Some ideas as to how this hypothesis could be investigated experimentally are discussed later (see *8.5.2 How does the Pitx2^{on} population operate as a whole?*).

8.4.2 Action selection in a modular motor map

Our findings of granularity in the representation of motor space open a number of questions regarding the population dynamics adopted in the SC during the selection of appropriate motor plans. Many hypotheses regarding the mechanisms of action selection have been formulated, and what model best fits the wealth of neurophysiological evidence gathered to date is still under debate[230]. One of the earliest speculations regarding collicular function revolves around the concept of "population coding"[231], whereby the metric of the generated movement vector is determined via a weighted sum, or vector average, of the activity of collicular neurons across the entire map. The amplitude and direction of the resulting executed motion typically matches the vector encoded at the site of maximal activity, located in the centre of the active population[232,233]. This model emerged from neurophysiological recordings in the primate SC, which established that, while individual SC neurons have a distinct tuning for saccades of a given motion metric, most saccade-related neurons fire during a range of saccadic displacements around their preferred one[232-234]. The main criticism moved to this model is that it relies on data of collicular activity triggered by the presence of single stimuli in the visual field, an unlikely setting for the generation of accurate orienting movements in naturalistic behaviour. Several studies have studied collicular networks during the presentation of multiple visual stimuli; these experiments have led to the formulation of a winner-takes-all code for collicular networks, in which the population of neurons discharging at the highest levels determines the metric of the motion produced[230].

How would a modular representation of motor space fit into a winner-takes-all model of collicular function? In a competitive system such as that necessary for this model, modularity may represent an excellent strategy to segregate excitatory inputs that could drive movement initiation, minimizing noise in the area. These incoming inputs target Pitx2^{ON} neurons directly, as highlighted by our tracing results, but might also contact a number of local interneurons. The large number of excitatory Pitx2^{OFF} neurons detected within the dendritic arborisations of Pitx2^{ON} cells suggest that these anatomical clusters might also contain local excitatory microcircuits to reinforce their own activation. In parallel, GABAergic neurons situated within the module might be the direct recipients of the same

quality information, and contact premotor neurons across the SGI to inhibit movements of different metric. The concentration of all these circuit elements in discrete modules might provide an effective circuit design to maximize their spatial coherence, as well as the timing of their activation, while at the same time minimizing the likelihood that a given sensory or motor-related input might exert influence on premotor neurons linked to the execution of distinct motor plans.

8.5 Experimental outlook

8.5.1 How does the Pitx2^{on} module operate as a unit?

Our *in vivo* electrophysiological recordings using optetrodes were instrumental for determining the degree to which Pitx2^{ON} units partake in the production of spontaneously occurring head movements; their high temporal resolution allows to speculate on the fact that the activity of these units is not only correlated to the performance of head rotations of a given metric, but is in fact responsible for the initiation of such movements, confirming observations from optogenetic experiments. The major caveat of this approach for the purposes of this study is the limited number of units that can be simultaneously recorded, as well as its limited ability to reconstruct the spatial relationship between isolated units. Calcium imaging techniques would provide an experimental strategy to monitor the activity of groups of Pitx2^{ON} neurons and study the coherency of their firing pattern, as well as their homogeneity in motion tuning. In other words, this approach would effectively determine if all neurons within the module are recruited together during spontaneously occurring orienting; furthermore, we would be able to determine if the specific motor output of a module that we described in this study is the result of a local vectorial averaging mechanism or instead if neurons in a given patch fire preferentially for motor plans of similar metric. To this date, the only feasible experimental approach for calcium imaging of intermediate SC layers is the use of microendoscopes coupled to GRIN lenses[164]. The size of the field of view of this imaging setup (~350 μm in diameter) is compatible with the periodicity defined by Pitx2^{ON} units in the SC (Fig. 3.7), suggesting that we should be able to monitor the activity of one to two Pitx2^{ON} modules, according to implant position.

We started implementing this approach in WT animals injected with AAV vectors driving the constitutive expression of GCaMP6s in neurons in the SGI; we have now developed a pipeline for image registration, ROI detection and spike deconvolution, allowing us to

correlate the activity of local neurons with specific patterns of head-over-body displacement. Indeed, preliminary results from the lab show that microendoscopy is a valid approach to identify motor-related cells, characterise their tuning preferences and study the temporal correlation in their activity patterns (data not shown). We have now obtained a *Pitx2-CRE::Rosa-LSL-GCaMP6f* line and confirmed its validity as a reporter of Pitx2^{ON} cell activity *ex vivo* using 2P microscopy (Fig. 8.2). Applying microendoscopy techniques to this line holds the potential to reveal whether Pitx2^{ON} neurons within a module are all motor-related in nature and, if so, whether they are tuned to the same head movement vectors.

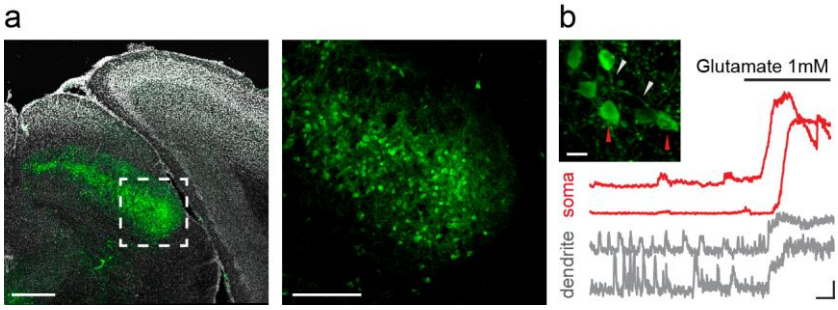

Figure 8.2 | 2P calcium imaging of Pitx2::GCaMP6f neurons in slice.
a, Coronal section through the SC of a *Pitx2-CRE::Rosa-LSL-GCaMP6f* mouse (scale bar: 250 µm). b, Example calcium traces recorded in the soma (*red*) and dendrites (*gray*) of Pitx2::GCaMP6f neurons shown; activity was elicited through application of 1mM glutamate (scale bars: 20 µm for image inset, 20%ΔF/F and 50s for calcium traces).

8.5.2 How does the Pitx2^{on} population operate as a whole?

Module-specific tracing. Combinatorial recruitment of different Pitx2^{ON} modules can be achieved in a network that allows the selective addressing of modules by its pre-synaptic population. As described in the *Introduction*, electrophysiological experiments in collicular slices have described a vertical organisation of the interlaminar circuits in the SC[141], suggesting that individual Pitx2^{ON} modules could be excited upon the presentation of sensory stimuli in a relevant portion of the visual field. Similarly, one could postulate the existence of such segregation of pre-synaptic partners in other input areas described in this study. To answer this question, we could perform a double retrograde tracing experiment, restricting the population of starter cells to neurons within two distinct modules and reconstructing their associated pre-synaptic networks using EnvA-ΔG-Rabies^{GFP} and EnvA-ΔG-Rabies^{mCherry}. This would allow us to appreciate whether distinct group of cells in sensory (eg. S1) and motor-related areas (eg. M1 and SNr) contain separate populations of input neurons for individual Pitx2^{ON} modules, and if so, further assess whether these distinct input cell groups are topographically organized or intermingled in the area. These anatomical observations

would help us gauge whether the decision to activate a module over others is initiated upstream, through the selective recruitment of input cells across the brain; alternatively, this selection process could be mainly the result of a competitive mechanism within the SC, whereby the expressed collicular motor output would be determined through a probabilistic model and correspond to those of modules that receive temporally aligned synaptic inputs from several brain regions.

Monitoring activity of multiple modules at once. In addition to understanding the principles underlying the function of Pitx2^{ON} modules as encoders of motion vectors, it would most informative to investigate how distinct modules are operated during orienting actions. Are multiple glomeruli recruited simultaneously? If so, how does the metric of movement performed compare to the motor plans encoded by individual modules? To this aim, we would need to be able to image large portions of the SC in the same session while monitoring head-over-body displacements. Because of their depth in the tissue, imaging Pitx2^{ON} cell bodies or dendritic processes is not easily achievable with 2P imaging techniques, even when the overlaying cortex is removed; furthermore, this head-fixed preparation would pose a limitation to our study of orienting. An alternative is found in fibre photometry[235,236], a technique that employs multimode optical fibres to provide excitation light and record the returning fluorescent signals from genetically encoded indicators of neuronal activity. Although this method lacks the cellular resolution of microendoscopy, fibre photometry relies on the manifestation of large changes in calcium signals in neural ensembles to attribute functional relevance to the activity of genetically identified neurons in an area. In an analogous experiment to that reported in this study for the stimulation of multiple Pitx2^{ON} modules in a single animal, we could use multi-fibre photometry to monitor large-scale collicular dynamics highlighted by the patterns of activation of Pitx2^{ON} cells. This low-resolution approach would be instrumental to address the general question of whether distinct modules are physiologically recruited simultaneously; if this was the case, photometry would also provide an indication of whether levels of activity in individual modules are predictive of the final motion produced.

Manipulating activity of multiple modules at once. In a complementary approach, we could also seek to determine what motor output would result from the concomitant optogenetic activation of multiple Pitx2^{ON} modules. Would we see mechanisms of vectorial averaging or would one of the two characteristic vectors be produced? And if so, which stimulation parameters can favour the execution of one motor plan over the other? Prompting the system through optogenetic manipulation will not provide conclusive evidence as to what recruitment strategies are adopted in collicular circuits; however, it holds

the potential to reveal what this modular system is capable of in terms of integration of motor plans, hence helping us refine our hypothesis regarding its physiological operation.

8.6 Concluding remarks

Although the SC has been implicated in the generation of spatially accurate orienting movements by multiple lines of research and across several animal species, the exact organisation of collicular networks that underlie sensorimotor integration remain elusive. Our results provide a genetic entry point to enhance our understanding of how the SC represents motor space, paving the way for the future investigation of principles of sensorimotor integration and action selection.

Appendix A

List of electrophysiological parameters employed in the hierarchical clustering of SGI neurons

Passive membrane properties		Active membrane properties			
		Action potential properties		Firing profile properties	
Parameter	**Unit**	**Parameter**	**Unit**	**Parameter**	**Unit**
Access resistance	MOhm	Threshold	mV	Frequency	Hz
Resting membrane potential	mV	Amplitude	mV	Frequency of adaptation	%
Input resistance	MOhm	Width	ms	Frequency between first and third action potentials	Hz
Tau	ms	After-hyperpolarisation amplitude	mV	Delay of the first action potential	ms
Capacitance	pF	After-hyperpolarisation width	ms	Delay of the last action potential	ms

Appendix B

Electrophysiological values for Pitx2^{ON}, vGluT2 ^{ON} and vGAT ^{ON} neurons

a

	n	Resting Membrane Potential (mV)	Input Resistance (MΩ)	Membrane Capacitance (pF)	Tau (ms)
Pitx2^{ON}					
Inactivating	16	-54.12 ± 6.64	259.15 ± 36.81	21.57 ±0.91	21.01 ± 5.42
vGluT2^{ON}					
Inactivating	21	-60.00 ± 2.23	279.19 ± 38.91	20.40 ± 1.49	14.24 ± 2.00
Regular Spiking	5	-65.82 ± 4.85	191.4 ± 22.05	21.12 ± 3.32	32.55 ± 18.06
vGAT^{ON}					
Inactivating	16	-61.63 ± 2.47	964.92 ± 31.54	48.42 ± 1.66	31.94 ± 1.66
Regular Spiking	3	-65.07 ± 2.25	210.57 ± 48.22	67.39 ± 19.85	15.26 ± 2.39
Stuttering	2	-71 ± 1.00	200.75 ± 37.25	27.288 ± 9.92	34.78 ± 26.19
Delayed	4	-71.57 ± 3.32	280.79 ± 45.62	24.41 ± 4.56	48.64 ± 35.11
Fast Spiking	20	-64.28 ± 1.73	306.67 ± 36.98	27.94 ± 5.44	23.63 ± 8.43

	n	AP Amplitude (mV)	AP width (ms)	AHP Amplitude (mV)	AHP width (ms)
Pitx2^{ON}					
Inactivating	16	75.63 ± 2.01	0.39 ± 0.009	-14.37 ± 0.80	4.07 ± 0.13
vGluT2^{ON}					
Inactivating	21	74.11 ± 1.91	5.75 ± 0.95	-12.52 ± 1.13	9.04 ± 1.18
Regular Spiking	5	70 ± 4.66	2.90 ± 1.18	-15.68 ± 1.33	10.88 ± 2.51
vGAT^{ON}					
Inactivating	16	63.73 ± 2.21	1.64 ± 0.43	-1.38 ± 1.43	25.51 ± 5.29
Regular Spiking	3	81.82 ± 2.36	0.66 ± 0.24	11.17 ± 11.32	88.42 ± 34.35
Stuttering	2	61.15 ± 18.24	1.5 ± 0.65	-13.96 ± 7.09	32.9 ± 29.50
Delayed	4	60.85 ± 4.41	0.79 ± 0.16	-3.79 ± 12.05	28.94 ± 9.07
Fast Spiking	20	64.93 ± 2.11	0.98 ± 0.16	4.53 ± 4.98	25.47 ± 6.06

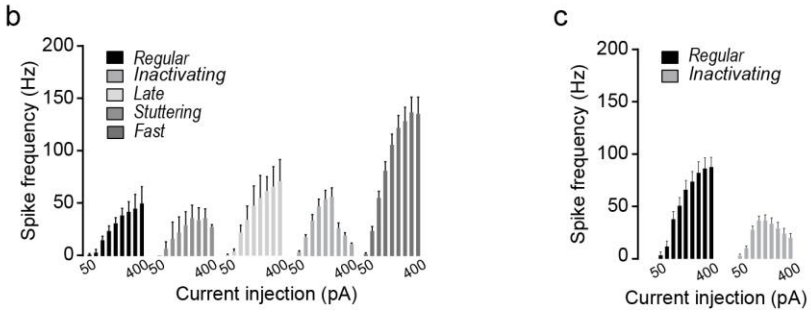

a, Passive membrane properties (top) and action potential properties (bottom).
b, **c**, Firing profile properties of vGAT^{ON} (**b**) and vGluT^{ON} (**c**) neurons.

Appendix C

RNAseq parameters for 20 most significantly enriched genes in the motor vs. sensory SC domain

Gene ID	Gene Name	AVG_motor	AVG_sensory	log_2FoldChange	Test_stat	p_{adj}
ENSMUSG00000014542	Clec4f	3.731	0.000	4.363	4.082E+00	8.264E-04
ENSMUSG00000098515	Gm27195	3.444	0.201	3.764	3.623E+00	4.012E-03
ENSMUSG00000079042	Apela	12.202	0.759	3.735	6.703E+00	2.220E-09
ENSMUSG00000047109	Cldn14	6.514	0.681	3.524	4.996E+00	2.100E-05
ENSMUSG00000001815	Evx2	4.249	0.532	3.098	4.250E+00	4.454E-04
ENSMUSG00000045518	Onecut3	157.160	18.832	3.039	1.347E+01	6.841E-38
ENSMUSG00000104494	Gm37111	4.607	0.584	2.974	3.337E+00	9.657E-03
ENSMUSG00000032517	Mobp	1032.984	132.580	2.962	5.097E+00	1.314E-05
ENSMUSG00000027356	Fermt1	3.817	0.414	2.851	3.771E+00	2.472E-03
ENSMUSG00000028023	Pitx2	370.237	53.222	2.797	4.107E+00	7.477E-04
ENSMUSG00000030158	Clec12b	5.669	0.845	2.620	3.667E+00	3.483E-03
ENSMUSG00000102298	Gm33707	3.918	0.580	2.539	3.413E+00	7.670E-03
ENSMUSG00000087351	Gm11464	3.543	0.603	2.505	2.981E+00	2.498E-02
ENSMUSG00000042596	Tfap2d	426.256	80.426	2.402	1.117E+01	6.811E-26
ENSMUSG00000114715	AC168056.3	3.883	0.796	2.397	3.116E+00	1.762E-02
ENSMUSG00000085992	Gm11515	7.595	1.304	2.391	4.319E+00	3.425E-04
ENSMUSG00000028357	Kif12	16.462	2.887	2.344	5.290E+00	5.444E-06
ENSMUSG00000016498	Pdcd1lg2	4.252878	0.577	2.302	1.752E-03	0.01698
ENSMUSG00000045991	Onecut2	212.3672	43.402	2.288	3.038E-43	1.05E-39
ENSMUSG00000108905	Gm44618	6.278466	1.100	2.287	4.925E-04	0.006182

Appendix D

Individual data from optogenetic study of Pitx2^{ON} neurons-driven head displacement

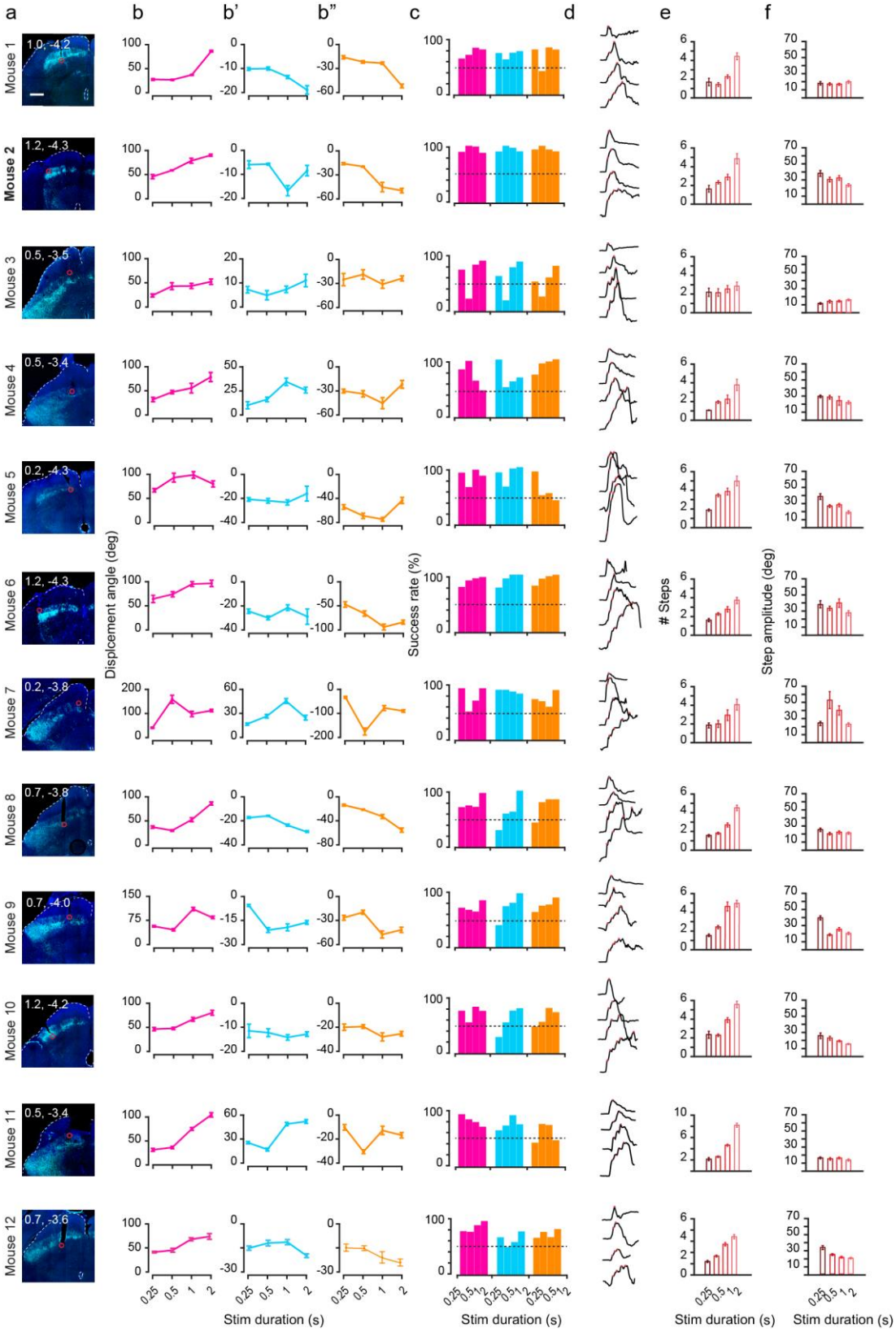

a, Histology of the implantation site for each tested mouse with estimated implant coordinates (x, y; scale bar: 500 µm)**.**
b-d, Effect of stimulus duration on the head displacement angle (**b-b”**) and the success rate of a head movement bout (**c**) for each mouse for yaw (*magenta*), pitch (*blue*) and roll (*orange*). Kinematics of head displacements for each mouse along the yaw dimension for increasing duration of stimulation (0.25, 0.5, 1 and 2 s); note the presence of step-wise trajectories for prolonged stimulations.
e, **f**, Trial-by-trial average of the number of recorded steps (**e**) and average step amplitude (**f**) for each mouse for increasing stimulus duration (n_{MICE} = 12, $n_{TRIALS/MOUSE}$ = 60).

List of references

1. Leibniz, G. W. & Clarke, S. *A Collection of Papers, Which Passed between the Late Learned Mr. Leibnitz, and Dr. Clarke, in the Years 1715 and 1716*. (Adamant Media Corporation, 2001).

2. Kant, I. & Meerbote, R. in *Theoretical Philosophy, 1755-1770* (ed. Walford, D.) 373–416 (Cambridge University Press, 1992).

3. Western, D. & Lindsay, W. K. Seasonal herd dynamics of a savanna elephant population. *African Journal of Ecology* **22,** 229–244 (1984).

4. Ruggiero, R. G. Seasonal forage utilization by elephants in central Africa. *African Journal of Ecology* **30,** 137–148 (1992).

5. Babaasa, D. Habitat selection by elephants in Bwindi Impenetrable National Park, south-western Uganda. *African Journal of Ecology* **38,** 116–122 (2000).

6. Leggett, K. E. A. Home range and seasonal movement of elephants in the Kunene Region, northwestern Namibia. *African Zoology* **41,** 17–36 (2015).

7. Pittman, S. E. *et al.* Homing of invasive Burmese pythons in South Florida: evidence for map and compass senses in snakes. *Biol. Lett.* **10,** 20140040 (2014).

8. Tolman, E. C. Cognitive maps in rats and men. *Psychol Rev* **55,** 189–208 (1948).

9. O'Keefe, J. & Dostrovsky, J. The hippocampus as a spatial map. Preliminary evidence from unit activity in the freely-moving rat. *Brain Res* **34,** 171–175 (1971).

10. Taube, J. S., Muller, R. U. & Ranck, J. B. Head-direction cells recorded from the postsubiculum in freely moving rats. I. Description and quantitative analysis. *Journal of Neuroscience* **10,** 420–435 (1990).

11. Taube, J. S., Muller, R. U. & Ranck, J. B. Head-direction cells recorded from the postsubiculum in freely moving rats. II. Effects of environmental manipulations. *Journal of Neuroscience* **10,** 436–447 (1990).

12. Fyhn, M., Molden, S., Witter, M. P., Moser, E. I. & Moser, M.-B. Spatial representation in the entorhinal cortex. *Science* **305,** 1258–1264 (2004).

13. Hafting, T., Fyhn, M., Molden, S., Moser, M.-B. & Moser, E. I. Microstructure of a spatial map in the entorhinal cortex. *Nature* **436,** 801–806 (2005).

14. Moser, E. I., Moser, M.-B. & McNaughton, B. L. Spatial representation in the hippocampal formation: a history. *Nature Publishing Group* **20,** 1448–1464 (2017).

15. Poincaré, H. in *The Foundations of Science* 66–80 (1913).

16. Hyvärinen, J. & Poranen, A. Function of the parietal associative area 7 as revealed from cellular discharges in alert monkeys. *Brain* **97,** 673–692 (1974).
17. Leinonen, L. & Nyman, G. II. Functional properties of cells in anterolateral part of area 7 associative face area of awake monkeys. *Experimental Brain Research* **34,** 321–333 (1979).
18. Rizzolatti, G., Scandolara, C., Matelli, M. & Gentilucci, M. Afferent properties of periarcuate neurons in macaque monkeys. I. Somatosensory responses. *Behav. Brain Res.* **2,** 125–146 (1981).
19. Rizzolatti, G., Scandolara, C., Matelli, M. & Gentilucci, M. Afferent properties of periarcuate neurons in macaque monkeys. II. Visual responses. *Behav. Brain Res.* **2,** 147–163 (1981).
20. Fogassi, L. *et al.* Space coding by premotor cortex. *Experimental Brain Research* **89,** 686–690 (1992).
21. Graziano, M. S., Yap, G. S. & Gross, C. G. Coding of visual space by premotor neurons. *Science* **266,** 1054–1057 (1994).
22. Graziano, M. S. & Gross, C. G. Spatial maps for the control of movement. *Current Opinion in Neurobiology* **8,** 195–201 (1998).
23. di Pellegrino, G. & Làdavas, E. Peripersonal space in the brain. *Neuropsychologia* **66,** 126–133 (2015).
24. Rizzolatti, G., Fadiga, L., Fogassi, L. & Gallese, V. The space around us. *Science* **277,** 190–191 (1997).
25. Guitton, D. & Volle, M. Gaze control in humans: eye-head coordination during orienting movements to targets within and beyond the oculomotor range. *Journal of Neurophysiology* **58,** 427–459 (1987).
26. Freedman, E. G. Coordination of the eyes and head during visual orienting. *Experimental Brain Research* **190,** 369–387 (2008).
27. Leigh, R. J. & Kennard, C. Using saccades as a research tool in the clinical neurosciences. *Brain* **127,** 460–477 (2004).
28. Becker, W. The neurobiology of saccadic eye movements. Metrics. *Rev Oculomot Res* **3,** 13–67 (1989).
29. Crawford, T., Goodrich, S., Henderson, L. & Kennard, C. Predictive responses in Parkinson's disease: manual keypresses and saccadic eye movements to regular stimulus events. *J. Neurol. Neurosurg. Psychiatry* **52,** 1033–1042 (1989).
30. Bizzi, E., Kalil, R. E. & Tagliasco, V. Eye-head coordination in monkeys: evidence for centrally patterned organization. *Science* **173,** 452–454 (1971).
31. Bizzi, E., Kalil, R. E. & Morasso, P. Two modes of active eye-head coordination in monkeys. *Brain Res* **40,** 45–48 (1972).
32. Morasso, P., Bizzi, E. & Dichgans, J. Adjustment of saccade characteristics during head movements. *Experimental Brain Research* **16,** 492–500 (1973).

33. Zangemeister, W. H. & Stark, L. Active head rotations and eye-head coordination. *Ann. N. Y. Acad. Sci.* **374,** 540–559 (1981).
34. Zangemeister, W. H. & Stark, L. Types of gaze movement: variable interactions of eye and head movements. *Exp. Neurol.* **77,** 563–577 (1982).
35. Freedman, E. G. & Sparks, D. L. Eye-head coordination during head-unrestrained gaze shifts in rhesus monkeys. *Journal of Neurophysiology* **77,** 2328–2348 (1997).
36. Lac, du, S. & Knudsen, E. I. Neural maps of head movement vector and speed in the optic tectum of the barn owl. *Journal of Neurophysiology* **63,** 131–146 (1990).
37. Valentine, D. E., Sinha, S. R. & Moss, C. F. Orienting responses and vocalizations produced by microstimulation in the superior colliculus of the echolocating bat, Eptesicus fuscus. *J Comp Physiol A* **188,** 89–108 (2002).
38. Leigh, R. J. & Zee, D. S. in *The Neurology of Eye Movements* 169–288 (Oxford University Press, 2015).
39. Koka, K., Read, H. L. & Tollin, D. J. The acoustical cues to sound location in the rat: Measurements of directional transfer functions. *The Journal of the Acoustical Society of America* **123,** 4297–4309 (2008).
40. Populin, L. C. & Yin, T. C. Pinna movements of the cat during sound localization. *Journal of Neuroscience* **18,** 4233–4243 (1998).
41. Griffin, D. R., Dunning, D. C., Cahlander, D. A. & WEBSTER, F. A. Correlated Orientation Sounds and Ear Movements of Horseshoe Bats. *Nature* **196,** 1185–1186 (1962).
42. Whittington, D. A., Hepp-Reymond, M. C. & Flood, W. Eye and head movements to auditory targets. *Experimental Brain Research* **41,** 358–363 (1981).
43. Kleinfeld, D., Ahissar, E. & Diamond, M. E. Active sensation: insights from the rodent vibrissa sensorimotor system. *Current Opinion in Neurobiology* **16,** 435–444 (2006).
44. Berg, R. W. & Kleinfeld, D. Rhythmic Whisking by Rat: Retraction as Well as Protraction of the Vibrissae Is Under Active Muscular Control. *Journal of Neurophysiology* **89,** 104–117 (2003).
45. Heffner, R. S. & Heffner, H. E. Degenerate hearing and sound localization in naked mole rats (Heterocephalus glaber), with an overview of central auditory structures. *J. Comp. Neurol.* **331,** 418–433 (1993).
46. Hetling, J. R. *et al.* Features of visual function in the naked mole-rat Heterocephalus glaber. *J Comp Physiol A* **191,** 317–330 (2005).
47. Park, T. J. *et al.* Somatosensory organization and behavior in naked mole-rats: II. Peripheral structures, innervation, and selective lack of neuropeptides associated with thermoregulation and pain. *J. Comp. Neurol.* **465,** 104–120 (2003).

48. Crish, S. D., Rice, F. L., Park, T. J. & Comer, C. M. Somatosensory Organization and Behavior in Naked Mole-Rats I: Vibrissa-Like Body Hairs Comprise a Sensory Array That Mediates Orientation to Tactile Stimuli. *Brain Behav. Evol.* **62,** 141–151 (2003).

49. Luo, J. & Moss, C. F. Echolocating bats rely on audiovocal feedback to adapt sonar signal design. *Proc Natl Acad Sci USA* **114,** 10978–10983 (2017).

50. Moss, C. F., Bohn, K., Gilkenson, H. & Surlykke, A. Active Listening for Spatial Orientation in a Complex Auditory Scene. *PLoS Biol* **4,** e79–12 (2006).

51. Kothari, N. B., Wohlgemuth, M. J. & Moss, C. F. Dynamic representation of 3D auditory space in the midbrain of the free-flying echolocating bat. *Elife* **7,** 1053 (2018).

52. Straschill, M. & Hoffmann, K. P. Activity of movement sensitive neurons of the cat's tectum opticum during spontaneous eye movements. *Experimental Brain Research* **11,** 318–326 (1970).

53. Wurtz, R. H. & Goldberg, M. E. Activity of superior colliculus in behaving monkey. 3. Cells discharging before eye movements. *Journal of Neurophysiology* **35,** 575–586 (1972).

54. Sparks, D. L., Holland, R. & Guthrie, B. L. Size and distribution of movement fields in the monkey superior colliculus. *Brain Res* **113,** 21–34 (1976).

55. Gandhi, N. J. & Katnani, H. A. Motor Functions of the Superior Colliculus. *Annu. Rev. Neurosci.* **34,** 205–231 (2011).

56. Robinson, D. A. Eye movements evoked by collicular stimulation in the alert monkey. *Vision Res.* **12,** 1795–1808 (1972).

57. Straschill, M. & Rieger, P. Eye movements evoked by focal stimulation of the cat's superior colliculus. *Brain Res* **59,** 211–227 (1973).

58. McHaffie, J. G. & Stein, B. E. Eye movements evoked by electrical stimulation in the superior colliculus of rats and hamsters. *Brain Res* **247,** 243–253 (1982).

59. Stanford, T. R., Freedman, E. G. & Sparks, D. L. Site and parameters of microstimulation: evidence for independent effects on the properties of saccades evoked from the primate superior colliculus. *Journal of Neurophysiology* **76,** 3360–3381 (1996).

60. Smit, A. C., Van Gisbergen, J. A. & Cools, A. R. A parametric analysis of human saccades in different experimental paradigms. *Vision Res.* **27,** 1745–1762 (1987).

61. Gnadt, J. W., Bracewell, R. M. & Andersen, R. A. Sensorimotor transformation during eye movements to remembered visual targets. *Vision Res.* **31,** 693–715 (1991).

62. Edelman, J. A. & Goldberg, M. E. Saccade-Related Activity in the Primate Superior Colliculus Depends on the Presence of Local Landmarks at the Saccade Endpoint. *Journal of Neurophysiology* **90,** 1728–1736 (2003).

63. Stryker, M. P. & Schiller, P. H. Eye and head movements evoked by electrical stimulation of monkey superior colliculus. *Experimental Brain Research* **23,** 103–112 (1975).

64. Breznen, B., Lu, S. M. & Gnadt, J. W. Analysis of the step response of the saccadic feedback: system behavior. *Experimental Brain Research* **111,** 337–344 (1996).

65. Missal, M., Lefèvre, P., Delinte, A., Crommelinck, M. & Roucoux, A. Smooth eye movements evoked by electrical stimulation of the cat's superior colliculus. *Experimental Brain Research* **107,** 382–390 (1996).

66. Freedman, E. G. & Sparks, D. L. Activity of cells in the deeper layers of the superior colliculus of the rhesus monkey: evidence for a gaze displacement command. *Journal of Neurophysiology* **78,** 1669–1690 (1997).

67. Harris, L. R. The superior colliculus and movements of the head and eyes in cats. *J Physiol* **300,** 367–391 (1980).

68. Freedman, E. G., Stanford, T. R. & Sparks, D. L. Combined eye-head gaze shifts produced by electrical stimulation of the superior colliculus in rhesus monkeys. *Journal of Neurophysiology* **76,** 927–952 (1996).

69. Guillaume, A. & Pélisson, D. Gaze shifts evoked by electrical stimulation of the superior colliculus in the head-unrestrained cat. I. Effect of the locus and of the parameters of stimulation. *Eur. J. Neurosci.* **14,** 1331–1344 (2001).

70. Klier, E. M., Wang, H. & Crawford, J. D. The superior colliculus encodes gaze commands in retinal coordinates. *Nat Neurosci* **4,** 627–632 (2001).

71. Guillaume, A. & Pélisson, D. Kinematics and eye-head coordination of gaze shifts evoked from different sites in the superior colliculus of the cat. *J Physiol* **577,** 779–794 (2006).

72. Corneil, B. D., Olivier, E. & Munoz, D. P. Neck muscle responses to stimulation of monkey superior colliculus. I. Topography and manipulation of stimulation parameters. *Journal of Neurophysiology* **88,** 1980–1999 (2002).

73. Pélisson, D., Goffart, L., Guillaume, A., Catz, N. & Raboyeau, G. Early head movements elicited by visual stimuli or collicular electrical stimulation in the cat. *Vision Res.* **41,** 3283–3294 (2001).

74. Corneil, B. D., Olivier, E. & Munoz, D. P. Neck muscle responses to stimulation of monkey superior colliculus. II. Gaze shift initiation and volitional head movements. *Journal of Neurophysiology* **88,** 2000–2018 (2002).

75. Guitton, D., Munoz, D. P. & Galiana, H. L. Gaze control in the cat: studies and modeling of the coupling between orienting eye and head movements in different behavioral tasks. *Journal of Neurophysiology* **64,** 509–531 (1990).

76. Gandhi, N. J. & Sparks, D. L. Dissociation of Eye and Head Components of Gaze Shifts by Stimulation of the Omnipause Neuron Region. *Journal of Neurophysiology* **98,** 360–373 (2007).

77. Grantyn, A., Kuze, B., Brandi, A.-M., Thomas, M.-A. & Quenech'du, N. Direct projections of omnipause neurons to reticulospinal neurons: A double-labeling light microscopic study in the cat. *J. Comp. Neurol.* **518,** 4792–4812 (2010).

78. Stein, B. E. & Clamann, H. P. Control of pinna movements and sensorimotor register in cat superior colliculus. *Brain Behav. Evol.* **19,** 180–192 (1981).

79. Hemelt, M. E. & Keller, A. Superior Colliculus Control of Vibrissa Movements. *Journal of Neurophysiology* **100,** 1245–1254 (2008).

80. Cramer, N. P. & Keller, A. Cortical control of a whisking central pattern generator. *Journal of Neurophysiology* **96,** 209–217 (2006).

81. Sprague, J. M. & Meikle, T. H. The role of the superior colliculus in visually guided behavior. *Exp. Neurol.* **11,** 115–146 (1965).

82. Schaefer, K. P. Unit analysis and electrical stimulation in the optic tectum of rabbits and cats. *Brain Behav. Evol.* **3,** 222–240 (1970).

83. Syka, J. & Radil-Weiss, T. Electrical stimulation of the tectum in freely moving cats. *Brain Res* **28,** 567–572 (1971).

84. Cowie, R. J. & Robinson, D. L. Subcortical contributions to head movements in macaques. I. Contrasting effects of electrical stimulation of a medial pontomedullary region and the superior colliculus. *Journal of Neurophysiology* **72,** 2648–2664 (1994).

85. Sinha, S. R. & Moss, C. F. Vocal Premotor Activity in the Superior Colliculus. *Journal of Neuroscience* **27,** 98–110 (2007).

86. Miller, G. A., Galanter, E. & Pribram, K. H. *Plans and the structure of behavior*. (Holt, Rinehart and Winston, 1970).

87. Gold, J. I. & Shadlen, M. N. Representation of a perceptual decision in developing oculomotor commands. *Nature* **404,** 390–394 (2000).

88. Hernández, A., Zainos, A. & Romo, R. Temporal evolution of a decision-making process in medial premotor cortex. *Neuron* **33,** 959–972 (2002).

89. Cisek, P. Cortical mechanisms of action selection: the affordance competition hypothesis. *Philosophical Transactions of the Royal Society B: Biological Sciences* **362,** 1585–1599 (2007).

90. Cisek, P. & Kalaska, J. F. Neural Mechanisms for Interacting with a World Full of Action Choices. *Annu. Rev. Neurosci.* **33,** 269–298 (2010).

91. Kustov, A. A. & Robinson, D. L. Shared neural control of attentional shifts and eye movements. *Nature* **384,** 74–77 (1996).

92. Bell, A. H., Fecteau, J. H. & Munoz, D. P. Using Auditory and Visual Stimuli to Investigate the Behavioral and Neuronal Consequences of Reflexive Covert Orienting. *Journal of Neurophysiology* **91,** 2172–2184 (2004).

93. Cavanaugh, J. Subcortical Modulation of Attention Counters Change Blindness. *Journal of Neuroscience* **24,** 11236–11243 (2004).

94. Cavanaugh, J., Alvarez, B. D. & Wurtz, R. H. Enhanced Performance with Brain Stimulation: Attentional Shift or Visual Cue? *Journal of Neuroscience* **26,** 11347–11358 (2006).

95. Rensink, R. A. Change detection. *Annu Rev Psychol* **53,** 245–277 (2002).

96. Lovejoy, L. P. & Krauzlis, R. J. Inactivation of primate superior colliculus impairs covert selection of signals for perceptual judgments. *Nature Publishing Group* **13,** 261–266 (2009).

97. May, P. J. The mammalian superior colliculus: laminar structure and connections. *Prog. Brain Res.* **151,** 321–378 (2006).

98. Ellis, E. M., Gauvain, G., Sivyer, B. & Murphy, G. J. Shared and distinct retinal input to the mouse superior colliculus and dorsal lateral geniculate nucleus. *Journal of Neurophysiology* **116,** 602–610 (2016).

99. Perry, V. H. & Cowey, A. Retinal ganglion cells that project to the superior colliculus and pretectum in the macaque monkey. *Neuroscience* **12,** 1125–1137 (1984).

100. Pollack, J. G. & Hickey, T. L. The distribution of retino-collicular axon terminals in rhesus monkey. *J. Comp. Neurol.* **185,** 587–602 (1979).

101. Hofbauer, A. & Holländer, H. Synaptic connections of cortical and retinal terminals in the superior colliculus of the rabbit: an electron microscopic double labelling study. *Experimental Brain Research* **65,** 145–155 (1986).

102. Feig, S., Van Lieshout, D. P. & Harting, J. K. Ultrastructural studies of retinal, visual cortical (area 17), and parabigeminal terminals within the superior colliculus of Galago crassicaudatus. *J. Comp. Neurol.* **319,** 85–99 (1992).

103. Schiller, P. H. & Koerner, F. Discharge characteristics of single units in superior colliculus of the alert rhesus monkey. *Journal of Neurophysiology* **34,** 920–936 (1971).

104. Middlebrooks, J. C. & Knudsen, E. I. A neural code for auditory space in the cat's superior colliculus. *Journal of Neuroscience* **4,** 2621–2634 (1984).

105. Jay, M. F. & Sparks, D. L. Sensorimotor integration in the primate superior colliculus. II. Coordinates of auditory signals. *Journal of Neurophysiology* **57,** 35–55 (1987).

106. Gaese, B. H. & Johnen, A. Coding for auditory space in the superior colliculus of the rat. *Eur. J. Neurosci.* **12,** 1739–1752 (2000).

107. Kadunce, D. C., Vaughan, J. W., Wallace, M. T., Benedek, G. & Stein, B. E. Mechanisms of within- and cross-modality suppression in the superior colliculus. *Journal of Neurophysiology* **78,** 2834–2847 (1997).

108. Populin, L. C. & Yin, T. C. T. Bimodal Interactions in the Superior Colliculus of the Behaving Cat. *Journal of Neuroscience* **22,** 2826–2834 (2002).

109. Dräger, U. C. & Hubel, D. H. Topography of visual and somatosensory projections to mouse superior colliculus. *Journal of Neurophysiology* **39,** 91–101 (1976).

110. Chalupa, L. M. & Rhoades, R. W. Responses of visual, somatosensory, and auditory neurones in the golden hamster's superior colliculus. *J Physiol* **270,** 595–626 (1977).

111. Wallace, M. T., Wilkinson, L. K. & Stein, B. E. Representation and integration of multiple sensory inputs in primate superior colliculus. *Journal of Neurophysiology* **76,** 1246–1266 (1996).

112. Hartline, P. H., Kass, L. & Loop, M. S. Merging of modalities in the optic tectum: infrared and visual integration in rattlesnakes. *Science* **199,** 1225–1229 (1978).

113. Grillner, S. & Robertson, B. The Basal Ganglia Over 500 Million Years. *Current Biology* **26,** R1088–R1100 (2016).

114. Hikosaka, O. & Wurtz, R. H. Visual and oculomotor functions of monkey substantia nigra pars reticulata. I. Relation of visual and auditory responses to saccades. *Journal of Neurophysiology* **49,** 1230–1253 (1983).

115. Joseph, J. P. & Boussaoud, D. Role of the cat substantia nigra pars reticulata in eye and head movements. I. Neural activity. *Experimental Brain Research* **57,** 286–296 (1985).

116. Hikosaka, O., neurophysiology, R. W. J. O.1985. Modification of saccadic eye movements by GABA-related substances. II. Effects of muscimol in monkey substantia nigra pars reticulata. *Journal of Neurophysiology* **53,** 292–308 (1985).

117. Mitrofanis, J. Some certainty for the 'zone of uncertainty'? Exploring the function of the zona incerta. *Neuroscience* **130,** 1–15 (2005).

118. Kobayashi, Y., Saito, Y. & Isa, T. Facilitation of saccade initiation by brainstem cholinergic system. *Brain Dev.* **23 Suppl 1,** S24–7 (2001).

119. Illing, R. B. & Graybiel, A. M. Convergence of afferents from frontal cortex and substantia nigra onto acetylcholinesterase-rich patches of the cat's superior colliculus. *Neuroscience* **14,** 455–482 (1985).

120. Mana, S. & Chevalier, G. Honeycomb-like structure of the intermediate layers of the rat superior colliculus: afferent and efferent connections. *Neuroscience* **103,** 673–693 (2001).

121. Illing, R. B. & Graybiel, A. M. Complementary and non-matching afferent compartments in the cat's superior colliculus: innervation of the acetylcholinesterase-poor domain of the intermediate gray layer. *Neuroscience* **18,** 373–394 (1986).

122. Illing, R. B., Vogt, D. M. & Spatz, W. B. Parvalbumin in rat superior colliculus. *Neurosci. Lett.* **120,** 197–200 (1990).

123. Harting, J. K., Feig, S. & Van Lieshout, D. P. Cortical somatosensory and trigeminal inputs to the cat superior colliculus: light and electron microscopic analyses. *J. Comp. Neurol.* **388,** 313–326 (1997).

124. Grantyn, A. & Grantyn, R. Axonal patterns and sites of termination of cat superior colliculus neurons projecting in the tecto-bulbo-spinal tract. *Experimental Brain Research* **46,** 243–256 (1982).

125. Horn, A. K. E. The reticular formation. *Prog. Brain Res.* **151,** 127–155 (2006).

126. Harting, J. K. Descending pathways from the superior colliculus: An autoradiographic analysis in the rhesus monkey (Macaca mulatta). *Journal of Comparative Neurology* **173,** 583–612 (1977).

127. Grantyn, A. & Berthoz, A. Burst activity of identified tecto-reticulo-spinal neurons in the alert cat. *Experimental Brain Research* **57,** 417–421 (1985).

128. Grantyn, A., Jacques, V. O.-M. & Berthoz, A. Reticulo-spinal neurons participating in the control of synergic eye and head movements during orienting in the cat. *Experimental Brain Research* **66,** 355–377 (1987).

129. Cowie, R. J. & Holstege, G. Dorsal mesencephalic projections to pons, medulla, and spinal cord in the cat: limbic and non-limbic components. *J. Comp. Neurol.* **319,** 536–559 (1992).

130. Huerta, M. F. & Harting, J. K. Projections of the superior colliculus to the supraspinal nucleus and the cervical spinal cord gray of the cat. *Brain Res* **242,** 326–331 (1982).

131. Huerta, M. F. & Harting, J. K. Tectal control of spinal cord activity: neuroanatomical demonstration of pathways connecting the superior colliculus with the cervical spinal cord grey. *Prog. Brain Res.* **57,** 293–328 (1982).

132. Harting, J. K., Huerta, M. F., Frankfurter, A. J., Strominger, N. L. & Royce, G. J. Ascending pathways from the monkey superior colliculus: an autoradiographic analysis. *J. Comp. Neurol.* **192,** 853–882 (1980).

133. Romanski, L. M., Giguere, M., Bates, J. F. & Goldman-Rakic, P. S. Topographic organization of medial pulvinar connections with the prefrontal cortex in the rhesus monkey. *J. Comp. Neurol.* **379,** 313–332 (1997).

134. Bisley, J. W. & Goldberg, M. E. Attention, intention, and priority in the parietal lobe. *Annu. Rev. Neurosci.* **33,** 1–21 (2010).

135. Desimone, R. & Duncan, J. Neural mechanisms of selective visual attention. *Annu. Rev. Neurosci.* **18,** 193–222 (1995).

136. Mundinano, I.-C. *et al.* Transient visual pathway critical for normal development of primate grasping behavior. *Proc. Natl. Acad. Sci. U.S.A.* **115,** 1364–1369 (2018).

137. Sommer, M. A., neurophysiology, R. W. J. O.2004. What the brainstem tells the frontal cortex. I. Oculomotor signals sent from superior colliculus to frontal eye field via mediodorsal thalamus. *Journal of Neurophysiology* **91,** 1381–1402 (2004).

138. Moore, T. & Armstrong, K. M. Selective gating of visual signals by microstimulation of frontal cortex. *Nature* **421,** 370–373 (2003).

139. Behan, M. & Appell, P. P. Intrinsic circuitry in the cat superior colliculus: projections from the superficial layers. *J. Comp. Neurol.* **315,** 230–243 (1992).

140. Hall, W. C. & Lee, P. Interlaminar connections of the superior colliculus in the tree shrew. I. The superficial gray layer. *J. Comp. Neurol.* **332,** 213–223 (1993).

141. Ozen, G., Helms, M. C. & Hall, W. C. in *The Superior Colliculus* (2004).

142. Sprague, J. M. Interaction of cortex and superior colliculus in mediation of visually guided behavior in the cat. *Science* **153,** 1544–1547 (1966).

143. Appell, P. P. & Behan, M. Sources of subcortical GABAergic projections to the superior colliculus in the cat. *J. Comp. Neurol.* **302,** 143–158 (1990).

144. Munoz, D. P. & Istvan, P. J. Lateral inhibitory interactions in the intermediate layers of the monkey superior colliculus. *Journal of Neurophysiology* **79,** 1193–1209 (1998).

145. Pettit, D. L., Helms, M. C., Lee, P., Augustine, G. J. & Hall, W. C. Local excitatory circuits in the intermediate gray layer of the superior colliculus. *Journal of Neurophysiology* **81,** 1424–1427 (1999).

146. Brenner, S. Sequences and consequences. *Philosophical Transactions of the Royal Society B: Biological Sciences* **365,** 207–212 (2010).

147. Shekhar, K. *et al.* Comprehensive Classification of Retinal Bipolar Neurons by Single-Cell Transcriptomics. *Cell* **166,** 1308–1323.e30 (2016).

148. Benzer, S. Behavioural mutants of Drosophila isolated by countercurrent distribution. *Proc Natl Acad Sci USA* **58,** 1112–1119 (1967).

149. Hotta, Y. & Benzer, S. Genetic dissection of the Drosophila nervous system by means of mosaics. *Proc Natl Acad Sci USA* **67,** 1156–1163 (1970).

150. Brenner, S. The genetics of Caenorhabditis elegans. *Genetics* **77,** 71–94 (1974).

151. White, J. G., Southgate, E., Thomson, J. N. & Brenner, S. The structure of the nervous system of the nematode Caenorhabditis elegans. *Philosophical Transactions of the Royal Society B: Biological Sciences* **314,** 1–340 (1986).

152. Brinster, R. L. *et al.* Somatic expression of herpes thymidine kinase in mice following injection of a fusion gene into eggs. *Cell* **27,** 223–231 (1981).

153. Costantini, F. & Lacy, E. Introduction of a rabbit beta-globin gene into the mouse germ line. *Nature* **294,** 92–94 (1981).

154. Gordon, J. W. & Ruddle, F. H. Integration and stable germ line transmission of genes injected into mouse pronuclei. *Science* **214,** 1244–1246 (1981).

155. Tsien, J. Z. *et al.* Subregion- and Cell Type-Restricted Gene Knockout in Mouse Brain. *Cell* **87,** 1317–1326 (1996).

156. Mouse Genome Sequencing Consortium *et al.* Initial sequencing and comparative analysis of the mouse genome. *Nature* **420,** 520–562 (2002).

157. Betley, J. N. & Sternson, S. M. Adeno-associated viral vectors for mapping, monitoring, and manipulating neural circuits. *Hum. Gene Ther.* **22,** 669–677 (2011).

158. Ugolini, G. Rabies virus as a transneuronal tracer of neuronal connections. *Adv. Virus Res.* **79,** 165–202 (2011).

159. Wickersham, I. R. *et al.* Monosynaptic restriction of transsynaptic tracing from single, genetically targeted neurons. *Neuron* **53,** 639–647 (2007).

160. Nagel, G. *et al.* Channelrhodopsin-1: a light-gated proton channel in green algae. *Science* **296,** 2395–2398 (2002).

161. Nagel, G. *et al.* Channelrhodopsin-2, a directly light-gated cation-selective membrane channel. *Proc Natl Acad Sci USA* **100,** 13940–13945 (2003).

162. Boyden, E. S., Zhang, F., Bamberg, E., Nagel, G. & Deisseroth, K. Millisecond-timescale, genetically targeted optical control of neural activity. *Nat Neurosci* **8,** 1263–1268 (2005).

163. Seki, A. *et al.* Heterologous Expression of Pharaonis Halorhodopsin in Xenopus laevis Oocytes and Electrophysiological Characterization of Its Light-Driven Cl− Pump Activity. *Biophysical Journal* **92,** 2559–2569 (2007).

164. Ziv, Y. *et al.* Long-term dynamics of CA1 hippocampal place codes. *Nature* **16,** 264–266 (2013).

165. Jun, J. J. *et al.* Fully integrated silicon probes for high-density recording of neural activity. *Nature* **551,** 232–236 (2017).

166. Anikeeva, P. *et al.* Optetrode: a multichannel readout for optogenetic control in freely moving mice. *Nat Neurosci* **15,** 163–170 (2011).

167. Dobin, A. *et al.* STAR: ultrafast universal RNA-seq aligner. *Bioinformatics* **29,** 15–21 (2012).

168. Love, M. I., Huber, W. & Anders, S. Moderated estimation of fold change and dispersion for RNA-seq data with DESeq2. *Genome Biol.* **15,** 31–21 (2014).

169. Susaki, E. A. *et al.* Advanced CUBIC protocols for whole-brain and whole-body clearing and imaging. *Nature Protocols* **10,** 1709–1727 (2015).

170. Wilson, J. J., Alexandre, N., Trentin, C. & Tripodi, M. Three-Dimensional Representation of Motor Space in the Mouse Superior Colliculus. *Current Biology* **28,** 1744–1755.e12 (2018).

171. Sidor, M. M. *et al.* In vivo optogenetic stimulation of the rodent central nervous system. *J Vis Exp* 51483 (2015).

172. Harris, K. D. & Mrsic-Flogel, T. D. Cortical connectivity and sensory coding. *Nature* **503,** 51–58 (2013).

173. Cruikshank, S. J., Lewis, T. J. & Connors, B. W. Synaptic basis for intense thalamocortical activation of feedforward inhibitory cells in neocortex. *Nat Neurosci* **10,** 462–468 (2007).

174. Jiang, X., Lachance, M. & Rossignol, E. Involvement of cortical fast-spiking parvalbumin-positive basket cells in epilepsy. *Prog. Brain Res.* **226,** 81–126 (2016).

175. Gentet, L. J. *et al.* Unique functional properties of somatostatin-expressing GABAergic neurons in mouse barrel cortex. *Nat Neurosci* **15,** 607–612 (2012).

176. Lee, S., Kruglikov, I., Huang, Z. J., Fishell, G. & Rudy, B. A disinhibitory circuit mediates motor integration in the somatosensory cortex. *Nat Neurosci* **16,** 1662–1670 (2013).

177. Markram, H. *et al.* Interneurons of the neocortical inhibitory system. *Nat Rev Neurosci* **5,** 793–807 (2004).

178. Herzog, E. *et al.* The existence of a second vesicular glutamate transporter specifies subpopulations of glutamatergic neurons. *J. Neurosci.* **21,** RC181 (2001).

179. Chaudhry, F. A. *et al.* The vesicular GABA transporter, VGAT, localizes to synaptic vesicles in sets of glycinergic as well as GABAergic neurons. *Journal of Neuroscience* **18,** 9733–9750 (1998).

180. Jackman, S. L., Beneduce, B. M., Drew, I. R. & Regehr, W. G. Achieving high-frequency optical control of synaptic transmission. *J. Neurosci.* **34,** 7704–7714 (2014).

181. Petersen, C. C. H. The functional organization of the barrel cortex. *Neuron* **56,** 339–355 (2007).

182. Woolsey, T. A. & Van der Loos, H. The structural organization of layer IV in the somatosensory region (SI) of mouse cerebral cortex. The description of a cortical field composed of discrete cytoarchitectonic units. *Brain Res* **17,** 205–242 (1970).

183. Amemori, K.-I., Gibb, L. G. & Graybiel, A. M. Shifting responsibly: the importance of striatal modularity to reinforcement learning in uncertain environments. *Front Hum Neurosci* **5,** 47 (2011).

184. Ressler, K. J., Sullivan, S. L. & Buck, L. B. Information coding in the olfactory system: evidence for a stereotyped and highly organized epitope map in the olfactory bulb. *Cell* **79,** 1245–1255 (1994).

185. Vassar, R. *et al.* Topographic organization of sensory projections to the olfactory bulb. *Cell* **79,** 981–991 (1994).

186. Mombaerts, P. *et al.* Visualizing an olfactory sensory map. *Cell* **87,** 675–686 (1996).

187. Graybiel, A. M. Organization of the nigrotectal connection: an experimental tracer study in the cat. *Brain Res* **143,** 339–348 (1978).

188. Kohl, J. *et al.* Functional circuit architecture underlying parental behaviour. *Nature* **556,** 326–331 (2018).

189. Evans, D. A. *et al.* A synaptic threshold mechanism for computing escape decisions. *Nature* **558,** 590–594 (2018).

190. Capelli, P., Pivetta, C., Esposito, M. S. & Arber, S. Locomotor speed control circuits in the caudal brainstem. *Nature* **551,** 373–377 (2017).

191. Bourane, S. *et al.* Identification of a Spinal Circuit for Light Touch and Fine Motor Control. *Cell* **160,** 503–515 (2015).

192. Radau, P., Tweed, D. & Vilis, T. Three-dimensional eye, head, and chest orientations after large gaze shifts and the underlying neural strategies. *Journal of Neurophysiology* **72,** 2840–2852 (1994).

193. Felsen, G. & Mainen, Z. F. Neural Substrates of Sensory-Guided Locomotor Decisions in the Rat Superior Colliculus. *Neuron* **60,** 137–148 (2008).

194. Sooksawate, T. *et al.* Viral vector-mediated selective and reversible blockade of the pathway for visual orienting in mice. *Front Neural Circuits* **7,** 162 (2013).

195. Tehovnik, E. J. Head and body movements evoked electrically from the caudal superior colliculus of rats: pulse frequency effects. *Behav. Brain Res.* **34,** 71–78 (1989).

196. Mooney, R. D., Klein, B. G. & Rhoades, R. W. Correlations between the structural and functional characteristics of neurons in the superficial laminae and the hamster's superior colliculus. *Journal of Neuroscience* **5,** 2989–3009 (1985).

197. Moschovakis, A. K., Karabelas, A. B. & Highstein, S. M. Structure-function relationships in the primate superior colliculus. I. Morphological classification of efferent neurons. *Journal of Neurophysiology* **60,** 232–262 (1988).

198. Moschovakis, A. K., Karabelas, A. B. & Highstein, S. M. Structure-function relationships in the primate superior colliculus. II. Morphological identity of presaccadic neurons. *Journal of Neurophysiology* **60,** 263–302 (1988).

199. Saito, Y. & Isa, T. Electrophysiological and morphological properties of neurons in the rat superior colliculus. I. Neurons in the intermediate layer. *Journal of Neurophysiology* **82,** 754–767 (1999).

200. Tremblay, R., Lee, S. & Rudy, B. GABAergic Interneurons in the Neocortex: From Cellular Properties to Circuits. *Neuron* **91,** 260–292 (2016).

201. Semina, E. V. *et al.* Cloning and characterization of a novel bicoid-related homeobox transcription factor gene, RIEG, involved in Rieger syndrome. *Nat. Genet.* **14,** 392–399 (1996).

202. Muccielli, M. L., Martinez, S., Pattyn, A., Goridis, C. & Brunet, J. F. Otlx2, an Otx-related homeobox gene expressed in the pituitary gland and in a restricted pattern in the forebrain. *Mol. Cell. Neurosci.* **8,** 258–271 (1996).

203. Gage, P. J. & Camper, S. A. Pituitary homeobox 2, a novel member of the bicoid-related family of homeobox genes, is a potential regulator of anterior structure formation. *Hum. Mol. Genet.* **6,** 457–464 (1997).

204. Westmoreland, J. J., McEwen, J., Moore, B. A., Jin, Y. & Condie, B. G. Conserved function of Caenorhabditis elegans UNC-30 and mouse Pitx2 in controlling GABAergic neuron differentiation. *J. Neurosci.* **21,** 6810–6819 (2001).

205. Zagoraiou, L. *et al.* A Cluster of Cholinergic Premotor Interneurons Modulates Mouse Locomotor Activity. *Neuron* **64,** 645–662 (2009).

206. Rozani, I. *et al.* Pitx2 cholinergic interneurons are the source of C bouton synapses on brainstem motor neurons. *Scientific Reports* **9,** 1–13 (2019).

207. Sooksawate, T. & Isa, T. Properties of cholinergic responses in neurons in the intermediate grey layer of rat superior colliculus. *European Journal of Neuroscience* **24,** 3096–3108 (2006).

208. Bolton, A. D. *et al.* A Diencephalic Dopamine Source Provides Input to the Superior Colliculus, where D1 and D2 Receptors Segregate to Distinct Functional Zones. *CellReports* **13,** 1003–1015 (2015).

209. Bittencourt, A. S., Nakamura-Palacios, E. M., Mauad, H., Tufik, S. & Schenberg, L. C. Organization of electrically and chemically evoked defensive behaviors within the deeper collicular layers as compared to the periaqueductal gray matter of the rat. *Neuroscience* **133,** 873–892 (2005).

210. Shang, C. *et al.* A parvalbumin-positive excitatory visual pathway to trigger fear responses in mice. *Science* **348,** 1472–1477 (2015).

211. Shang, C. *et al.* Divergent midbrain circuits orchestrate escape and freezing responses to looming stimuli in mice. *Nature Communications* **9,** 1–17 (2018).

212. Comoli, E. *et al.* Segregated anatomical input to sub-regions of the rodent superior colliculus associated with approach and defense. *Front Neuroanat* **6,** 9 (2012).

213. Tervo, D. G. R. *et al.* A Designer AAV Variant Permits Efficient Retrograde Access to Projection Neurons. *Neuron* **92,** 372–382 (2016).

214. Eriksen, C. W. & St James, J. D. Visual attention within and around the field of focal attention: a zoom lens model. *Percept Psychophys* **40,** 225–240 (1986).

215. Reynolds, J. H. & Chelazzi, L. Attentional modulation of visual processing. *Annu. Rev. Neurosci.* **27,** 611–647 (2004).

216. Treue, S. & Martínez Trujillo, J. C. Feature-based attention influences motion processing gain in macaque visual cortex. *Nature* **399,** 575–579 (1999).

217. Reynolds, J. H. & Heeger, D. J. The normalization model of attention. *Neuron* **61,** 168–185 (2009).

218. Kastner, S. & Ungerleider, L. G. Mechanisms of visual attention in the human cortex. *Annu. Rev. Neurosci.* **23,** 315–341 (2000).

219. Fecteau, J. H. & Munoz, D. P. Salience, relevance, and firing: a priority map for target selection. *Trends Cogn. Sci. (Regul. Ed.)* **10,** 382–390 (2006).

220. Krauzlis, R. J., Bollimunta, A., Arcizet, F. & Wang, L. Attention as an effect not a cause. *Trends Cogn. Sci. (Regul. Ed.)* **18,** 457–464 (2014).

221. Ding, L. & Gold, J. I. The Basal Ganglia's Contributions to Perceptual Decision Making. *Neuron* **79,** 640–649 (2013).

222. Wall, N. R., La Parra, De, M., Callaway, E. M. & Kreitzer, A. C. Differential Innervation of Direct- and Indirect-Pathway Striatal Projection Neurons. *Neuron* **79,** 347–360 (2013).

223. Redgrave, P., Gurney, K. & Reynolds, J. What is reinforced by phasic dopamine signals? *Brain Research Reviews* **58,** 322–339 (2008).

224. Lin, J. Y. A user's guide to channelrhodopsin variants: features, limitations and future developments. *Experimental Physiology* **96,** 19–25 (2010).

225. Ahmadlou, M. & Heimel, J. A. Preference for concentric orientations in the mouse superior colliculus. *Nature Communications* **6,** 1–11 (2015).

226. Walton, M. M. G., Bechara, B. & Gandhi, N. J. Role of the Primate Superior Colliculus in the Control of Head Movements. *Journal of Neurophysiology* **98,** 2022–2037 (2007).

227. Feinberg, E. H. & Meister, M. Orientation columns in the mouse superior colliculus. *Nature* **519,** 299–232 (2015).

228. Bizzi, E., Mussa-Ivaldi, F. A. & Giszter, S. Computations underlying the execution of movement: a biological perspective. *Science* **253,** 287–291 (1991).

229. Hafed, Z. M. & Chen, C.-Y. Sharper, Stronger, Faster Upper Visual Field Representation in Primate Superior Colliculus. *Current Biology* **26,** 1647–1658 (2016).

230. Basso, M. A. & May, P. J. Circuits for Action and Cognition: A View from the Superior Colliculus. *Annu Rev Vis Sci* **3,** 197–226 (2017).

231. McIlwain, J. T. Distributed spatial coding in the superior colliculus: a review. *Vis. Neurosci.* **6,** 3–13 (1991).

232. Anderson, R. W., Keller, E. L., Gandhi, N. J. & Das, S. Two-dimensional saccade-related population activity in superior colliculus in monkey. *Journal of Neurophysiology* **80,** 798–817 (1998).

233. van Opstal, A. J. & Goossens, H. H. L. M. Linear ensemble-coding in midbrain superior colliculus specifies the saccade kinematics. *Biol Cybern* **98,** 561–577 (2008).

234. Munoz, D. P. & Wurtz, R. H. Saccade-related activity in monkey superior colliculus. II. Spread of activity during saccades. *Journal of Neurophysiology* **73,** 2334–2348 (1995).

235. Cui, G. *et al.* Concurrent activation of striatal direct and indirect pathways during action initiation. *Nature* **494,** 238–242 (2013).

236. Gunaydin, L. A. *et al.* Natural Neural Projection Dynamics Underlying Social Behavior. *Cell* **157,** 1535–1551 (2014).